Obtaining temperature profiles from superior mirage data

by

William C. Kropla

A thesis

presented to the University of Manitoba

in partial fulfillment of the

requirements for the degree of

Master of Science

in

Interdisciplinary Studies

Winnipeg, Manitoba, 1988

ISBN 0-315-51692-5

OBTAINING TEMPERATURE PROFILES FROM SUPERIOR MIRAGE DATA

BY

WILLIAM C. KROPLA

A thesis submitted to the Faculty of Graduate Studies of the University of Manitoba in partial fulfillment of the requirements of the degree of

MASTER OF SCIENCE

I hereby declare that I am the sole author of this thesis.

I authorize the University of Manitoba to lend this thesis to other institutions or individuals for the purpose of scholarly research.

William C. Kropla

I further authorize the University of Manitoba to reproduce this thesis by photocopying or by other means, in total or in part, at the request of other institutions or individuals for the purpose of scholarly research.

The University of Manitoba requires the signature of all persons using or photocopying this thesis. Please sign below, and give address and date.

Abstract

Fraser's inversion method is applied to superior mirages and the results analysed. The ray equation is solved explicitly to express refractive profile in terms of the equation of the ray path. Differential geometric techniques are used to model the optical properties of the atmosphere and it is demonstrated that the assumption of constant Gaussian curvature can produce accurate refractive profiles. A mechanical analog of atmospheric refraction is derived and the fitting of optical data to derive refractive profiles is investigated.

I wish to thank Professor Waldemar Lehn for his guidance and insight throughout the course of the work presented here. Thanks are also due to Donald E. Knuth for his help in preparation of the manuscript. Finally I would like to express my gratitude to Linda, for her support and perseverance and also for her interest in Kruskal coordinates.

Table of Contents

List of Figures

CHAPTER 1: INTRODUCTION

1.1 Some Previous Work

The refractive index of an optical medium is defined to be the ratio between the speed of light in vacuo and the speed of light in the medium. In a medium of constant refractive index light rays will travel in straight lines. If, however, refractive index is not constant light rays will follow curved paths. Examining the ray equation

$$\frac{d}{ds}\left(n\frac{d\mathbf{r}}{ds}\right) = \nabla n$$

where the vector **r** locates a point on the ray path and **s** is arc length, we see that the ray will always turn in the direction of the gradient of n. If we restrict our attention to a laterally homogeneous, stratified atmosphere, then it should be clear that if refractive index increases with elevation rays will curve up and if it decreases with elevation rays will curve down.

In some cases, the refractive profile will result in two or more rays from each point on the target reaching the eye. These extra rays are perceived as images, distorted and displaced above or below the image resulting from the more direct rays. Superior mirages are images displaced above the direct image and inferior mirages are displaced below.

Knowing refractive index as a function of position in a region will allow us to

determine the path followed by a ray of light within that region by a straightforward solution of the ray equation The *inverse* problem stated simply is this: From observable optical distortions due to variations in refractive index, can we determine the refractive index as a function of position?

In the simplest case the atmosphere is assumed to be horizontally stratified, with refractive index constant within each layer. We view a target at some distance from the observer and record the elevation of a ray at the eye, the elevation angle of the ray and elevation of the ray at the target. It is not clear that this optical data, or a set of such triples, will allow us to deduce the refractive profile.

Sparkman [1], used a library technique and compared optical data with results from a two parameter logarithmic profile. The validity of this method of inversion rests on the implicit assumption that similar refractive profiles would result from similar optical data. It is clear from the ray equation that the inversion process is nonlinear, and as well, in the case of mirage phenomena, that the mapping that transforms rays at the target into rays at the eye is discontinuous — neighboring points on the target are widely separated at the eye. This casts serious doubt on the validity of the assumption underlying the method.

Fraser [2], assumed a series expansion for a refractive profile resulting in an

inferior mirage and sought to fit the constant coefficients of the truncated series to the optical data. While a fortunate choice of series can result in a good fit to a known profile, we can conclude only that the resulting fit is a good linear, good quadratic, etc. approximation to the true profile. Should Nature choose to select a different functional form for the refractive index, our set of fitting constants will be no more than a guess. As well, the optical data cannot force convergence of the series, and so leaves us without any estimate of the error incurred by truncation. Fraser's method is examined more closely in § 2.1, where we attempt to fit a Taylor series to superior mirage data and in § 2.3 where we analyse the failure of this attempt.

Neither of these two methods is theoretically enlightening. More promising is an iterative scheme proposed by Lehn[3], that traced rays through an approximation profile and followed by an adjustment of the approximation in each layer to reduce the elevation error for each ray at the target. Lehn assumed a constant radius of curvature in each layer, but this is not a strong constraint, since in the limit as layer depth goes to zero the radius of curvature of the ray path becomes constant. The iterative method converges experimentally, that is, when applied to several atmospheres with known temperature profiles.

1.2 Geometry

By Fermat's principle, the curved path that a ray follows in an atmosphere of nonconstant refractive index, minimizes the time of travel between any two points A and B, on the path. This is equivalent to minimizing the optical path length between A and B. A length minimizing curve is a geodesic. Clearly, the curved path between A and B is not the shortest Euclidean path.

We can, however, define a metric or distance function in terms of the optical path length. If the atmosphere is laterally homogeneous, this metric will determine, locally, a two dimensional surface related to the Euclidean plane by a set of differentiable, invertible mappings. Such a surface is called a differentiable manifold. In Chapter 3 it is shown that the image of the ray equation under these mappings is the set of geodesic equations of the manifold.

The consequences of constraining the Gaussian curvature of such a manifold are examined and it is shown that assuming constant curvature yields accurate refractive profiles for elevations below 20 meters.

1.3 A Mechanical Analogue

In Chapter 4 a mechanical analogue of atmospheric refraction is described. Its utility for inversion is examined and some calculations presented. While the model has some paedagogical utility it was found to be ineffective for calculation.

1.4 Definitions

This work uses three refractive and associated temperature profiles labelled Profile 1, Profile 2 and Profile 3. The details of each and ray plots generated from each profile are contained in the Appendix.

Table 1.1 defines the various symbols and constants used.

Symbol	Definition	Value	Dimensions
g	acceleration of gravity	9.8	$m\ s^{-2}$
β	1 / specific gas constant	0.00348	$°K\ s^2\ m^{-2}$
ϵ	constant	226×10^{-6}	$m^3\ kg^{-1}$
p	atmospheric pressure	—	$N\ m^{-2}$
ρ	air density	—	$kg\ m^{-3}$
n	refractive index	—	—
r	refractivity	$n - 1 \times 10^6$	—
K	Gaussian curvature	—	m^{-2}
k	ray curvature	—	m^{-1}
R_e	radius of the earth	6378	km
y_d	displacement of surface	—	m

Table 1.1

CHAPTER 2: SOME ANALYTICAL RESULTS

2.1 Fraser's Method

The differential equation describing the path of a light ray in a medium with refractive index n is

$$dx = \cot\beta dz \tag{2.1.1}$$

where β is the elevation angle of the ray and we assume that $n = n(z)$. Snell's law can be written

$$d(n\cos\beta)/ds = 0. \tag{2.1.2}$$

Fraser[2] defined the following transformation

$$\begin{aligned} \tau &= 1 - (n/n_o)^2 \\ \phi &= \tan\beta\cos\beta_o \\ \xi &= x\sec\beta_o \\ \varsigma &= z \end{aligned} \tag{2.1.3}$$

where z is the ray elevation at distance x from the observer, and β and n are respectively, the elevation angle of the ray and the refractive index. β_o and n_o are the values of these quantities at some reference level. Subscripts e, v, and t will refer to values of a quantity at the eye, vertex of the ray path, and target respectively. We assume throughout that the earth is flat.

The transformed variables allow us to rewrite Eq. (2.1.1)

$$d\xi = \phi^{-1} d\zeta \tag{2.1.4}$$

and Snell's law (Eq. (2.1.2))

$$d(\phi^2 + \tau)/ds = 0, \tag{2.1.5}$$

the solutions of which, for various initial conditions, are

$$\begin{aligned} \tau &= {\phi_o}^2 - \phi^2 \\ \tau_v &= {\phi_o}^2 \\ \tau_e &= {\phi_o}^2 - {\phi_e}^2 \\ \tau - \tau_e &= {\phi_e}^2 - \phi^2. \end{aligned} \tag{2.1.6}$$

Equation (2.1.4) and the chain rule allow us to write

$$d\xi = \frac{1}{\phi}\frac{d\zeta}{d\tau} d\tau$$

but from Eq. (2.1.6)

$$d\tau = -2\phi d\phi$$

hence

$$\xi_t = -2 \int_{\phi_e}^{\phi_t} \zeta' d\phi \tag{2.1.7}$$

where $\xi_e = 0$ and $\varsigma' \equiv d\varsigma/d\tau \equiv \varsigma^{(1)}$. A singularity exists that is not apparent when Eq. (2.1.4) is expressed in this form. If the ray path possesses a vertex between eye and target, then $\tan(\beta)$ vanishes there and the implicit division that cancels the ϕ's is not defined. However, Eq. (2.1.7) can still be valid and possess a continuous integrand, if we interpret the value of the integrand as a limit as $\beta \to 0$. We are, in effect, replacing the discontinuity with a point that will make the integrand continuous. The insertion of this single point will not affect the integral.

By the fundamental theorem of calculus

$$\varsigma = \int_0^\tau \varsigma' d\tau, \tag{2.1.8}$$

with ς' independent of ξ. Equation (2.1.8) and the unnumbered equation preceding Eq. (2.1.7) give us

$$\varsigma_t = -2 \int_{\phi_e}^{\phi_t} \varsigma' \phi d\phi. \tag{2.1.9}$$

Equations (2.1.7) and (2.1.9) are the parametric equations (with parameter ϕ_t) of the ray path. To solve these equations the temperature profile must be known.

Fraser assumes a series expansion for his elevation variable ς. He truncates this expansion and solves for the constants in terms of the inferior mirage data. The procedure is highly nonlinear, interactive and intuitive. Applying this method

to superior mirages yields results "inferior" to those obtained using the method described in Chapter 3.

We choose a set of polynomials ψ_m in τ, and write

$$\varsigma' = \sum_{m=1}^{\infty} a_m \psi_m(\tau) = \sum_{m=1}^{\infty} a_m \psi_m(\phi_o^2 - \phi^2). \tag{2.1.10}$$

Inserting into Eqs. (2.1.7) and (2.1.9) and reversing the order of integration and summation we get

$$\begin{aligned} -\xi_t/2 &= \sum_{m=1}^{\infty} a_m \hat{\psi}_m \\ -\varsigma_t/2 &= \sum_{m=1}^{\infty} a_m \tilde{\psi}_m, \end{aligned} \tag{2.1.11}$$

where we have

$$\begin{aligned} \hat{\psi}_m &= \hat{\psi}_m(\phi_e, \phi_t) = \int_{\phi_e}^{\phi_t} \psi_m({\phi_o}^2 - \phi^2) d\phi \\ \tilde{\psi}_m &= \tilde{\psi}_m(\phi_e, \phi_t) = \int_{\phi_e}^{\phi_t} \psi_m({\phi_o}^2 - \phi^2) \phi d\phi. \end{aligned} \tag{2.1.12}$$

In order to justify the interchange of summation and integration we require that the integrals in Eqs. (2.1.7) and (2.1.9) converge, that the series in Eq. (2.1.10) converge uniformly and each term in the series be continuous on the interval of interest. The first of these conditions is met by assuming a sufficiently differentiable $\varsigma(\tau)$ and by the insertion of a point if a vertex exists. The last two conditions will depend on the specific series expansion chosen. Presumably no one would attempt to expand ς in a series of discontinuous terms. Whether the series chosen will converge uniformly can be a more difficult question to answer.

We now suppose a Maclaurin expansion for ς in terms of τ. This converges absolutely within its radius of convergence (which may consist of the single point $\tau = 0$), and it converges uniformly on any open interval contained within the radius of convergence. We have, retaining only the first p terms,

$$\varsigma = \sum_{m=0}^{p} \varsigma_o{}^{(m)} \frac{\tau^m}{m!} \tag{2.1.13}$$

so that

$$\varsigma' = \sum_{m=1}^{p} \varsigma_o{}^{(m)} \frac{\tau^{m-1}}{(m-1)!}. \tag{2.1.14}$$

From Eq. (2.1.6), $\tau = \phi_o{}^2 - \phi^2$, so that Eq. (2.1.9) becomes (assuming that $\phi_e = \phi_o$),

$$\begin{aligned} \varsigma_t &= -2 \int_{\phi_o}^{\phi_t} \left(\sum_{m=1}^{p} \varsigma_o{}^{(m)} \frac{\tau^{m-1}}{(m-1)!} \right) \phi d\phi \\ &= -2 \int_{\phi_o}^{\phi_t} \left(\sum_{m=1}^{p} \varsigma_o{}^{(m)} \frac{(\phi_o{}^2 - \phi^2)^{m-1}}{(m-1)!} \right) \phi d\phi \end{aligned} \tag{2.1.15}$$

Letting $u = \phi_o{}^2 - \phi^2$ and $du = -2\phi d\phi$, substitution into this last integral yields

$$\varsigma_t = \sum_{m=1}^{p} \varsigma_o{}^{(m)} \frac{(\phi_o{}^2 - \phi_t{}^2)^m}{m!}. \tag{2.1.16}$$

In a similar manner

$$\begin{aligned} \xi_t = \sum_{m=1}^{p} \varsigma_o{}^{(m)} \Bigg[& \frac{2^{2m-1}(m-1)!}{(2m-1)!} \phi_o{}^{2m-1} \\ & - \sum_{s=1}^{m} \frac{2^{2s-1}(s-1)!}{(m-s)!(2s-1)!} \phi_t{}^{2s-1} (\phi_o{}^2 - \phi_t{}^2)^{m-s} \Bigg]. \end{aligned} \tag{2.1.17}$$

Taking a one term expansion ($p = 1$) we get

$$\begin{aligned} \xi_t &= 2\varsigma_o{}'(\phi_o - \phi_t) \\ \varsigma_t &= \varsigma_o{}'(\phi_o{}^2 - \phi_t{}^2). \end{aligned} \tag{2.1.18}$$

This result, following equation (16) in Fraser[2], is misprinted. As well, the following derivation (as presented by Fraser) is marred by repeated typographical errors. Eliminating ϕ_t from the previous pair of equations, we obtain

$$\frac{\xi_t{}^2}{4\varsigma_o{}'} = \xi_t\phi_o - \varsigma_t.$$

But the apparent elevation of the target point $\varsigma_a = \varsigma_e + \xi_t\phi_e$, which, since $\varsigma_e = 0 = \varsigma_o$, means that $\xi_t\phi_o = \varsigma_a$. Hence, the vertical separation between object and image

$$\begin{aligned} \delta\varsigma = \varsigma_a - \varsigma_t &= \frac{\xi_t{}^2}{4\varsigma_o{}'} \\ &= \frac{x^2 \sec^2\beta_o}{4d\varsigma_o/d\tau}. \end{aligned}$$

Assuming a temperature of approximately 273° K, typical atmospheric conditions and small β_o Fraser obtains

$$\delta\varsigma \approx \frac{x^2 10^{-6}}{2} \left.\frac{dT}{dz}\right|_{z=0},$$

similar to a result due to Fleagle [5].

If we know the vertical separation between points on the image and points on the target we can employ this equation to express the derivative dT/dz as a function

of departure angle β. Vertical separation data from Profile 1 for a target at 25 km were used and the result is presented in Fig. 2.1.1. For comparison purposes the figure also contains a graph of the temperature derivative required to displace the ground surface at the target an amount equal to the departure angle.

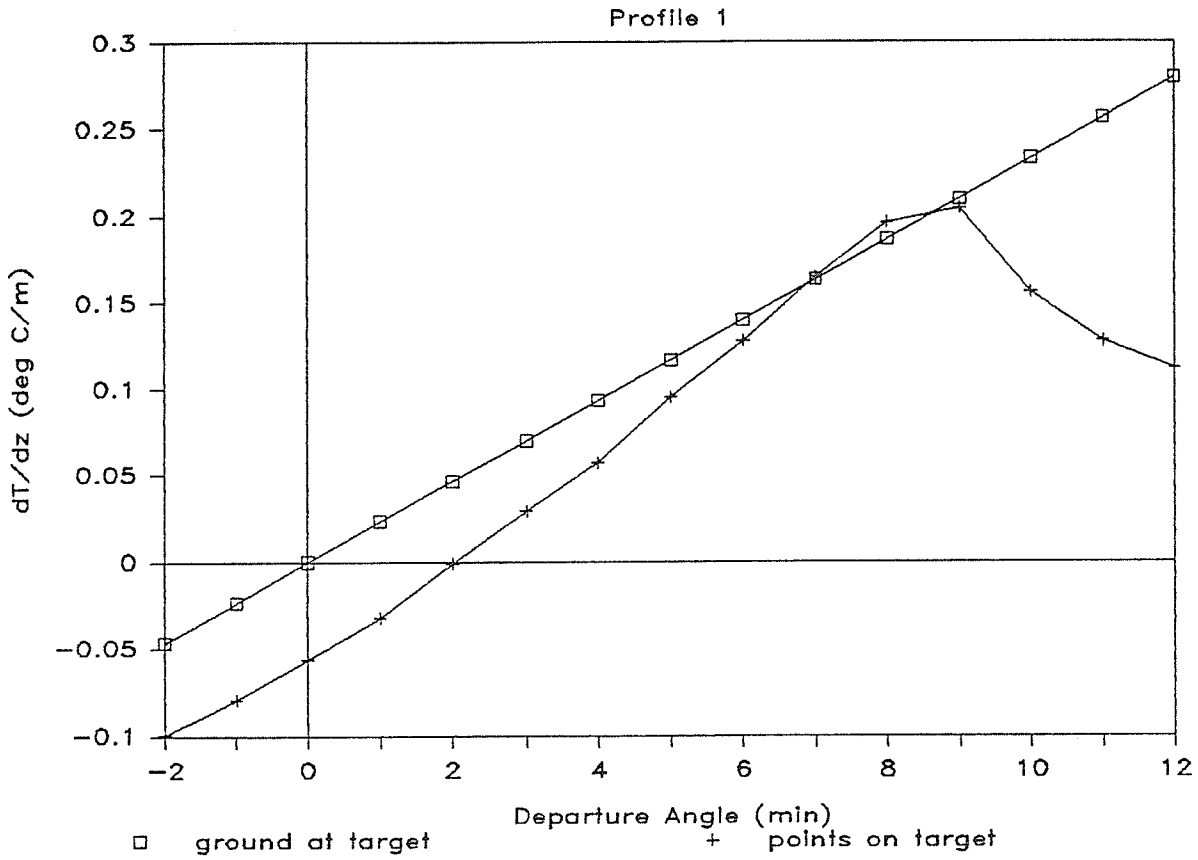

Fig. 2.1.1 Gradient required to produce vertical separation

It is to be noted that the temperature gradient is an approximately linear function of departure angle from -2 to 9 minutes of arc and then abruptly starts to decrease. It is also in this region that the ray paths start to flatten. The relationship, if one exists between these two phenomena, was not investigated.

From Profile 1 (see Appendix), between 0 and 15 meters, the actual mean temperature gradient is approximately 0.07° K/m, and between 15 meters and 30 meters it it approximately 0.4° K/m. Comparing with Fig. 2.1.1, we see that the temperature gradient below 15 meters can be obtained by properly selecting the ray upon which to base the calculation. We have, however, no *a priori* basis upon which to make such a selection. For the temperature gradient between 15 and 30 meters it is not possible to select a ray that results in a calculated temperature gradient greater than 0.22° K/m. Clearly a single term expansion is not a good model for the temperature profile examined here.

If we select $p = 2$ rays then Eqs. (2.1.16) and (2.1.17) will give us a system of four equations in four unknowns, namely, a ϕ_t for each ray and the first two constants in the Taylor expansion, $\varsigma_o^{(1)}$ and $\varsigma_o^{(2)}$. For each ray chosen we will have

the following pair of parametric equations

$$\begin{aligned} \varsigma_t &= \varsigma_o{}^{(1)}(\phi_o{}^2 - \phi_t{}^2) + \varsigma_o{}^{(2)}(\phi_o{}^2 - \phi_t{}^2)^2/2! \\ \xi_t &= 2\varsigma_o{}^{(1)}(\phi_o - \phi_t) + \varsigma_o{}^{(2)}\frac{8}{3!}(\phi_o{}^3 - \phi_t{}^3) - 2\varsigma_o{}^{(2)}\phi_t(\phi_o{}^2 - \phi_t{}^2). \end{aligned} \tag{2.1.19}$$

A program employing Newton's method, was used to solve this system of equations for two rays from Profile 1 and two rays from Profile 2. Each pair consisted of one ray with a departure angle of zero minutes of arc and one ray with a departure angle of one minute of arc. Two different solutions were found for each profile. The results are presented in Table 2.1 below, where $\phi_t{}^{(k)}$ is the arrival angle of the k^{th} ray at the target.

	Profile 1		Profile 2	
$\varsigma_o{}^{(1)}$	-3.0158×10^{6}	-3.4714×10^{6}	1.9423×10^{7}	4.3714×10^{7}
$\varsigma_o{}^{(2)}$	7.5118×10^{11}	-4.5304×10^{11}	3.8340×10^{14}	9.3382×10^{14}
$\phi_t{}^{(1)}$	1.4202×10^{-3}	1.6281×10^{-3}	5.6908×10^{-4}	4.7443×10^{-4}
$\phi_t{}^{(2)}$	1.6236×10^{-3}	3.3884×10^{-3}	-6.3161×10^{-4}	5.5110×10^{-4}

Table 2.1

Now, from Eq. (2.1.13)

$$z = \varsigma = \sum_{m=1}^{2} \varsigma_o{}^{(m)} \frac{\tau^m}{m!}.$$

Hence

$$\tau^2 \left(\frac{\varsigma_o{}^{(2)}}{2} \right) + \tau \varsigma_o{}^{(1)} - z = 0,$$

so that

$$\tau = -\frac{\varsigma_o^{(1)}}{\varsigma_o^{(2)}} + sgn\left(\frac{\varsigma_o^{(1)}}{\varsigma_o^{(2)}}\right)\sqrt{\left(\frac{\varsigma_o^{(1)}}{\varsigma_o^{(2)}}\right)^2 + \frac{2z}{\varsigma_o^{(2)}}}, \tag{2.1.20}$$

where, in order that $\tau(z=0)=0$, we have chosen the sign of the square root to be the sign of $\varsigma_o^{(1)}/\varsigma_o^{(2)}$. From Eqs. (2.1.3) we have $n/n_o = \sqrt{1-\tau}$, so

$$n = n_o\sqrt{1 + \frac{\varsigma_o^{(1)}}{\varsigma_o^{(2)}} - sgn\left(\frac{\varsigma_o^{(1)}}{\varsigma_o^{(2)}}\right)\sqrt{\left(\frac{\varsigma_o^{(1)}}{\varsigma_o^{(2)}}\right)^2 + \frac{2z}{\varsigma_o^{(2)}}}}. \tag{2.1.21}$$

Refractive indices resulting from Eq. (2.1.21) and the values in Table 2.1 are presented in Figs. 2.1.2 and 2.1.3. In both cases the eye is at the origin at the center of the graph.

The results for Profile 1 are qualitatively incorrect. One solution provides a refractive profile not defined for elevations greater than 13.3 meters. The other is defined for all positive elevations. Both, however, produce a refractive index that increases with elevation. This is inconsistent with the requirement that an inversion be present to produce a superior mirage.

While qualitatively correct, that is, the results for Profile 2 provide a decreasing refractive index, the decrease is so shallow that for both solutions the temperature at 45 meters is just 0.12° C. Furthermore, the two solutions provide indistinguishable refractive and temperature profiles. These results are presented in Fig. 2.1.4.

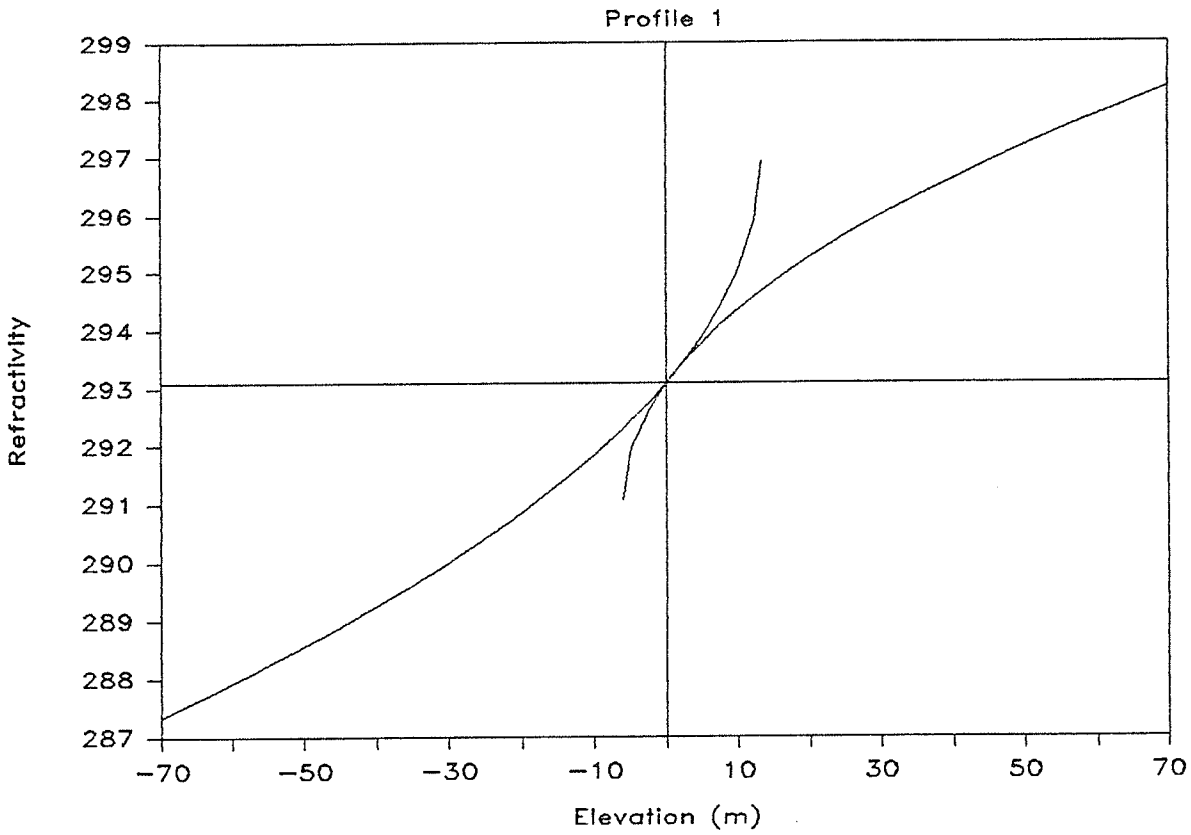

Fig. 2.1.2 Profile 1 first solution (p=2).

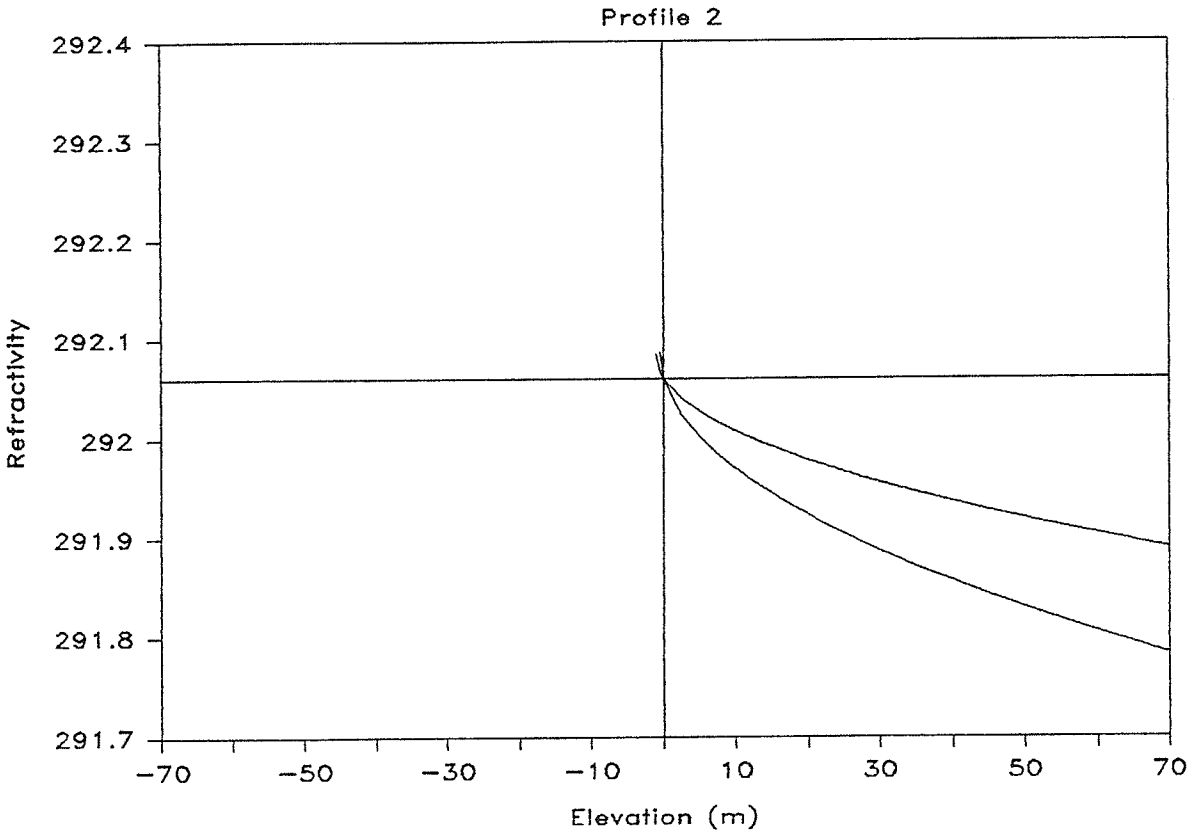

Fig. 2.1.3 Profile 1 second solution (p=2).

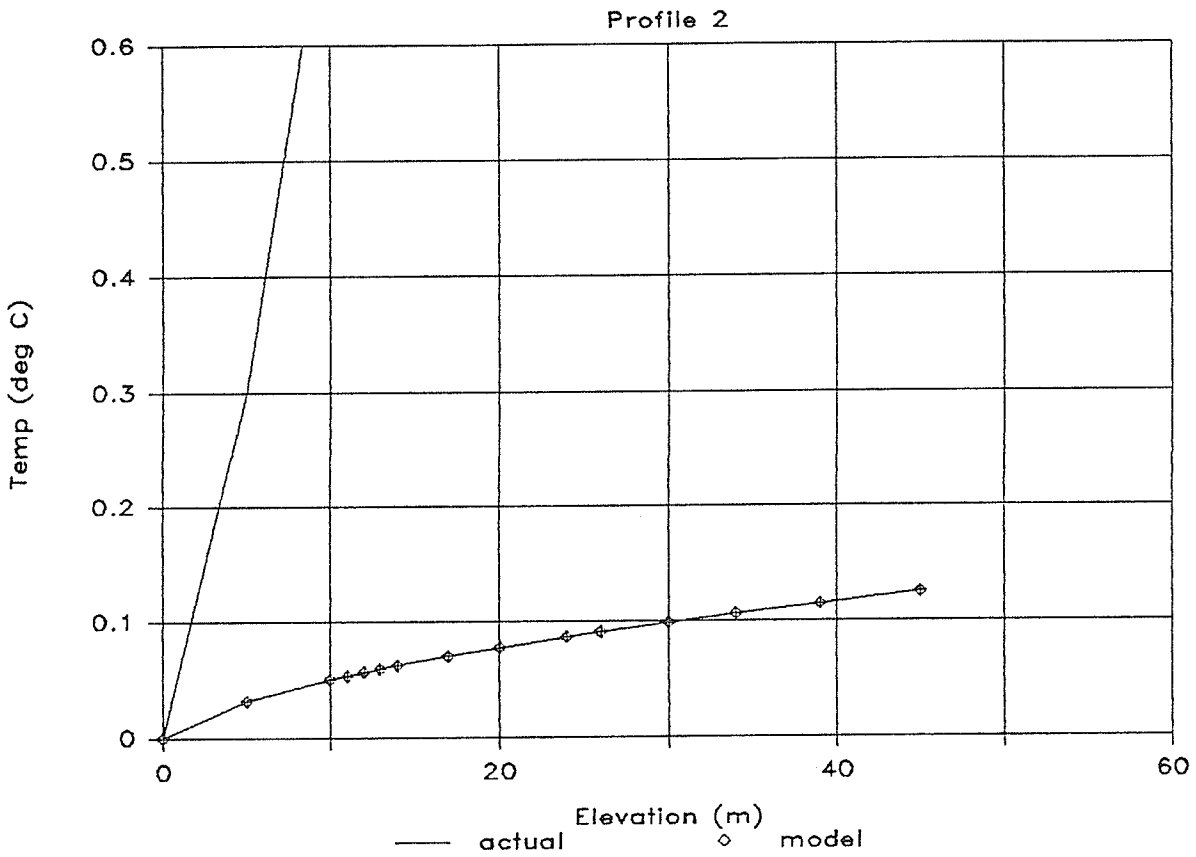

Fig. 2.1.4 Profile 2 first and second solutions are indistiguishable (p=2).

Clearly, employing Fraser's method with a two term expansion describes inadequately the temperature profile associated with a superior mirage.

For reasonable refractive indices, the variable τ is on the order of $\pm 10^{-5}$. So, in order to account for the large excursions of the ray path that occur in superior mirage situations, the Taylor coefficients in the ς expansion must be very large. We see in Table 1.1, that the ratio between first and second coefficients is on the order of 10^5 to 10^7. If a third, or higher term, contributes significantly to the expansion, then clearly the coefficient associated with that term must be even larger. The solution of Eqs. (2.1.19) and higher degree analogs, involve unknown quantities that differ by at least 14 to 17 orders of magnitude. As well, we take differences of small quantities. We are also not assured of finding all solutions. An investigation of these numerical concerns in the context of this problem have not been attempted. It appears that Fraser's power series approach is not well suited for superior mirage work.

2.2 A Direct Solution of the Ray Equation

If a ray of light in a nonhomogeneous medium follows a path given parametrically by $\mathbf{r} = (x(s), y(s), z(s))$ where s denotes path length and $\mathbf{r}$ locates a point on

the path, then the path must satisfy

$$\frac{d}{ds}\left(n\frac{d\mathbf{r}}{ds}\right) = \nabla n \tag{2.2.1}$$

where $n = n(x, y, z)$ is the refractive index of the medium through which the ray passes. We can rewrite the ray equation as

$$n\frac{d^2\mathbf{r}}{ds^2} + \frac{dn}{ds}\frac{d\mathbf{r}}{ds} = \nabla n. \tag{2.2.2}$$

Denoting derivatives with respect to s by primes we can write

$$\begin{aligned} nx'' + n'x' &= \frac{\partial n}{\partial x} \\ ny'' + n'y' &= \frac{\partial n}{\partial y} \\ nz'' + n'z' &= \frac{\partial n}{\partial z}. \end{aligned} \tag{2.2.3}$$

Noting that

$$\frac{dn}{ds} = \frac{\partial n}{\partial x}x' + \frac{\partial n}{\partial y}y' + \frac{\partial n}{\partial z}z' \tag{2.2.4}$$

and denoting partials by subscripts we have

$$\begin{aligned} (x'^2 - 1)n_x + x'y'n_y + x'z'n_z &= -nx'' \\ x'y'n_x + (y'^2 - 1)n_y + y'z'n_z &= -ny'' \\ x'z'n_x + y'z'n_y + (z'^2 - 1)n_z &= -nz''. \end{aligned} \tag{2.2.5}$$

We wish to solve these three equations for the three partial derivatives of n. The determinant of the matrix of coefficients is

$$\Delta = \begin{vmatrix} x'^2 - 1 & x'y' & x'z' \\ x'y' & y'^2 - 1 & y'z' \\ x'z' & y'z' & z'^2 - 1 \end{vmatrix} \tag{2.2.6}$$

Evaluating this we find that

$$\Delta = x'^2 + y'^2 + z'^2 - 1. \tag{2.2.7}$$

If a curve α is parametrized by arc length s, then $\alpha(s) = (x(s), y(s), z(s))$ and the tangent of the curve is defined to be $\alpha' = (x', y', z')$, which, since the path is parametrized by arc length, must have unit magnitude. Hence $\Delta = 0$ and the system is undetermined.

If the ray path lies in the x-y plane then we have

$$\begin{aligned} (x'^2 - 1)n_x + x'y'n_y &= -nx'' \\ x'y'n_x + (y'^2 - 1)n_y &= -ny'' \end{aligned} \tag{2.2.8}$$

and again

$$\Delta = \begin{vmatrix} x'^2 - 1 & x'y' \\ x'y' & y'^2 - 1 \end{vmatrix} = 0. \tag{2.2.9}$$

The reason for this is not hard to see. Since $x' = \cos\phi$ and $y' = \sin\phi$, (where ϕ is the tangent angle to the ray) substitution yields

$$n_x \sin\phi - n_y \cos\phi = -n\frac{d\phi}{ds}$$

for both of Eqs. (2.2.8). We note that $d\phi/ds$ is the curvature k, of the ray path. Now, if we assume that n is a function of y alone, this means that $n_y/n = \sec\phi(d\phi/ds)$, and, since $\phi = \tan^{-1}(dy/dx)$,

$$\frac{n_y}{n} = k\sec\phi = \sec\phi\frac{d\phi}{ds} = \sqrt{1 + \left(\frac{dy}{dx}\right)^2}\frac{d\phi}{ds}. \tag{2.2.10}$$

The curvature of a plane curve is given by

$$\frac{d\phi}{ds} = \frac{d^2y/dx^2}{\left(1+(dy/dx)^2\right)^{3/2}},$$

so that we have, integrating with respect to y, from the elevation of the eye

$$\ln\left(\frac{n}{n_e}\right) = \int_{y_e}^{y} \frac{n_y}{n} dy = \int_{y_e}^{y} \frac{d^2y/dx^2}{1+(dy/dx)^2} dy. \tag{2.2.11}$$

This gives us a relation between elevation and refractive index independent of arc length. We select a ray path $y = f(x)$ and express dy/dx and d^2y/dx^2 as functions of y. (Finding the inverse function may not be a trivial problem.) Performing the integration we obtain refractive index n as a function of elevation.

	Path	n
Parabola	$y = a - b(x - x_v)^2$	$n_e\sqrt{(\alpha-\beta y)/(\alpha-\beta y_e)}^{\dagger}$
Cycloid	$x = a\cos^{-1}(1-y/a) \pm \sqrt{2ay-y^2}$	$n_e\sqrt{y_e/y}$
Circle	$y = \sqrt{2ax-x^2}$	$n_e y_e/y$
Catenary	$y = a - a\cosh x/a$	$n_e(1-y/a)/(1-y_e/a)$

$\dagger\alpha = 1+4ab, \quad \beta = 4b, \quad x_v =$ vertex range

Table 2.2

Table (2.2) gives the dependence of refractive index on elevation for four ray paths: parabola, cycloid, circle and catenary. These are similar to results obtained by Lyusternik [6].

Suppose that the ray path is given by

$$y = a - b(x - x_v)^2, \tag{2.2.12}$$

then

$$\ln\left(\frac{n}{n_e}\right) = \int_{y_e}^{y} \frac{-2b}{1 + 4ab - 4by} dy. \tag{2.2.13}$$

Integration yields

$$n(y) = n_e \sqrt{\frac{1 + 4ab - 4by}{1 + 4ab - 4by_e}}. \tag{2.2.14}$$

A ray from Profile 2, with departure angle 5 minutes of arc, was selected because its shape seemed reasonably parabolic. The ray elevation at the eye was 2.00 meters, and at the target range of 25 kilometers, it was 2.42 meters. These values, plus the initial ray slope, allowed us to fit the parabola given by Eq. (2.2.12) yielding values of:

$$a = 11.1969 \qquad b = 5.7508 \times 10^{-8} \qquad x_v = 12646$$

The fit to the ray path is shown in Fig. (2.2.1). The resulting refractivity and temperature profiles are shown in Figs. (2.2.2) and (2.2.3) respectively.

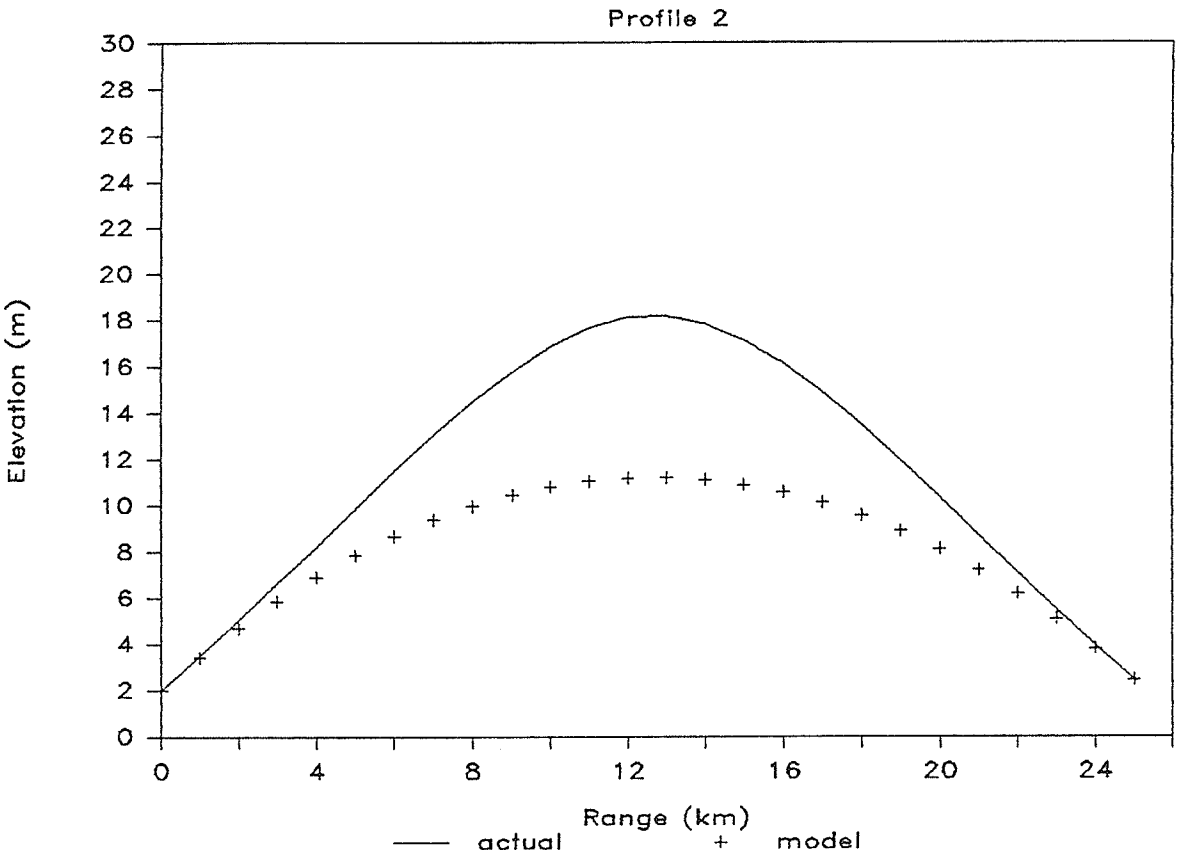

Fig. 2.2.1 Parabola fitted to a ray from Profile 2

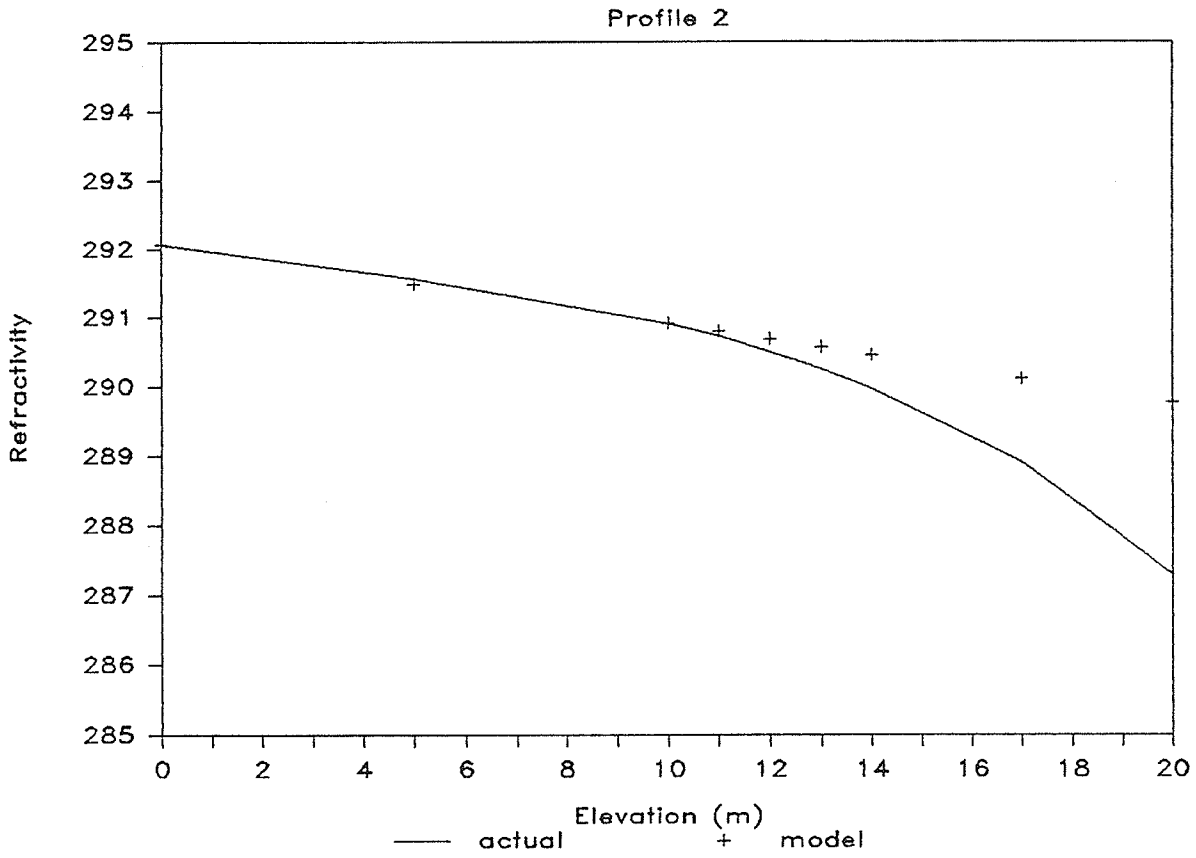

Fig. 2.2.2 Refractive profile corresponding to Fig. 2.2.1

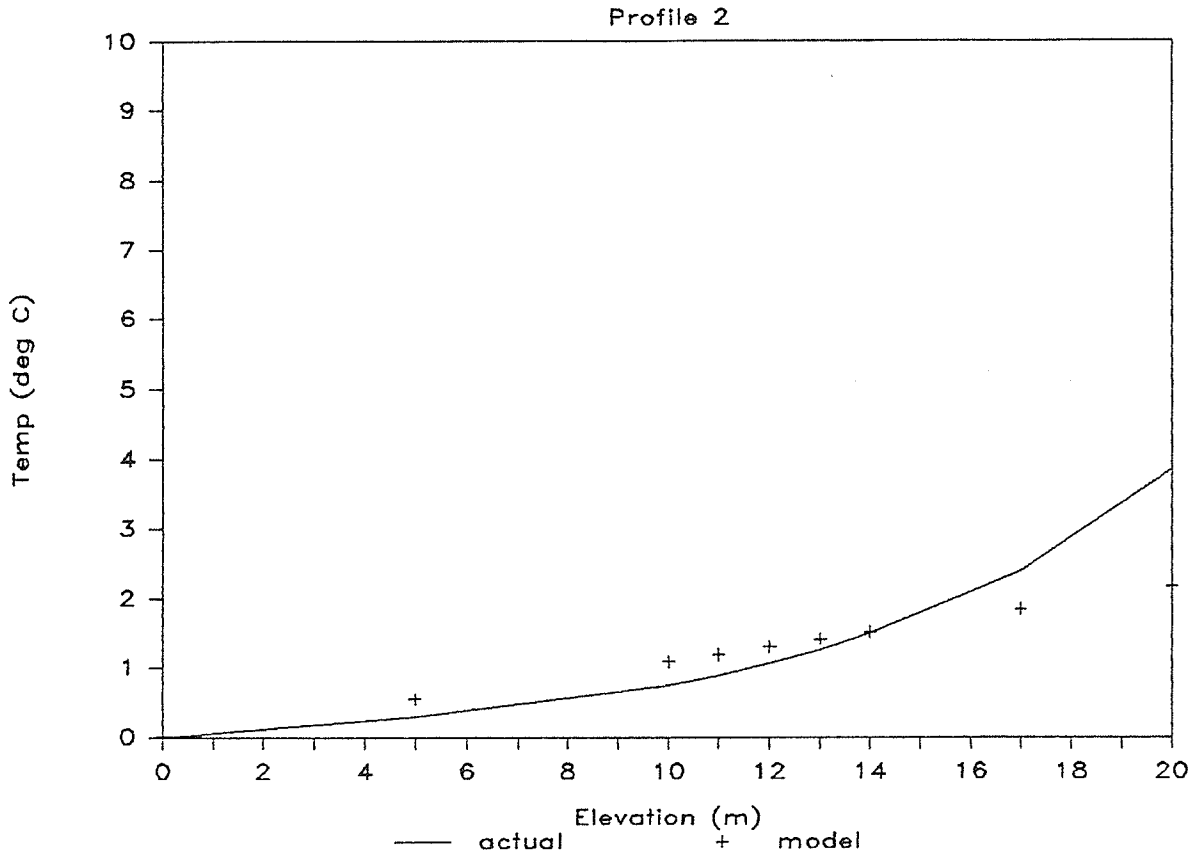

Fig. 2.2.3 Temperature profile coresponding to Fig. 2.2.1

The parabola was fitted to observable quantities and clearly the fit to the ray path is poor. If we simplify the problem and fit a parabola to the observable elevations at eye and target and the unobservable elevation at the vertex (18.17 meters), we get

$$a = 18.1854 \qquad b = 1.0224 \times 10^{-7} \qquad x_v = 12582$$

From Fig. (2.2.4), it is clear that these values provide a better fit to the ray path. But Figs. (2.2.5) and (2.2.6) indicate that the errors in refractive index and temperature are larger over most of the range of elevation treated.

Cartesian coordinates are convenient for calculation on the flat earth, but when we take the curvature of the earth into account (as we must for distant targets), we must employ plane polar coordinates.

The derivatives of the position vector $\mathbf{r}$, are given by

$$\begin{aligned} \frac{d\mathrm{r}}{ds} &= r'\hat{r} + r\theta'\hat{\theta} \\ \frac{d^2\mathrm{r}}{ds^2} &= (r'' - r\theta'^2)\hat{r} + (r\theta'' + 2r'\theta')\hat{\theta}, \end{aligned} \tag{2.2.15}$$

and the gradient of n,

$$\nabla n = \frac{\partial n}{\partial r}\hat{r} + \frac{1}{r}\frac{\partial n}{\partial \theta}\hat{\theta}, \tag{2.2.16}$$

where $\hat{r}$ and $\hat{\theta}$ are unit vectors, and primes denote differentiation with respect to

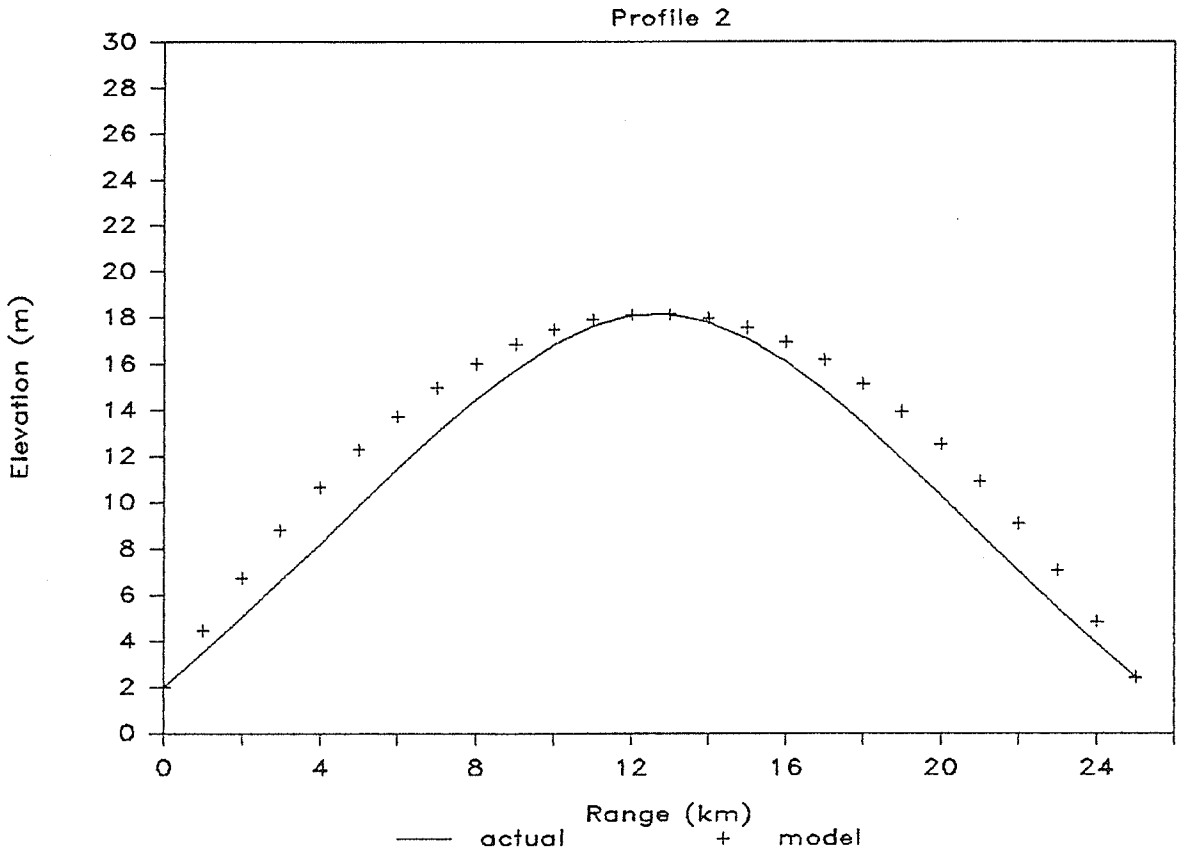

Fig. 2.2.4 Parabola fitted to a ray from Profile 2

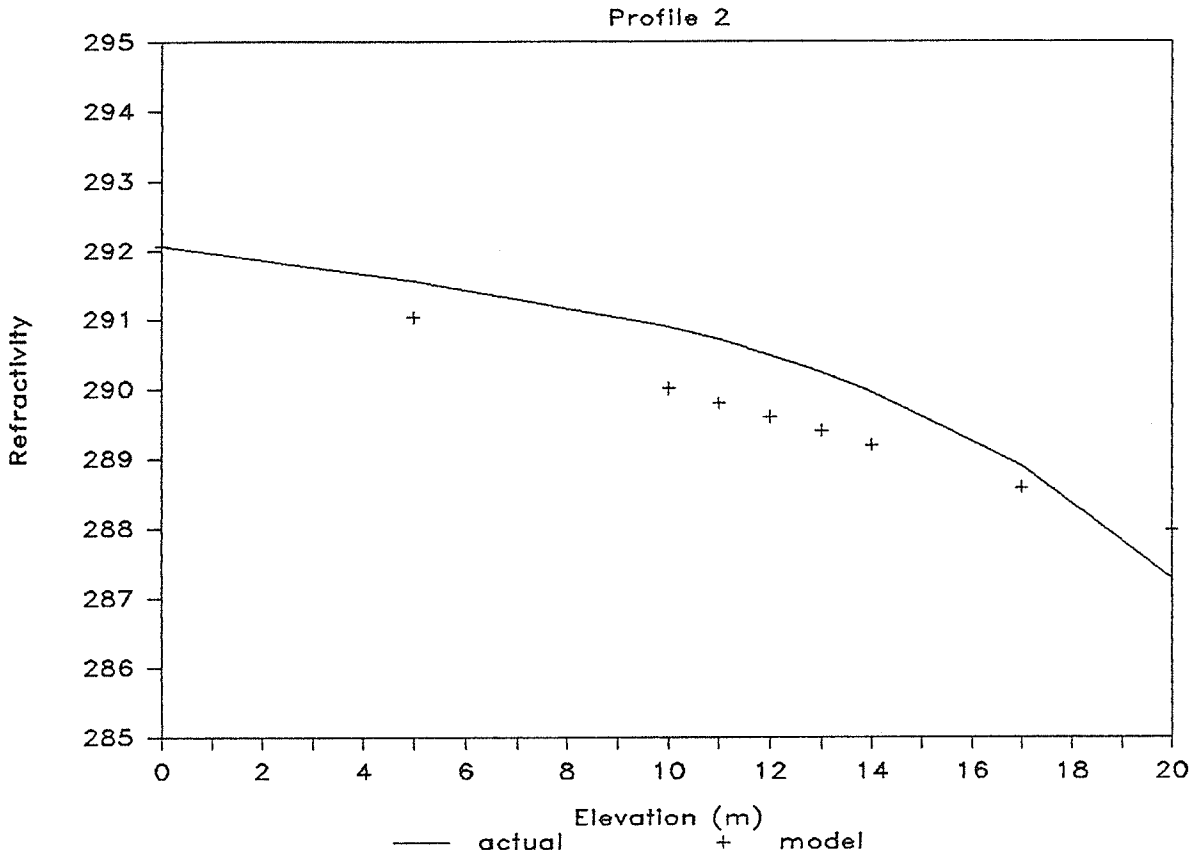

Fig. 2.2.5 Refractive profile corresponding to Fig. 2.2.5

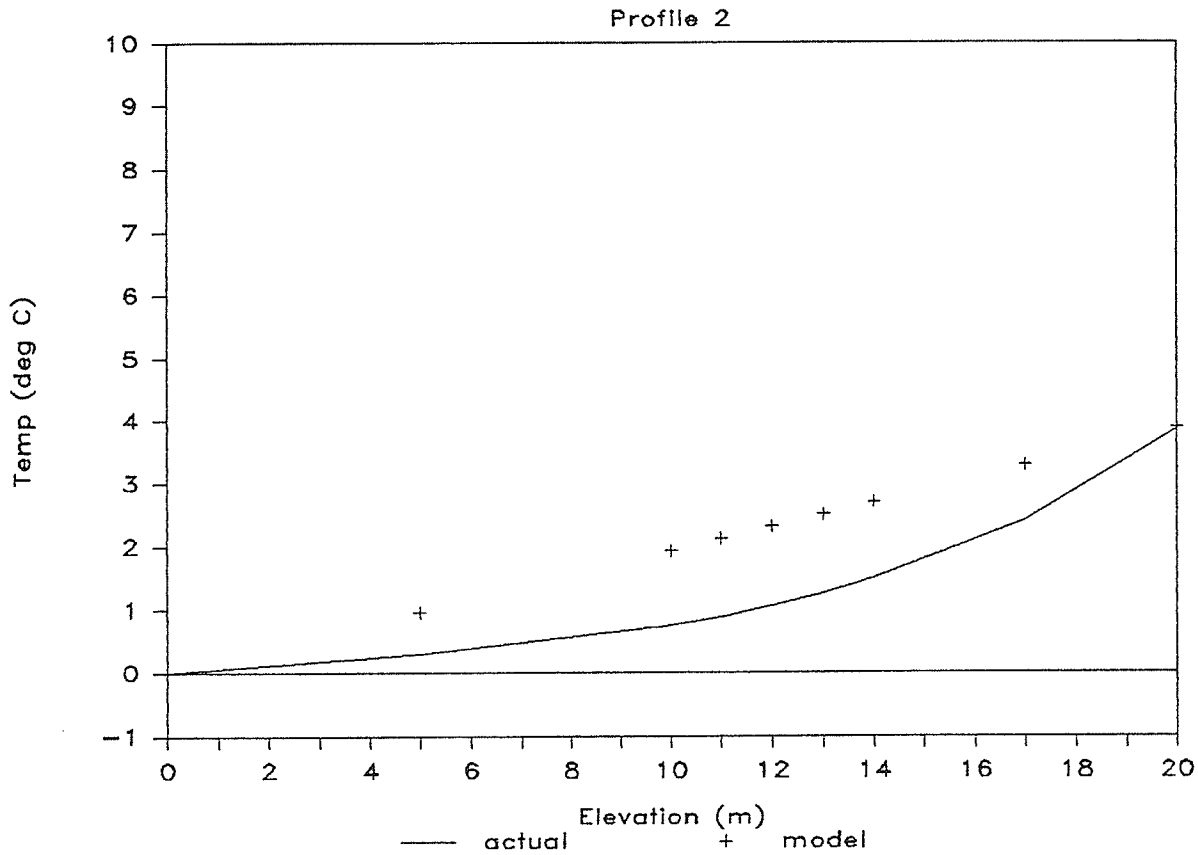

Fig. 2.2.6 Temperature profile corresponding to Fig. 2.2.5

arc length s. Employing Eqs. (2.2.15) and (2.2.16) we write the ray equation in component form,

$$n(r'' - r\theta'^2) + n'r' = n_r$$

$$n(r\theta'' + 2r'\theta') + n'r\theta' = \frac{1}{r}n_\theta.$$

Since

$$\frac{dn}{ds} = n_r r' + n_\theta \theta'$$

we have

$$\begin{aligned} n_r(1 - r'^2) - n_\theta r'\theta' &= n(r'' - r\theta'^2) \\ -n_r(rr'\theta') + n_\theta(\frac{1}{r} - r\theta'^2) &= n(r\theta'' + 2r'\theta'). \end{aligned} \tag{2.2.17}$$

We wish to solve these equations for n_r and n_θ, the partial derivatives of n with respect to r and θ. Evaluating the determinant of the matrix of coefficients, we find that

$$\Delta = \begin{vmatrix} (1 - r'^2) & -r'\theta' \\ -rr'\theta' & (\frac{1}{r} - r\theta'^2) \end{vmatrix} = \frac{1}{r}(1 - r'^2 - r^2\theta'^2), \tag{2.2.18}$$

which, since $(r'^2 + r^2\theta'^2)$ is the magnitude of the *unit* tangent to the path, must vanish. Again the system of equations is undetermined.

The orthogonal components of the unit tangent are: $r\theta' = \cos\phi$ and $r' = \sin\phi$, where ϕ is the tangent angle with respect to the normal to the radius vector $\mathbf{r}$. Differentiating these we obtain

$$r\theta'' = -\frac{d\phi}{ds}\sin\phi - (\frac{\sin\phi\cos\phi}{r}) \qquad \text{and} \qquad r'' = \frac{d\phi}{ds}\cos\phi.$$

Substituting in Eqs. (2.2.17), and noting that the tangent of ϕ has unit magnitude, some algebra yields

$$\begin{aligned} n_r \cos\phi - n_\theta \frac{\sin\phi}{r} &= n\left(\frac{d\phi}{ds} - \frac{\cos\phi}{r}\right) \\ -n_r \cos\phi + n_\theta \frac{\sin\phi}{r} &= n\left(-\frac{d\phi}{ds} + \frac{\cos\phi}{r}\right), \end{aligned} \tag{2.2.19}$$

where the linear dependence is obvious.

If we assume that n is a function of r alone, that is, $n = n(r)$ then Eqs. (2.2.19), become

$$\frac{n_r}{n} = \frac{d\phi}{ds}\sec\phi - \frac{1}{r} \tag{2.2.20}$$

so that integrating with respect to r, from the elevation of the eye,

$$\ln\left(\frac{n}{n_e}\right) = \int_{r_e}^{r} \frac{n_r}{n} dr = \int_{r_e}^{r} \left(\frac{d\phi}{ds}\sec\phi - \frac{1}{r}\right) dr. \tag{2.2.21}$$

Intuitively, the $1/r$ term accounts for the curvature inherent in the coordinate system. For example, if the ray paths are circles centered on the origin, then $d\phi/ds = 0$, $\sec\phi = 1$ and performing the integration yields

$$n = n_e\left(\frac{r_e}{r}\right).$$

Note that for level rays on a curved earth, $\phi < 1°$, so that rays with constant ϕ have true curvature very nearly equal to the curvature of the earth.

Since the quantity $d\phi/ds$ will, in general, be difficult to calculate we will not proceed as we did in the cartesian case, that is, perform the integration in Eq. (2.2.21). It will be easier to integrate either one of Eqs. (2.2.17) directly.

With $n = n(r)$ the first of Eqs. (2.2.17) becomes

$$\frac{n_r}{n} = \frac{(r'' - r\theta'^2)}{(1 - r'^2)}. \tag{2.2.22}$$

If we consider a parabolic ray path with focus at the center of the earth, then the path can be described by

$$r(1 - \cos\theta) = 2a \tag{2.2.23}$$

where $a - R_e$ is the elevation of the vertex and R_e is the radius of the earth. Then

$$\theta = \cos^{-1}\left(1 - \frac{2a}{r}\right) \qquad \text{and} \qquad \frac{d\theta}{dr} = -\frac{1}{\sqrt{1-u^2}}\left(\frac{2a}{r^2}\right) \tag{2.2.24}$$

where $u = (1 - 2a/r)$ so that

$$\theta' = r'\frac{d\theta}{dr} \qquad \Longrightarrow \qquad \theta'^2 = \frac{r'^2}{1-u^2}\frac{4a^2}{r^4}. \tag{2.2.25}$$

Since the magnitude of the unit tangent is given by $r'^2 + r^2\theta'^2$ we find that

$$r'^2 = \frac{r-a}{r} \qquad \text{and} \qquad r'' = \frac{a}{2r^2}. \tag{2.2.26}$$

Inserting these formulae into Eq. (2.2.22) and integrating from the elevation of the eye, we have

$$\ln\left(\frac{n}{n_e}\right) = \int_{r_e}^{r} \frac{n_r}{n} dr = \int_{r_e}^{r} -\frac{1}{2r} dr \tag{2.2.27}$$

which yields

$$n = n_e \sqrt{\frac{r_e}{r}}. \tag{2.2.28}$$

Since $r - r_e = z$ and z is small we can write

$$n = n_e \sqrt{\frac{r_e}{r_e + z}} \approx \frac{n_e}{1 + \frac{1}{2}\frac{z}{r_e}} \approx n_e \left(1 - \frac{1}{2}\frac{z}{r_e}\right) \approx n_e(1 - 0.79 \times 10^{-7} z), \tag{2.2.29}$$

where we have expanded the square root and retained only the linear term. This linearized refractive index differs from the square root by less than 4 parts in 10^6 at 20 meters.

Unfortunately, a ray described by Eq. (2.2.23) will never intersect the surface of the earth. We employ polar coordinates with origin at the center of the Earth in order to account, in a straightforward manner, for the Earth's curvature and the resulting spherical symmetry of the atmosphere. In this context a useful profile is characterized by a lack of dependence on polar angle.

While Eq. (2.2.23) certainly leads to a profile with the required symmetry, its failure to intersect the surface severely limits its utility.

We could relocate both focus and origin to the same point on the surface. Equation (2.2.23) will still describe the path but a becomes the elevation of the vertex and the polar angle θ will sweep out π radians from horizon through zenith

to horizon. Now however, when tracing a ray through such an atmosphere, the elevation of any point above the surface depends on both coordinates r and θ. Our profile, expressed in this coordinate system, has lost its symmetry.

By relocating just the focus of the parabolic path, the profile retains its symmetry but the calculations required to convert the path to a profile become very complicated. For example, if we shift the focus of Eq. (2.2.23) p units to the left, the polar equation of this parabola becomes

$$r^2(1-\cos^2\theta) - 4ar\cos\theta = 4a^2 + 4ap. \tag{2.2.30}$$

Recalling the derivatives required to solve Eq. (2.2.22) it should be clear that the problem is cumbersome at best. Considering that the resulting profile will be essentially linearly, investigation of parabolic paths in a polar coordinate system will be abandoned.

In the cartesian case we have

$$n = n_e\sqrt{\frac{1+4ab-4by}{1+4ab-4by_e}},$$

expanding the square root and keeping only the linear term we get

$$n \approx n_e(1 - 2.04\times 10^{-7}z). \tag{2.2.31}$$

Comparing with the linearized square root, we see that the cartesian refractive profile requires a larger slope to produce the same degree of ray curvature that occurred in the polar case as a consequence of the radial symmetry.

Clearly, modelling an entire ray path by a single parabola will, for all practical purposes, produce a linear refractive profile. The method, as it stands, has little applicability to the problem of determining temperature profiles from mirage data. It does however possess some utility. Since we know the departure angle and the initial and final elevations of the ray, the highest degree polynomial that can be fitted to these conditions is second degree. The assumption of a parabolic path allows a rough refractive profile to be obtained from observable quantities. And, for shallow rays, the parabola may provide a sufficiently accurate refractive profile.

A problem that arises when fitting rays to parabolas, is that each parabola is, in a sense, uncoupled from the others. Each is fitted separately and no parameters from one are related to another. This means that we cannot find an *optimal* (in some sense) set of parabolas derived from a set of mirage data and use some commom parameter to determine a refractive profile statistically. We discuss this problem in Chapter 4, where we fit mirage data to sinusoidal paths and relate refractive index to the common frequency.

The selection of a parabola as the approximate shape of the ray path, is to some extent arbitrary. There are other functions that can be fitted to the known ray data: Gaussians, sinusoids, Legendre polynomials etc. But whatever function we choose, we are *guessing* that the temperature structure of the atmosphere will produce rays with approximately that shape. We have no way of knowing, a priori, if that is the case. Furthermore, it is possible for the optical data to mimic (at least for a single ray) the result of another refractive profile. A ray can be perturbed in the region between eye and target in such a way that the initial and final conditions remain unchanged. No analysis of a single ray, or analysis of uncoupled rays can hope to determine the nature of this perturbation.

It seems pointless then, to compile a library of path/profile pairs and seek to fit mirage data by searching for the *best* path. While this method might solve the practical problem of obtaining atmospheric temperature profiles from mirage data, it does not constitute, in any mathematical sense, a solution to the inversion problem. We can not be sure that the profile associated with the best fitted path is a good fit to the true profile. A mathematical solution, even a statistical solution, should not stumble over a quirky atmosphere, the boundary of its region of applicability should be derivable a priori and the initial conditions of the problem should

tell us if the atmosphere under investigation falls within the boundary.

2.3 An Analysis of the Ray Path

We examine here the effect of ray path shape on the temperature structure of the atmosphere. We will limit the discussion to ray paths that possess a single vertex and no points of inflection. Note that at a point of inflection the ray curvature, and hence the refractive gradient, change sign. Thus, the restriction is equivalent to requiring that the refractive index be a monotonic function of elevation.

The lowest ray observed in an inferior mirage exits the eye with negative slope, strikes the surface tangentially at the vertex, and travels on to intersect the target. Let us suppose that the ray path is given explicitly by $y = f(x)$.

Since we have assumed that $f(x)$ possesses no points of inflection, $f''(x) > 0$ for all x. This implies that the slope of the ray path always increases with increasing x. Furthermore, the initial slope is bounded below by the requirement that the ray be tangent to the surface at the vertex. Hence, the slope of the ray path, between eye and vertex, must lie between the initial (negative) value and zero.

We can suppose that all of the temperature variation between the eye and the surface occurs, discontinuously, at the surface. The ray path in this case would be

a pair of straight lines intersecting at the vertex. The path is not differentiable at this point and the ray curvature is infinite. Convective, conductive and radiative mechanisms will, however, guarantee a non-zero lapse rate between surface and eye. This serves to limit the magnitude of ray curvature and hence places a physical upper bound on $f''(x)$. (Ray curvature is, of course, one of the parameters that we are trying to deduce from the mirage data.)

We expand $f(x)$ in a Maclaurin series,

$$f(x) = f(0) + f'(0)x + f''(0)\frac{x^2}{2} + f'''(0)\frac{x^3}{3!} + \cdots$$

where the first two coefficients, $f(0)$ and $f'(0)$ are known. To adequately model the temperature structure of the atmosphere, we must select second (and higher) order terms that will reduce the slope from a *known* initial value to zero, in a *known* distance.

Let $f_p(x)$ be the cubic approximation to the ray path $f(x)$. The approximation has the same origin and initial slope as $f(x)$, and is tangent to the surface at the vertex of $f(x)$ so that

$$f_p(x) = f(0) + f'(0)x + f_p''(0)\frac{x^2}{2!} + f_p'''(0)\frac{x^3}{3!}$$

where $f(0)$ and $f'(0)$ come from the Taylor expansion of $f(x)$, and $f_p''(0)$ and

$f_p'''(0)$ are fitting constants. Define the cubic defect

$$\Delta_p = f_p(x) - f(x).$$

Since $f(x)$ has one vertex and no points of inflection, $f(x)$ must lie between $f_p(x)$ and the straight line

$$y = f(0) + f'(0)x$$

obtained by allowing the line tangent to the ray at the eye to intersect the x-axis at $x_p = -f(0)/f'(0)$. Figure 2.3.1 shows the region that $f(x)$ must inhabit. It follows that the maximum cubic defect will be

$$\begin{aligned}\Delta_p &= f(0) + f'(0)x_p + f_p''(0)\frac{{x_p}^2}{2} + f_p'''(0)\frac{{x_p}^3}{6} \\ &= \frac{1}{2}f_p''(0)\left(-\frac{f(0)}{f'(0)}\right)^2 + \frac{1}{6}f_p'''(0)\left(-\frac{f(0)}{f'(0)}\right)^3.\end{aligned}$$

If we fit a cubic to a ray that is tangent to the surface at a range of 2500 meters, that exits the eye with departure angle -3 minutes of arc and initial elevation of 1.0 meter, then we obtain the results shown in Table 2.3, from which we determine that the maximum cubic defect is 0.269 meters.

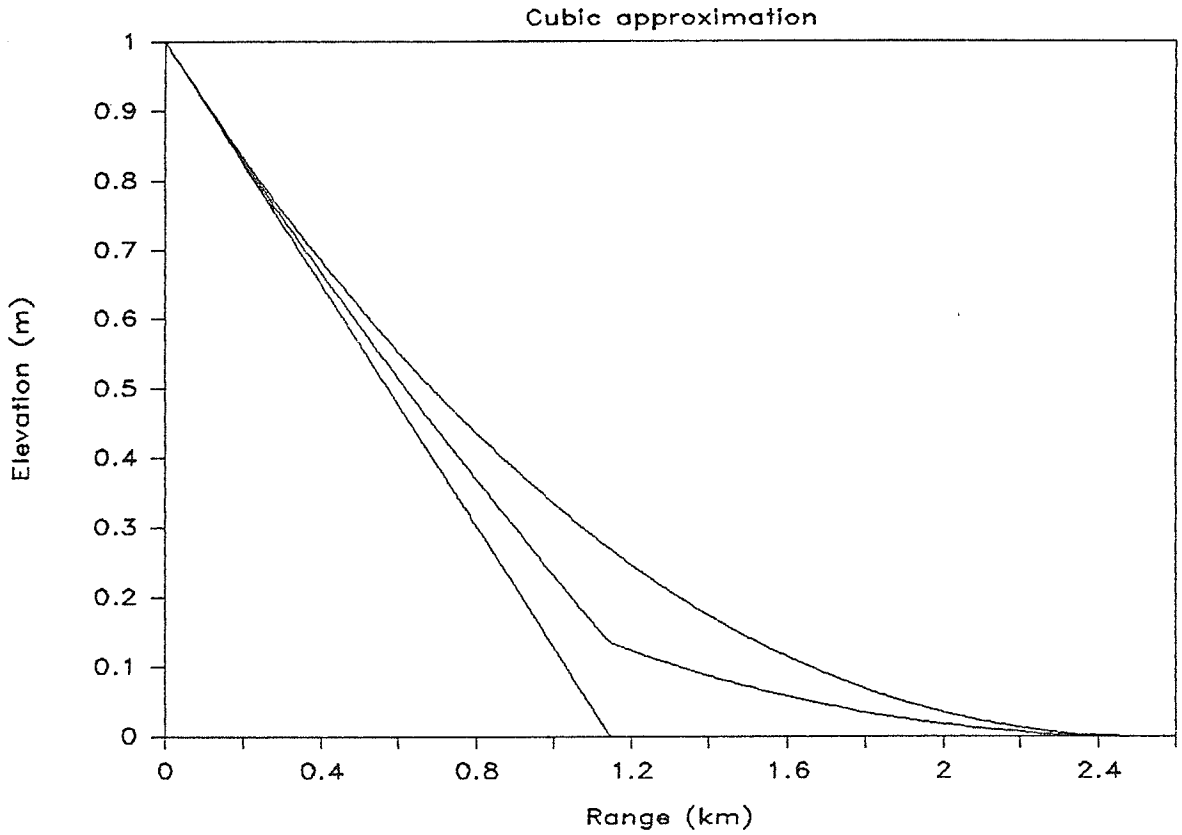

Fig. 2.3.1 Cubic approximation of a ray.

$f(0)$	$f'(0)$	$f''(0)$	$f'''(0)$
1.0	-8.7270×10^{-4}	4.3632×10^{-7}	-6.9792×10^{-11}

Table 2.3

Under the present constraints, an actual ray would never exhibit this maximum defect since the defect occurs at a point of infinite ray curvature, namely at the corner at $x = x_p$. We can even relax, slightly, the constraint that $f(x)$ possess no points of inflection. As long as any deviation resulting from such a relaxation does not cause the ray to stray from the region bounded by the straight line, the x-axis and the cubic approximation, the cubic defect will be bounded as before. Such deviations in the ray path would indicate the presence of a fine structure in the temperature profile that the cubic model ignores. From the preceding analysis, it is clear that the magnitude of this fine structure *must* be bounded for the cubic approximation to adequately model the ray trajectory.

The highest ray observed in a superior mirage exits the eye with positive slope, reaches its highest elevation at the vertex, and then continues on to intersect the target. An analysis similar to the one above is not possible since we can not locate the vertex. We know, given the constraints on $f(x)$, that the vertex must lie below a line tangent to the ray at the eye, but we can not determine either its range

or elevation. Neither can we fit a cubic to the known conditions since we lack information about the location of the vertex.

As well, the vertical displacement of a ray under superior mirage conditions can be orders of magnitude greater than the displacement under inferior mirage conditions. As a consequence, disallowing points of inflection on the ray path is unrealistic. We do not, however, possess, a *priori*, a sensible scheme for relaxing this constraint. Indeed, thermodynamically relevant quantities aloft depend on the entire column of air below, and this column can be very tall. Even if rates of change of these quantities are small, integrating over the height of the column can produce large changes.

These factors suggest that the failure of Fraser's method to produce accurate temperature profiles from the superior mirage data used, results from attempting to extend the method beyond its domain of validity.

CHAPTER 3: GEOMETRY

3.1 Optical Path Length

The optical path length along a ray from a point A to a point B, in a medium with varying refractive index n is defined by

$$\Delta l = \int_A^B \frac{c}{v}\, ds = \int_A^B n(x,y,z)ds \tag{3.1.1}$$

where c is the velocity of light in vacuo, v the velocity in the medium and the integration is performed along the path of the ray. Now, $v = ds/dt$, so that along the ray one can write $cds/v = cdt$ and hence

$$\Delta l = \int_A^B cdt = c\Delta t. \tag{3.1.2}$$

Thus the optical path length is proportional to travel time for light along the path. Fermat's principle tells us that the path followed by a ray will be that path which minimizes time of traversal. From Eq. (3.1.2) we see that this implies minimization of optical path length. Any length minimizing path on a surface is a geodesic. This has some interesting consequences.

3.2 Metrics and Geodesics

If we restrict our attention to a ray that travels in the x-y plane, then for arbitrarily close points on the ray, the optical path length (now denoted by dl), is

approximately

$$dl = n(x, y)ds. \tag{3.2.1}$$

Note that line element ds lies in the euclidean plane (denoted by $\mathbf{R}^2$) and that dl is the line element on a two dimensional surface that is defined (at least locally) by Eq. (3.2.1). Since $dl^2 = n^2(dx^2 + dy^2) = n^2\delta_{ij}dx^i dx^j = g_{ij}dx^i dx^j$, this surface has metric

$$g_{ij} = n^2\delta_{ij}. \tag{3.2.2}$$

We make the assumption that n is a function of elevation alone, explicitly

$$n = n(y). \tag{3.2.3}$$

Then the covariant metric tensor is

$$g_{ij} = n^2(y)\delta_{ij} \tag{3.2.4}$$

and its contravariant counterpart becomes

$$g^{ij} = \frac{1}{n^2}\delta^{ij}. \tag{3.2.5}$$

We can now begin the calculation of the quantities required to describe the surface in terms of the metric given by Eq. (3.2.2). The details of these calculations are

contained in Appendix I, where the Christoffel symbols of the first and second kinds are defined. The nonvanishing Christoffel symbols of the first kind are

$$\begin{aligned} \Gamma_{112} &= n(dn/dy) \\ \Gamma_{121} &= -n(dn/dy) \\ \Gamma_{211} &= n(dn/dy) \\ \Gamma_{222} &= n(dn/dy). \end{aligned} \tag{3.2.6}$$

and of the second kind are

$$\begin{aligned} \Gamma_1{}^2{}_1 &= -(1/n)(dn/dy) \\ \Gamma_2{}^2{}_2 &= (1/n)(dn/dy) \\ \Gamma_1{}^1{}_2 &= (1/n)(dn/dy) \\ \Gamma_2{}^1{}_1 &= (1/n)(dn/dy). \end{aligned} \tag{3.2.7}$$

The equations defining a geodesic on a surface, in terms of arc length are

$$\frac{d^2x^i}{ds^2} + \Gamma_j{}^i{}_k \frac{dx^j}{ds}\frac{dx^k}{ds} = 0. \tag{3.2.8}$$

Substituting Eq. (3.2.7) into equations (3.2.8) and noting that we are now measuring arc length by l, we obtain the geodesic equations for the surface under discussion

$$\begin{aligned} \frac{d^2x}{dl^2} + \frac{2}{n}\frac{dn}{dy}\frac{dx}{dl}\frac{dy}{dl} &= 0 \\ \frac{d^2y}{dl^2} + \frac{1}{n}\frac{dn}{dy}\left[\left(\frac{dy}{dl}\right)^2 - \left(\frac{dx}{dl}\right)^2\right] &= 0. \end{aligned} \tag{3.2.9}$$

3.3 Geodesics and the Ray Equation

We have defined the line element on the surface so that $dl = nds$. The chain rule allows us to write

$$\begin{aligned} \frac{dx}{dl} &= \frac{dx}{ds}\frac{ds}{dl} = \frac{1}{n}\frac{dx}{ds} \\ \frac{dy}{dl} &= \frac{dy}{ds}\frac{ds}{dl} = \frac{1}{n}\frac{dy}{ds} \end{aligned} \tag{3.3.1}$$

and

$$\begin{aligned} \frac{d^2x}{dl^2} &= \frac{1}{n^2}\frac{d^2x}{ds^2} + \frac{1}{n}\frac{d}{dy}\left(\frac{1}{n}\frac{dx}{ds}\frac{dy}{ds}\right) \\ \frac{d^2y}{dl^2} &= \frac{1}{n^2}\frac{d^2y}{ds^2} + \frac{1}{n}\frac{d}{dy}\left(\frac{1}{n}\frac{dy}{ds}\frac{dy}{ds}\right). \end{aligned} \tag{3.3.2}$$

Substituting Eq. (3.3.1) and (3.3.2) into the geodesic Eq. (3.2.9) we obtain (after some manipulation)

$$\begin{aligned} n\frac{d^2x}{ds^2} + \frac{dn}{ds}\frac{dx}{ds} &= 0 \\ n\frac{d^2y}{ds^2} + \frac{dn}{ds}\frac{dy}{ds} &= \frac{dn}{dy} \end{aligned} \tag{3.3.3}$$

which can be written in the more familiar form

$$\frac{d}{ds}\left(n\frac{d\mathbf{r}}{ds}\right) = \nabla n \tag{3.3.4}$$

known as the ray equation. Here the vector $\mathbf{r}$, which locates a point on the ray path and arc length s, are creatures of R^2.

3.4 Gaussian Curvature

If $\alpha(s)$ is a plane curve, parametrized by arc length s, then the *curvature* $k = k(s)$ of α is defined to be

$$k(s) = \frac{d\mathbf{T}}{ds} \cdot \mathbf{N} \tag{3.4.1}$$

where $\mathbf{T}$ and $\mathbf{N}$ are the unit tangent and unit normal respectively of α. Intuitively, k measures the rate of change of the tangent direction with respect to arc length.

Now, suppose that we have a surface imbedded in $\mathbf{R}^3$ and that at every point on this surface we can define a unique (up to sign) normal vector. The intersection of the surface and a plane containing the normal, defines a plane curve, the curvature of which is called the normal curvature of the surface. If we allow this plane to rotate about the normal at $\mathbf{p}$, the curvature at $\mathbf{p}$ will be given as a function of the rotation angle. There are two cases. Either the curvature will be constant as the angle changes, or the curvature will attain a maximum *and* a minimum. The directions in which the extrema occur will be orthogonal. These two directions are called principal directions and the curvatures in the principal directions are called principal curvatures.

The Gaussian curvature at a point is defined to be the product of the principal curvatures. If, for example, our surface is a circular cylinder of radius r, the principal

directions are parallel and perpendicular to the axis of the cylinder. The normal curvature in the perpendicular direction is just the curvature of a circle $1/r$. In the other direction the curvature is zero since the normal plane in that direction cuts a straight line from the cylinder. Hence, the Gaussian curvature of a circular cylinder is zero. Similarly, any pair of orthogonal directions on the surface of a sphere of radius r will be principal directions. Then each principal curvature will be $1/r$ so that the Gaussian curvature of a sphere is $1/r^2$.

Surfaces whose Gaussian curvatures vanish, can be simpler than those in which this is not the case. But such surfaces are not, for our purposes, without utility. For example, if we allow a straight line, called a ruling, to move smoothly along a fixed line, not colinear with it, the ruling sweeps out a surface called a ruled surface. Cylinders and cones are simple examples of such surfaces. The important feature of a ruled surface in the present context, is the fact that its Gaussian curvature $K \leq 0$. In fact, if the tangent planes remain parallel along the rulings then $K = 0$.

The discussion above describes a surface and its Gaussian curvature in terms of an *extrinsic* feature of the surface, ie. the rate at which the normal topples. The normal does not exist in the surface and requires that we embed the surface in $\mathbf{R}^3$. This limits us to surfaces which *can* be embedded. We would like a characterization

of curvature that is based on intrinsic properties of the surface. The simplest such property is geodesic spreading.

We consider a geodesic polar mapping of the surface at the point $\mathbf{p}$. Such a mapping is defined by

$$\mathbf{x}(u, v) = \gamma_{\cos v\mathbf{e}_1 + \sin v\mathbf{e}_2}(u),$$

where $\mathbf{e}_1$ and $\mathbf{e}_2$ constitute a basis at $\mathbf{p}$, the curves of constant u are the analogue of polar circles and the curves of constant v are geodesics radiating from $\mathbf{p}$.

If the Gaussian curvature vanishes, then geodesics will spread at the same rate as straight lines emanating from a point in the plane, that is, in a neighborhood of $\mathbf{p}$, $(v - v_o)/u = \theta$, where θ is the angle subtended at u by $v - v_o$. Locally, this surface is planar.

If Gaussian curvature is positive, then locally, the surface acts like a sphere. In that case geodesics do not spread as fast as on a plane. Intuitively, this can be demonstrated by forcing an orange peel onto a flat surface. It spreads and finally tears as its geodesics are forced to spread at the same rate as the geodesics of the flat surface. (Note that this intuition is an extrinsic one.)

If the Gaussian curvature is negative the surface is, locally, like a saddle, and geodesics spread faster than geodesics in the plane. Imagine forcing a saddle onto

flat surface; as we proceed it doesn't tear but folds over on itself. The geodesic spreading gives us more surface than the plane can accomodate. If we are careful and the saddle is elastic we can force its points into a one to one correspondence with the points of the plane by squeezing the geodesics closer together so that they spread less.

In Appendix I we determine the components of the Riemann and covariant curvature tensors. These results allow us to express the Gaussian curvature of our surface as

$$K = \frac{R_{1212}}{|g|} \tag{3.4.2}$$

where K is the Gaussian curvature, R_{1212} the [1212] component of the covariant curvature tensor and $|g|$ is the determinant of the contravariant metric tensor, treated as a matrix. Performing the calculations implicit in Eq. (3.4.2) we obtain

$$\frac{d^2n}{dy^2} - \frac{1}{n}\left(\frac{dn}{dy}\right)^2 = -n^3K. \tag{3.4.3}$$

For $K = 0$, let $v = \ln n$ then Eq. (3.4.3) becomes $v'' = 0$ (where $'$ indicates differentiation with respect to y) so that

$$n = ae^{by}. \tag{3.4.4}$$

If the temperature (and hence refractive index) is known at two points, $y = 0$ and

$y = y_e$, then

$$a = n(0) = n_o \qquad \text{and} \qquad b = \frac{1}{y_e} \ln\left(\frac{n_e}{n_o}\right). \tag{3.4.5}$$

and finally

$$n = n_o \left(\frac{n_e}{n_o}\right)^{y/y_e} \tag{3.4.6}$$

Since $n = 1 + \epsilon\beta \mathrm{p}/T$ we have

$$T = \epsilon\beta \mathrm{p} \left[n_o \left(\frac{n_e}{n_o}\right)^{y/y_e} - 1 \right]^{-1}. \tag{3.4.7}$$

A fit of Eq. (3.4.7) was attempted, using the data from Profile 1. Elevations zero and 35 meters were chosen for y and y_e, respectively. The resulting temperature profile did not agree with the known temperature profile at the selected elevations. It was determined that this was due to a difference in air pressure p, at zero and 35 meters. Since pressure as a function of altitude was not known a refractive profile, Eq. (3.4.6), was fitted to the known refractive index at these same elevations. The fitted profile and actual refractivity are shown in Fig. (3.4.1). The profile from Eq. (3.4.6) appeared to be a straight line, as is apparent from the figure. Similar results occurred when other points were chosen to fit. We can write Eq. (3.4.6) as

$$\ln\left(\frac{n}{n_o}\right) = \frac{y}{y_e} \ln\left(\frac{n_e}{n_o}\right).$$

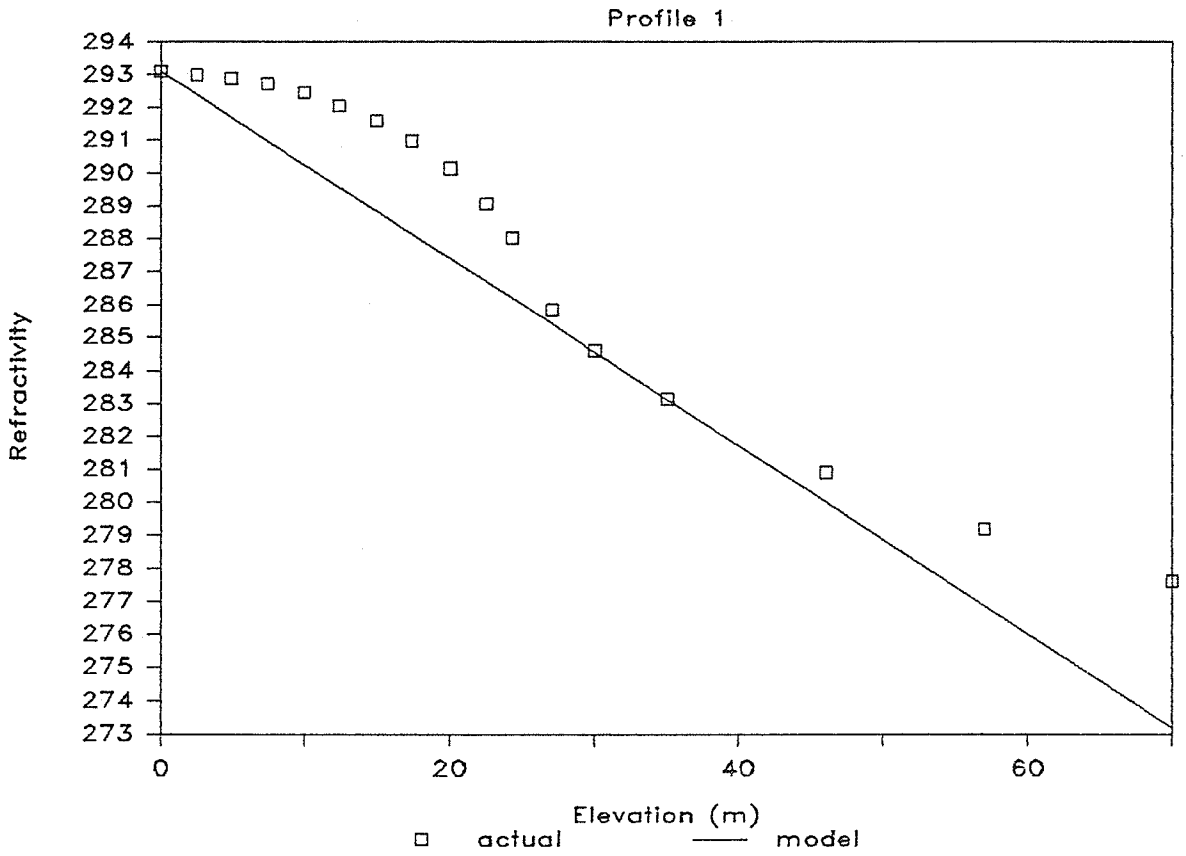

Fig. 3.4.1 Profile 1 refractivity — K = 0.

For $0 < x \leq 2$,

$$\ln x = (x-1) - \frac{1}{2}(x-1)^2 + \frac{1}{3}(x-1)^3 - \cdots$$

Since $n/n_o - 1$ is small we have

$$y \approx \frac{y_e}{\ln(n_e/n_o)} \left(\frac{n}{n_o} - 1 \right)$$

so that n is approximately a linear function of y. Linear refractive profiles do not cover many cases.

For K = constant, the same change of variable gives us $v'' = -n^2 K$. An application of the chain rule allows us to write this as $v'' = v' dv'/dv$. Integrating this with respect to v we obtain

$$n' = \pm n\sqrt{a^2 - Kn^2} \tag{3.4.8}$$

where a is the constant of integration. Note that, under conditions that produce a superior mirage, n is a decreasing function of y so that we choose the negative root. Then changing variables and integrating Eq. 3.4.8 with respect to y gives us

$$n = \frac{2ac}{\sqrt{K}} \frac{e^{-ay}}{e^{-2ay} + c^2} \tag{3.4.9}$$

where c is the second constant of integration. We have three parameters to adjust to fit the refractive index, namely, the two integration constants and the Gaussian

curvature. The refractive index at three elevations, 0, 10 and 20 m, was taken from each of the profiles and Newton's method used to fit a, c and K. The results are presented in Table (3.1).

Profile	a	c	K
1	$1.2920296665 \times 10^{-4}$	0.99984996067	$1.6683625101 \times 10^{-8}$
2	$1.5682137495 \times 10^{-4}$	0.99972591717	$2.4578594157 \times 10^{-8}$
3	$1.0236447124 \times 10^{-4}$	1.00028519580	$1.0471349362 \times 10^{-8}$

Table 3.1

Note that, since pressure as a function of altitude was not known, the derived refractive profile was converted to a temperature profile by means of the relation

$$n = 1 + \frac{\epsilon\beta \mathrm{p}}{T} = 1 + \frac{0.07968}{T}$$

where atmospheric pressure, p, was assumed to have a constant value of 101.3 kp and $\epsilon = 226 \times 10^{-6}$ and $\beta = 3.48 \times 10^{-3}$ are constants. This assumption of constant pressure led to an essentially constant difference between the derived and actual temperature profiles. In the absence of more refined pressure data, this disagreement was minimized by using the relation above to derive *actual* temperature profiles from the known refractive profiles. This procedure will not affect the accuracy of

the model since, a more sophisticated pressure-altitude relation could be substituted to convert the accurate refractive profiles to true *actual* temperature profiles.

The refractive and temperature profiles are presented in Figs. (3.4.2) through (3.4.7). The correspondence is remarkable. The errors are presented in Figs. (3.4.8) through (3.4.10). The maximum error is less than 0.1° C below twenty meters, and for Profile 2, the maximum error is 0.005° C.

We note that the value determined for the integration constant c is very nearly unity, for each profile. If we assume that $c = 1$ in Eq. (3.4.9), then

$$n = \frac{a}{\sqrt{K}} \operatorname{sech}(ay). \tag{3.4.10}$$

The refractive index at elevations of zero and 20m, was taken from each of the profiles and Newton's method used to fit a and K of Eq. (3.4.9) under the assumption that $c = 1$. The numerical results are presented in Table 3.2. The errors are presented in Figs. (3.4.11) through(3.4.13). While the two point fit results in larger temperature errors, the maximum error is still just 0.2° C. Some images generated

from constant Gaussian curvature profiles are presented in the appendix.

Profile	a	K
1	$1.2146893214 \times 10^{-4}$	$1.4746056301 \times 10^{-8}$
2	$1.4245751976 \times 10^{-4}$	$2.0282305240 \times 10^{-8}$
3	$1.1574739001 \times 10^{-4}$	$1.3388336018 \times 10^{-8}$

Table 3.2

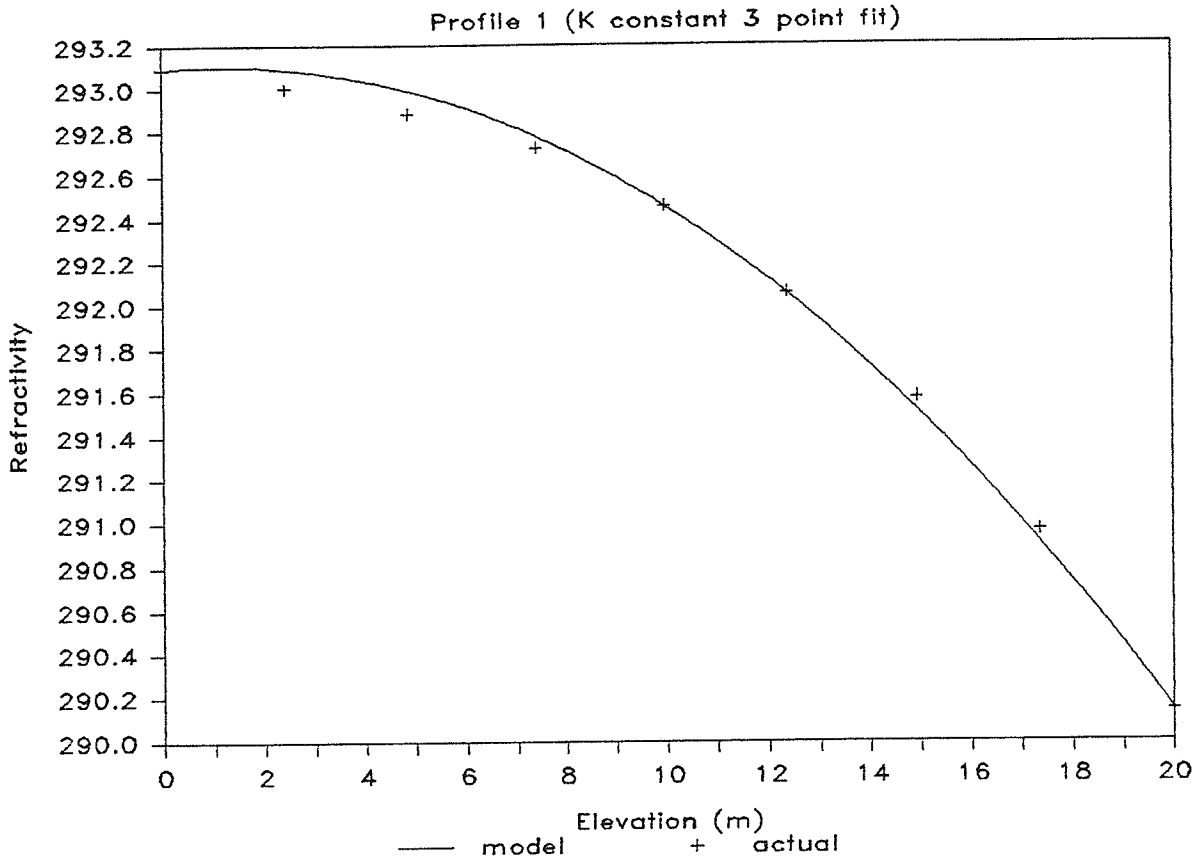

Fig. 3.4.2 Profile 1 refractivity. Constant K, no approximation of c.

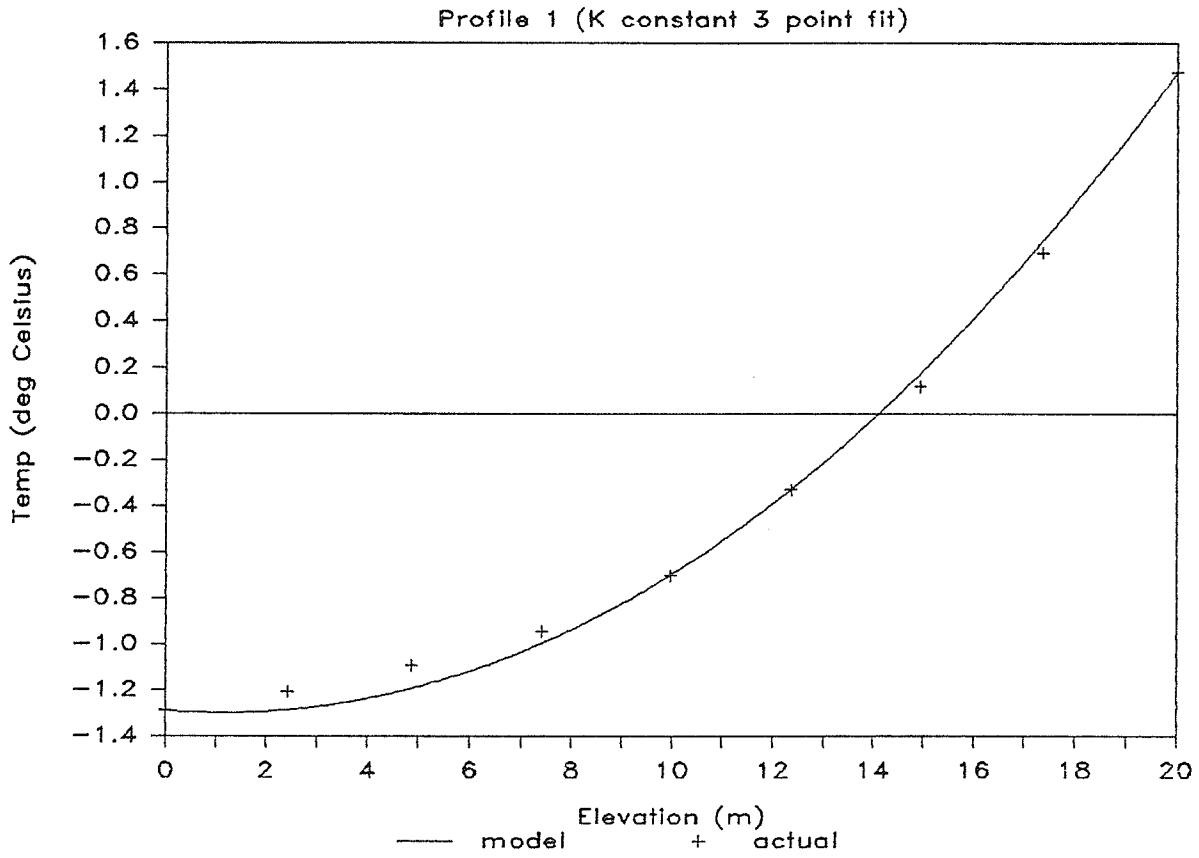

Fig. 3.4.3 Profile 1 temperature. Constant K, no approximation of c.

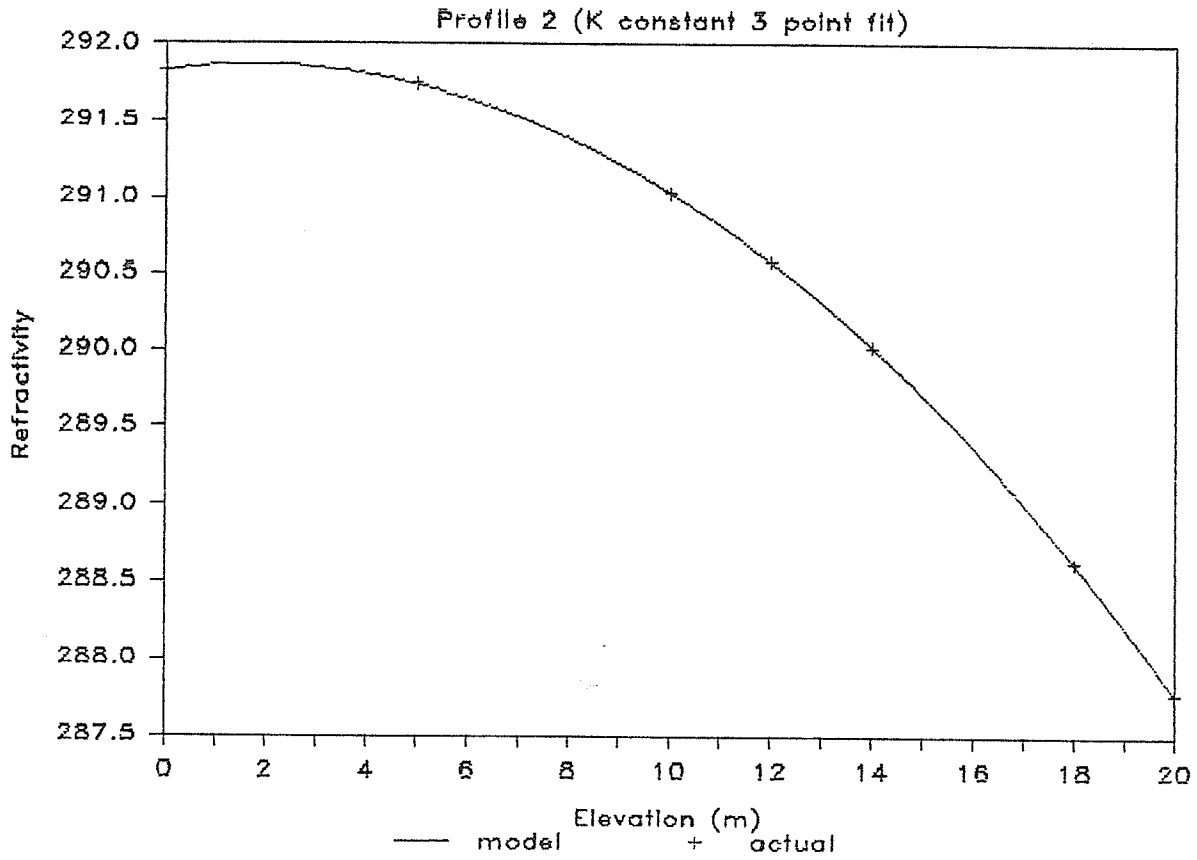

Fig. 3.4.4 Profile 2 refractivity. Constant K, no approximation of c.

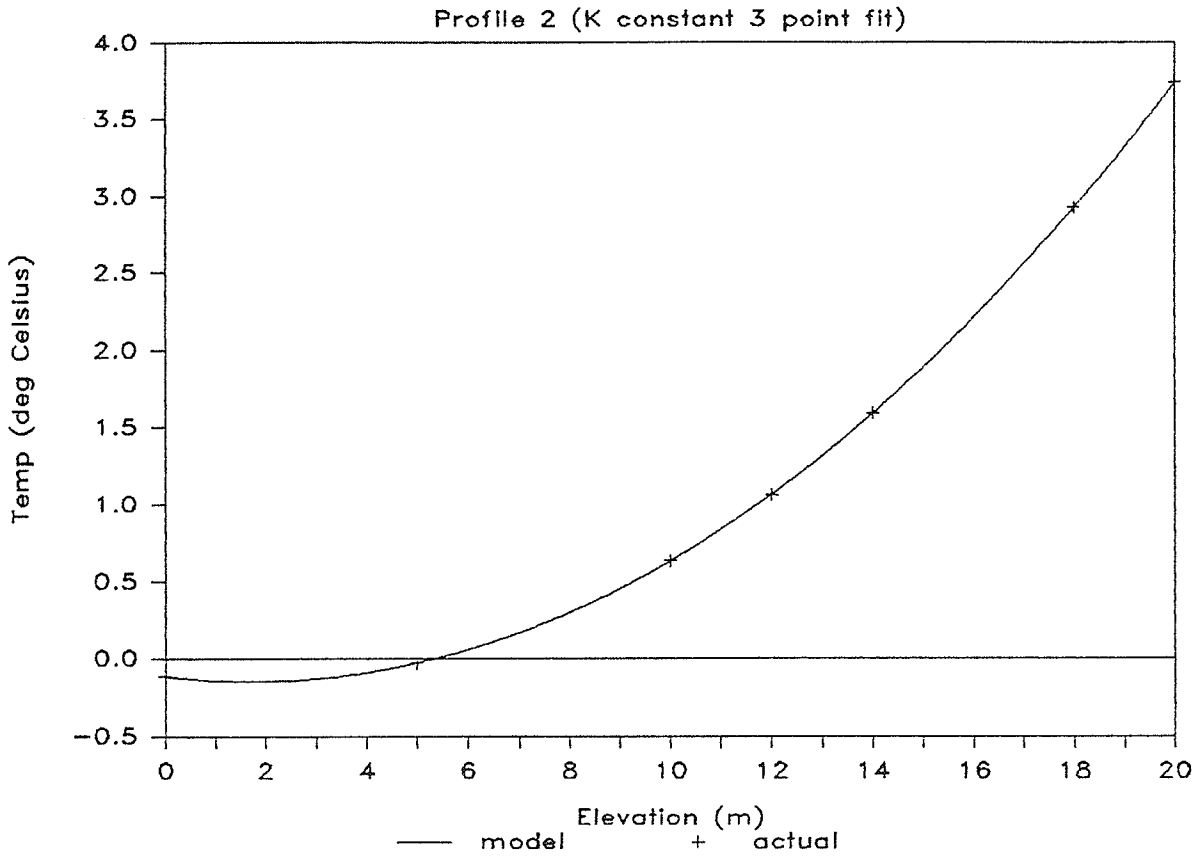

Fig. 3.4.5 Profile 2 temperature. Constant K, no approximation of c.

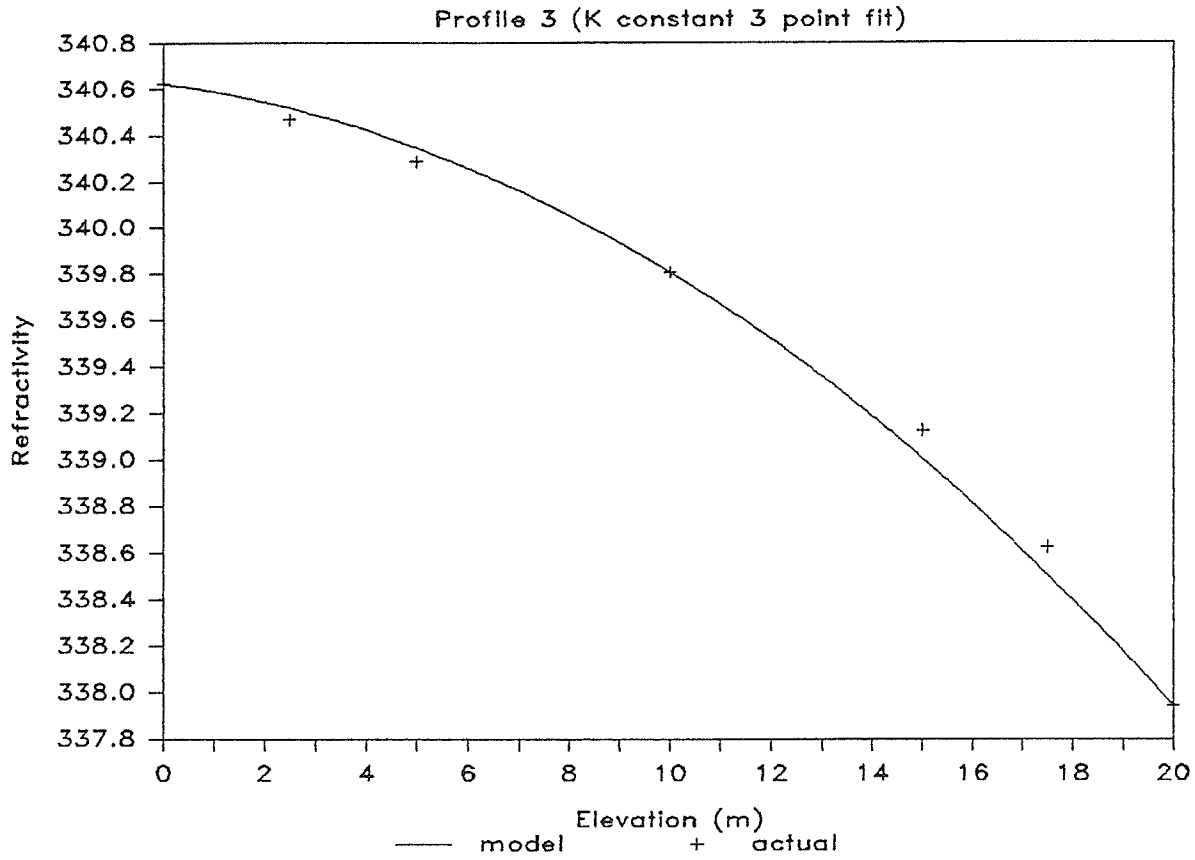

Fig. 3.4.6 Profile 3 refractivity. Constant K, no approximation of c.

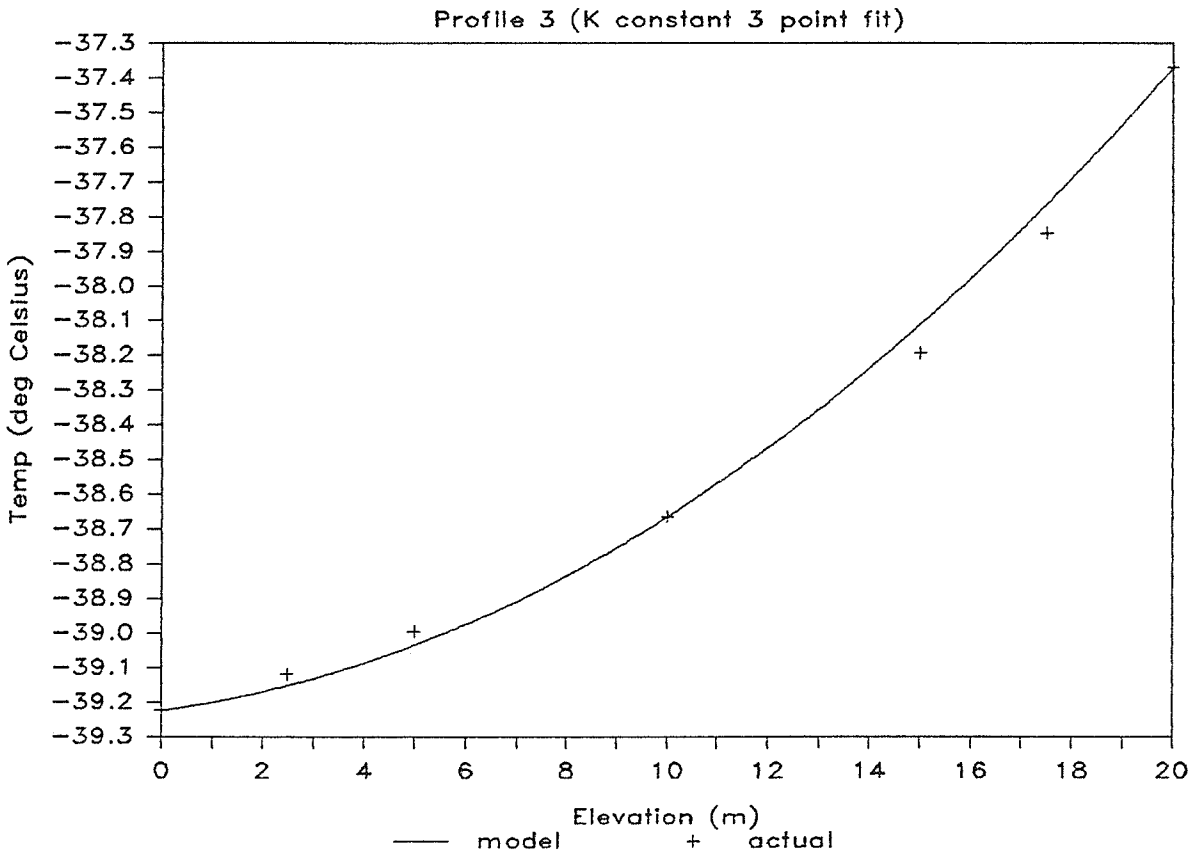

Fig. 3.4.7 Profile 3 temperature. Constant K, no approximation of c.

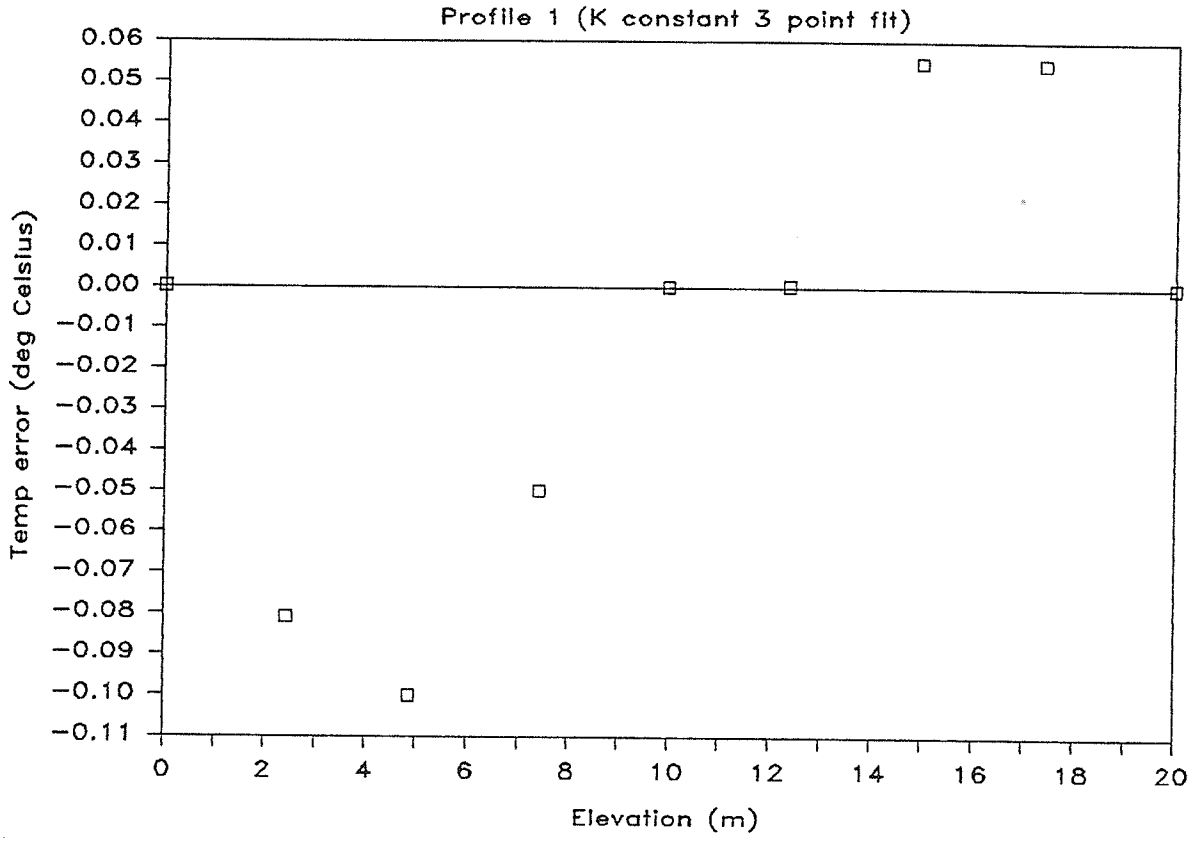

Fig. 3.4.8 Profile 1 temperature error. Constant K, no approximation of c.

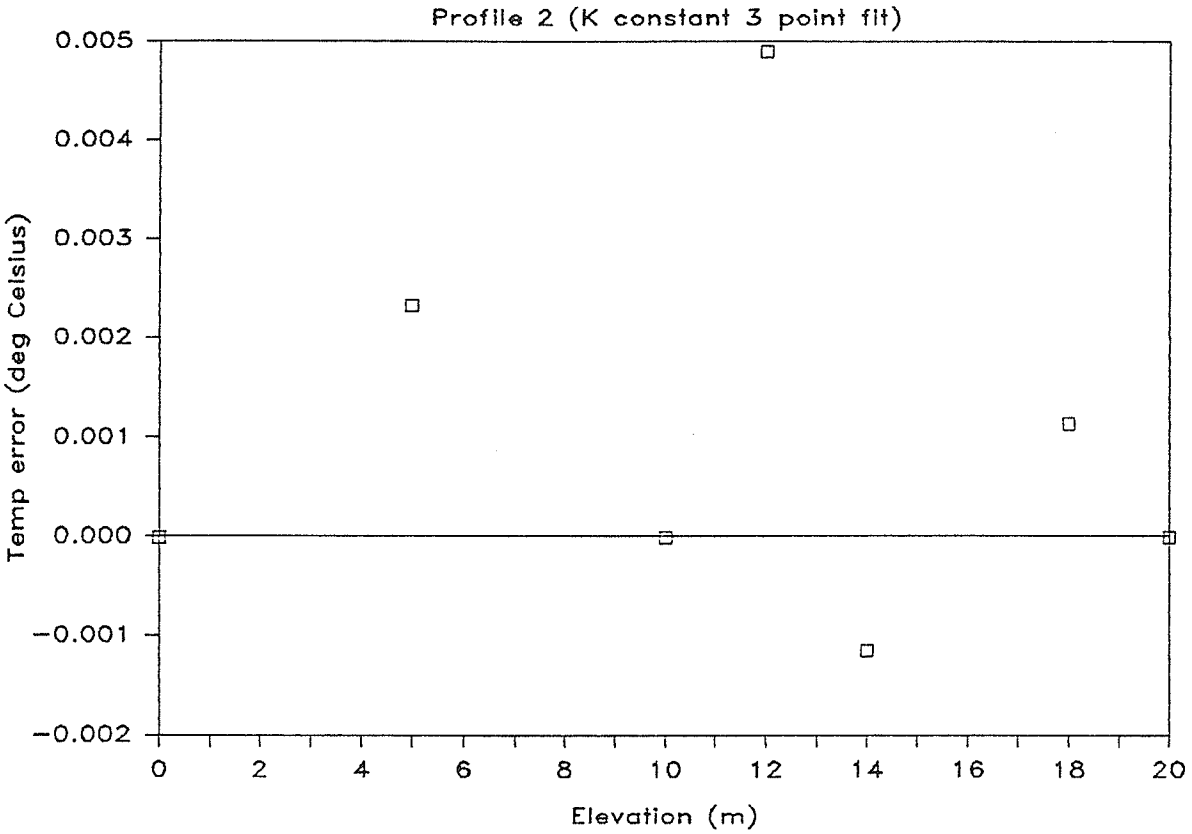

Fig. 3.4.9 Profile 2 temperature error. Constant K, no approximation of c.

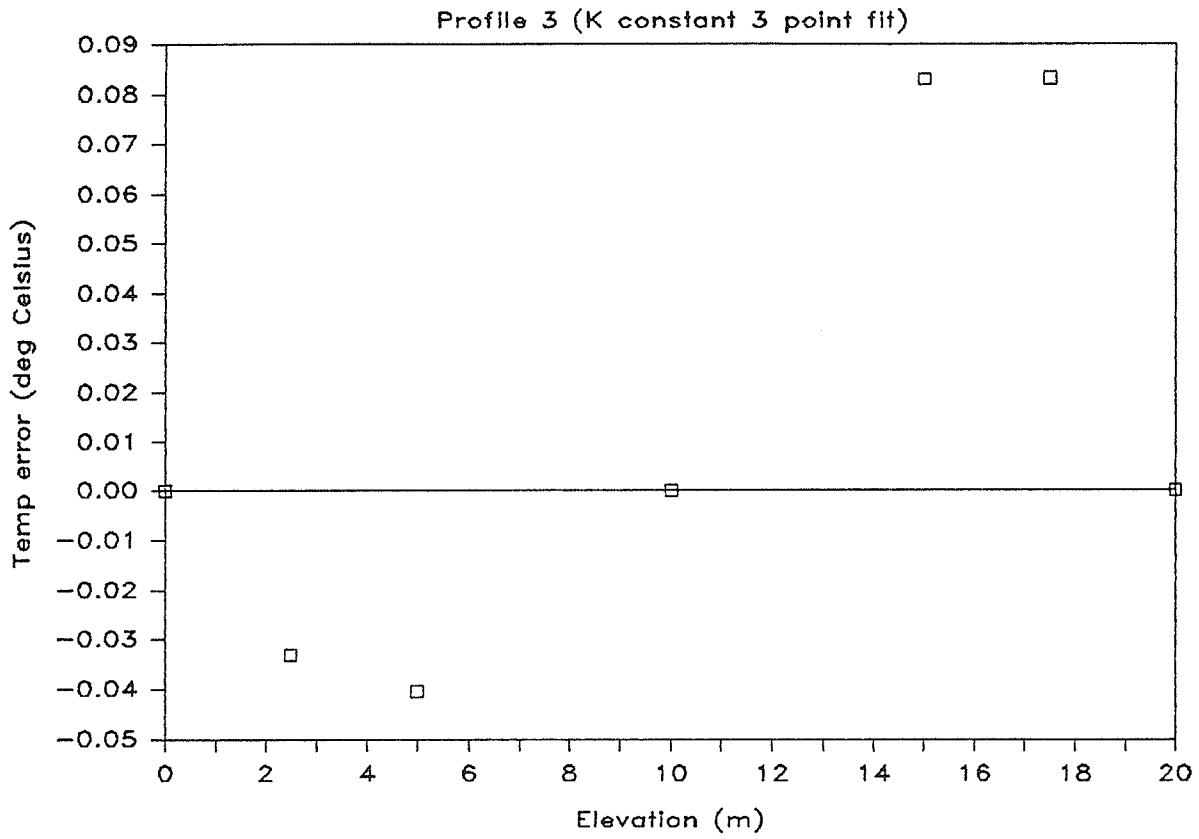

Fig. 3.4.10 Profile 3 temperature error. Constant K, no approximation of c.

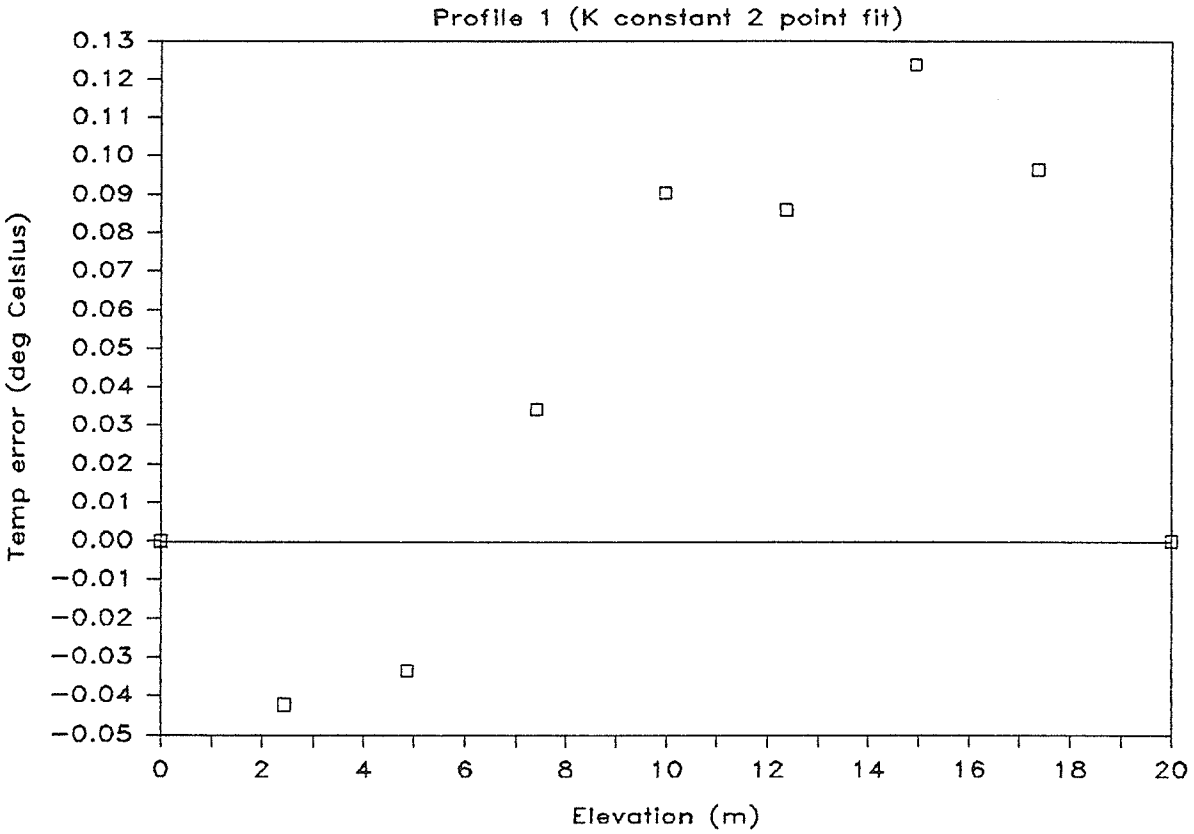

Fig. 3.4.11 Profile 1 temperature error. Constant K, $c = 1$.

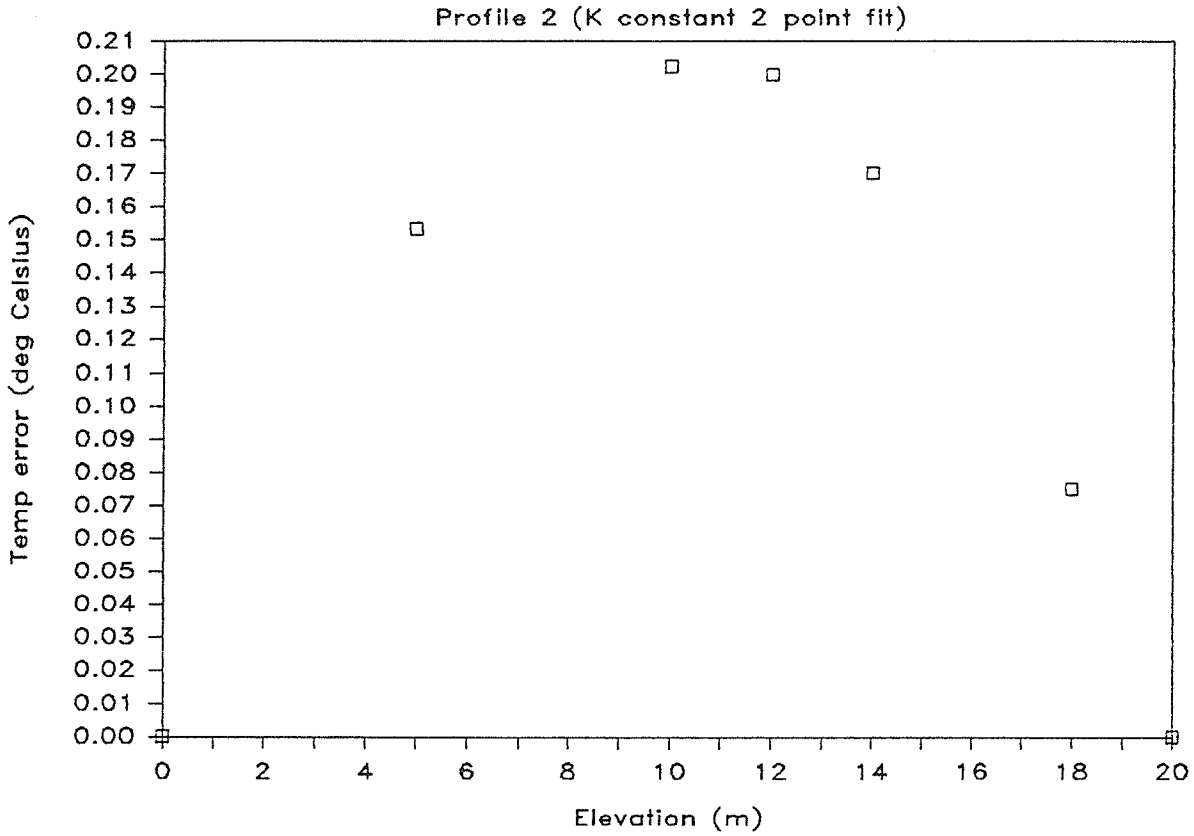

Fig. 3.4.12 Profile 2 temperature error. Constant K, $c = 1$.

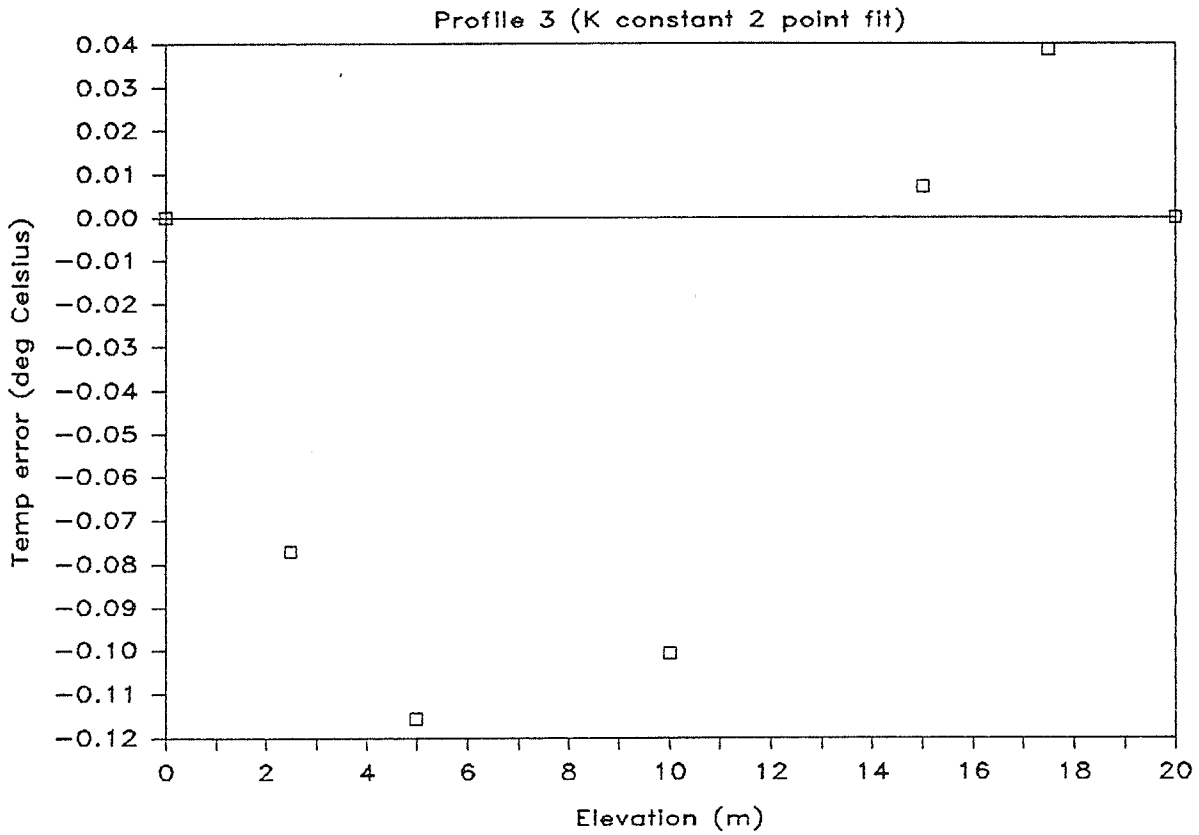

Fig. 3.4.13 Profile 3 temperature error. Constant K, $c = 1$.

3.5 The Radially Symmetric Manifold

In the preceding sections we have examined the consequences of the metric specified by Eq. (3.2.4). This metric was stated in terms of Cartesian coordinates (that is, the earth was assumed to be flat). In order to take into account the curvature of the earth we must express the metric in terms of plane polar coordinates, with origin at the center of the earth.

The polar line element ds is given by

$$ds^2 = dr^2 + r^2 d\theta^2 \tag{3.5.1}$$

so that our metric becomes

$$\begin{aligned} dl^2 = n^2 ds^2 &= n^2(dr^2 + r^2 d\theta^2) \\ &= g_{ij} dx^i dx^j \end{aligned} \tag{3.5.2}$$

where

$$g_{ij} = n^2 \begin{pmatrix} 1 & 0 \\ 0 & r^2 \end{pmatrix}$$

and

$$g^{ij} = \frac{1}{n^2} \begin{pmatrix} 1 & 0 \\ 0 & \frac{1}{r^2} \end{pmatrix}$$

We assume that $n = n(r)$. The Christoffel symbols of the first and second kind are defined in the Appendix. A derivation identical to the one above leads to the

following relation between Gaussian curvature and refractive index:

$$\frac{d^2n}{dr^2} - \frac{1}{n}\left(\frac{dn}{dr}\right)^2 + \frac{1}{r}\frac{dn}{dr} = -n^3K. \tag{3.5.3}$$

This differs from its cartesian analog by the third term on the left.

We let $v = \ln n$. So that

$$v'' + \frac{v'}{r} = -Ke^{2v}. \tag{3.5.4}$$

For $K = 0$, we get

$$n = br^a = bR_e{}^a\left(1 + \frac{y}{R_e}\right)^a,$$

where R_e is the radius of the earth. Two points of known refractive index will allow us to fit the integration constants, a and b. Noting that $\ln(1 + x) \approx x$ for $x \ll 1$, we get, after some manipulation

$$n = n_o\left(\frac{n_e}{n_o}\right)^{y/y_e} \tag{3.5.5}$$

This result produces an essentially linear refractive profile for the range of elevations of interest and is (absent the approximation used), the same as Eq. (3.4.6).

To obtain an approximate solution of Eq. (3.5.4) for the case $K \neq 0$, we note that

$$n^2 = e^{2v} = 1 + 2v + \frac{(2v)^2}{2} + \cdots \approx 1$$

which leads to

$$v'' + \frac{v'}{r} = -K. \tag{3.5.6}$$

Multiplying Eq. (3.5.6) by r^2 and letting $r = e^t$ we obtain

$$\ddot{v} = -Ke^{2t} \tag{3.5.7}$$

where the dots indicate differentiation with respect to t. The general solution to Eq. (3.5.7) is

$$v = at + b - \frac{Ke^{2t}}{4}$$

or, with suitably relabelled constants,

$$n = br^a e^{-Kr^2/4}. \tag{3.5.8}$$

Inserting this result into the lefthand side of Eq. (3.5.3) we obtain

$$\frac{d^2n}{dr^2} - \frac{1}{n}\left(\frac{dn}{dr}\right)^2 + \frac{1}{r}\frac{dn}{dr} = -nK, \tag{3.5.9}$$

which is wrong by a factor of n^2 on the righthand side. The absence of this quadratic variation of n is sufficient to prevent a reasonable fit of the constants in Eq. (3.5.8).

Newton's method was applied to the refractive index at three elevations. This attempt to fit resulted in ill conditioned matrices and so failed. A singular value decomposition with back substitution (Press[7]) resulted in a Gaussian curvature

of approximately 1×10^{-28}, hence the exponential term was essentially unity and the fit was the same as the $K = 0$ case examined earlier. Since variation of n with elevation is very small and Gaussian curvature smaller still, it seems inappropriate to attempt further approximate solutions to Eq. (3.5.3).

By imposing radial symmetry on the manifold, we have in effect determined a scale for the problem. In the Cartesian case, the location of the origin can be arbitrarily specified so this scaling does not occur. However, the layer of atmosphere that we are attempting to model geometrically has a depth on the order of 20 m and it sits at the top of 6000 km of *constantly* curving manifold. We cannot expect to model an atmosphere over such a large distance in such a way that the last 20 m will accurately reflect the refractive profile. In the absence of an exact solution, the problem of geometrizing the temperature structure of the radially symmetric atmosphere must remain open.

3.6 Accounting for Curvature

While the results of the preceding section are disappointing, it is possible to use the flat earth model with a term that corrects for the curvature of the earth and temperature strata.

The surface of the earth curves away from the tangent plane at the location of the observer so that the temperature strata, which are concentric with the center of the earth, lose altitude (with respect to a cartesian coordinate system) as range increases. This serves to increase the elevation of a ray with respect to the *local* profile. The loss of altitude is, to a high degree of accuracy, given by

$$\Delta y = \frac{x^2}{2R_e}, \tag{3.6.1}$$

where x is the horizontal target range and R_e, the radius of the earth. The error incurred by using the horizontal range rather than the arc range is negligible.

Any ray with cartesian elevation y at a distance x from the observer, has an *actual* height above ground of $y + \Delta y$, so that we can write the modified versions of Eqs. (3.4.9) and (3.4.10)

$$n = \frac{2ac}{\sqrt{K}} \frac{e^{-a(y+x^2/2R_e)}}{e^{-2a(y+x^2/2R_e)} + c^2} \tag{3.6.2}$$

and

$$n = \frac{a}{\sqrt{K}} \operatorname{sech}(a(y + x^2/2R_e)). \tag{3.6.3}$$

The presence of this correction term does not imply that the local profile varies from location to location; it is, rather, a device for transporting the profiles given

by Eqs. (3.4.9) and (3.4.10) around the curve of the earth as light rays propagate in a cartesian frame.

CHAPTER 4: A CYLINDRICAL MODEL

4.1 A Mechanical Analogue

The relation that allows us to trace the path of a ray of light in an optical system or in a medium of varying refractive index is Snell's law, namely

$$n_1 \sin\theta_1 = n_2 \sin\theta_2, \tag{4.1.1}$$

where, n_i is the refractive index in medium i and θ_i is the angle between the ray in medium i and the normal to the interface between the two media, at the point of incidence.

If a particle moves in a conservative potential field then there is a relation, formally identical to Snell's law, describing the path of the particle in terms of its kinetic energy and directions of its path at a discontinuity of the potential function.

Suppose we have a particle with unit mass and total energy E, passing from a region with a conservative potential V_1 to a region of conservative potential V_2. In region 1 we have

$$\mathrm{T}_1 = E - V_1 = \frac{1}{2}{v_1}^2 \tag{4.1.2}$$

and in region 2

$$\mathrm{T}_2 = E - V_2 = \frac{1}{2}{v_2}^2. \tag{4.1.3}$$

The change in kinetic energy

$$\Delta \mathrm{T} = \mathrm{T}_1 - \mathrm{T}_2 = V_2 - V_1 = \frac{1}{2}({v_1}^2 - {v_2}^2) \tag{4.1.4}$$

is the consequence of an impulsive force F normal to the line (or surface) of discontinuity, ie. the component of velocity normal to the line changes but the component tangent to the line remains constant. If v_i is the speed of the particle in region i, then, across the discontinuity

$$v_1 \sin\theta_1 = v_2 \sin\theta_2. \tag{4.1.5}$$

By conservation of energy

$$\frac{1}{2}m{v_1}^2 = E - V_1 \quad \text{and} \quad \frac{1}{2}m{v_2}^2 = E - V_2 \tag{4.1.6}$$

so that we have

$$\sqrt{E - V_1}\sin\theta_1 = \sqrt{E - V_2}\sin\theta_2. \tag{4.1.7}$$

The function $\sqrt{E-V}$ differs from the speed of the particle by a multiplicative constant. Clearly, if refractive index and speed possess the same functional dependence on position, then a ray and a particle with the same initial position and direction will follow the same path.

4.2 Cylindrical Kinematics

Consider a particle i with unit mass and total energy E, sliding without friction on the interior of a right circular cylinder of radius R. The cylinder is oriented so that its axis lies in a plane parallel to the x-y plane and along the x-axis. Gravity acts along the $-z$-axis.

For small excursions about the bottom of the cylindrical trough, the particle will exhibit simple harmonic motion, with the position of the particle (projected onto the x-y plane) given parametrically by

$$\begin{aligned} x_i &= v_{ix}t \\ y_i &= A_i \sin(\omega t + \delta_i) \end{aligned} \tag{4.2.1}$$

where $\omega = \sqrt{g/R}$ and t = time. The potential in which the particle moves is given by

$$\mathrm{V} = gR\left(1 - \sqrt{1 - \frac{{y_i}^2}{R^2}}\right), \tag{4.2.2}$$

so that its kinetic energy T is

$$\mathrm{T} = E - V = E - gR\left(1 - \sqrt{1 - \frac{{y_i}^2}{R^2}}\right). \tag{4.2.3}$$

We will assume that at $t = 0$ the displacement of the particle is y_{ie} and that the particle has unit speed. Then, since

$$\mathrm{T} = E - gR\left(1 - \sqrt{1 - \frac{{y_{ie}}^2}{R^2}}\right) = \frac{1}{2}, \tag{4.2.4}$$

we have

$$\mathrm{T} = \frac{1}{2} + g\left(\sqrt{R^2 - {y_i}^2} - \sqrt{R^2 - {y_{ie}}^2}\right). \tag{4.2.5}$$

At time $t = 0$ the tangent to the path of the particle makes an angle ϕ_{i0} with the x-axis. We will refer to this angle as the departure angle of the particle. The assumption of unit speed means that ${v_{ix}}^2 + {v_{iy}}^2 = 1$. This implies

$$\begin{aligned} v_{ix} &= \cos\phi_{i0} \\ v_{iy} &= \sin\phi_{i0}. \end{aligned} \tag{4.2.6}$$

Now, suppose that we know the departure angle and the initial and final displacement of the particle from some reference level which we will take to be ground level. Can we determine the frequency ω (and hence R) and the elevation, y_d, of ground level with respect to our coordinate system with axis along the axis of the cylinder?

We rewrite Eq. (4.2.1) as

$$y_d + y_i = A_i \sin(\omega t + \delta_i) \tag{4.2.7}$$

where y_i is now the displacement from the reference level. Differentiating Eq. (4.2.7) we obtain

$$\frac{dy_i}{dt} = \omega A_i \cos(\omega t + \delta_i). \tag{4.2.8}$$

At time $t = 0$, Eqs. (4.2.7) and (4.2.8) give us

$$\begin{aligned} y_d + y_{i0} &= A_i \sin(\delta_i) \\ \left.\frac{dy_i}{dt}\right|_{t=0} &= \sin\phi_{i0} = \omega A_i \cos(\delta_i) \end{aligned} \tag{4.2.9}$$

where we have used the second of Eqs. (4.2.6). Some manipulation yields

$$A_i = \pm\sqrt{(y_d + y_{i0})^2 + \left(\frac{\sin\phi_{i0}}{\omega}\right)^2} \tag{4.2.10}$$

and

$$\delta_i = \cos^{-1}\left(\frac{\sin\phi_{i0}}{\omega A_i}\right). \tag{4.2.11}$$

Noting Eqs. (4.2.1) and (4.2.6) we can now rewrite Eq. (4.2.7)

$$y_{if} = A_i \sin\left(\frac{\omega L}{\cos\phi_{i0}} + \delta_i\right) - y_d. \tag{4.2.12}$$

where y_{if} is the displacement of the path of the particle from the reference level at a distance L from the origin. As a consequence of Eqs. (4.2.10) and (4.2.11) there are only two unknowns in this equation, ω and y_d. The initial and final positions and departure angles of two particles that follow different paths will, in theory, suffice to determine these two quantities.

4.3 Interpreting the Radius of the Optical Cylinder

When we have determined the spatial frequency and reference level for the cylindrical model, we are left with the problem of fitting known conditions to the optical cylinder in order to deduce a temperature profile. Spatial frequency ω gives us the radius of the cylinder and the displacement of the reference level gives us the distance from the surface of the ground to the bottom of the cylinder. We have still, however, to determine the relationship between cylinder radius and refractive index.

From the previous discussion, we know that the refractive profile that governs the path of the light ray will have the same functional dependence on position as the *speed* profile that governs the path of the particle. This is given by

$$v_i = \sqrt{2\mathrm{T}} = \left(1 + 2g\sqrt{R^2 - {y_i}^2} - 2g\sqrt{R^2 - {y_{ie}}^2}\right)^{1/2}. \qquad (4.3.1)$$

Clearly, the unity term on the right is the square of the initial speed of the particle, (set $y_i = y_{ie}$). This follows from the assumption of unit speed and unit mass. We will explicitly assume that gravity is numerically equal to one. Thus we can write the positional dependence of refractive index as

$$n = \left({n_e}^2 + 2\sqrt{\mathrm{R}^2 - y^2} - 2\sqrt{\mathrm{R}^2 - {y_e}^2}\right)^{1/2}. \qquad (4.3.2)$$

The first term on the right, $n_e{}^2$, is the square of the refractive index at the eye, and serves to adjust the origin, up or down, to fit the optical data to the cylinder. Had we chosen the particle to have initial speed equal to refractive index at the eye, then we could have used Eq. (4.3.1) directly. Implicit in Eq. (4.3.2) is a unit constant with dimensions of acceleration.

4.4 Fitting the Cylinder

Equations (4.2.10), (4.2.11) and (4.2.12) are the equations to fit to the optical data in the cylindrical model. The equations are non-linear and Eq. (4.2.12) is periodic. This fact will be important later on. The data fitted consisted of three temperature profiles — Profile 1, 2 and 3.

Initially, two rays with departure angles of 0 and 1 minute of arc were chosen from Profile 1. The target elevations at a range of 25 km were 19.64m and 19.32m respectively. The departure angles and ray elevation at target gives us a system of two non-linear equations. Recall, that we wish to extract the values of ω and y_d from these equations. A straightforward iterative technique was used. The resulting fitting residuals became small for $\omega \approx 60$ radians/m and $y_d \approx -17$ meters. This is an enormous spatial frequency. Next a least squares procedure was used to determine

the fitting parameters. Again, values for ω and y_d were about 60 radians/meter and -17 meters, respectively.

Equation (4.2.12) was used to generate values for ray plots using the fitting parameters. It was clear that the frequency was grossly in error.

When however, elevation at target was plotted against departure angle the reason for the problem was obvious. At a spatial frequency of 57.9 radians/meter, the fit was excellent. This was the result of the periodic property of Eq. (4.2.12). The fitting programs generated the optimum fit by increasing the frequency until an optimum sum of squared errors was reached.

At this point the use of numerical techniques to fit the optical data to the cylinder was abandoned. Instead, Eq. (4.3.2) was solved for R and fitted directly to the refractive profile. Since

$$R^2 = {y_e}^2 + \left(\frac{{y_e}^2 - y^2 - N^2}{2N}\right)^2 \tag{4.4.1}$$

where $N = (n^2 - {n_e}^2)/2$, two points of known refractive index serve to determine R. For Profile 1 elevations of 2.44m and 20m, with refractive indexes of 1.0002930027 and 1.0002901404 respectively, were chosen for fitting. For Profile 2 elevations of 5m and 20m, with refractive indexes of 1.0002915588 and 1.0002872835 respectively, were chosen. For Profile 3 elevations of 5m and 20m, with refractive indexes of

1.0003402862 and 1.0003379416 respectively, were chosen. The calculations were performed with 15 digits of precision. The displacement y_d was found by noting that a ray that departs the eye horizontally at an elevation of y_e meters and intersects the target (approximately horizontally) at a range of l meters and an elevation of y_l meters, gives us an approximate displacement

$$y_d = y_e + \frac{(y_l - y_e)}{2}. \tag{4.4.2}$$

Recall that the observable quantities: y_e and y_l are given with respect to ground level and that y_d is the distance from the axis of the cylinder to ground level. Since the axis of the cylinder must lie midway between the peaks of the sine wave, and we have assumed that these peaks occur at eye and target, the elevation of ground level, y_d given by Eq. (4.4.2) follows. The displacement was then adjusted, while holding R fixed, to reproduce the correct target elevation of the ray.

Refractive and temperature profiles were generated, and rays with departure angles of zero were traced based on the generated profile and cylindrical model. The profiles and ray paths were compared with the original profiles and rays. The fitted values of R and y_d are presented in Table 4.1, the profiles in Figs. (4.4.1), (4.4.2) and (4.4.3), the associated refractive errors in Figs. (4.4.4), (4.4.5) and (4.4.6) and the ray traces in Figs (4.4.7), (4.4.8) and (4.4.9).

Profile	R	ω	y_d
1	6.881337796×10^7	$1.205489859 \times 10^{-4}$	-10.96835
2	4.384404620×10^7	$1.510235542 \times 10^{-4}$	-8.265950
3	7.994647856×10^7	$1.118408169 \times 10^{-4}$	-12.52100

Table 4.1

Examining the graphs of the fitted profiles it is evident that all three match well, for elevations below approximately 20 meters, the error being on the order of a few percent. (Per cent error is defined as absolute error as a fraction of the total range of temperature or refractive index, where range extends from ground level to approximately 30m.) However, the ray plots indicate that only for Profile 1 do the parameters of the model provide a good fit to the ray path.

Note, that when temperature profiles were constructed, the atmospheric pressure at the elevation of the observer's eye was adjusted until model temperature was equal to actual temperature. All cylinder radii were determined by solving Eq. (4.3.2) at lower elevations of 2.44, 5 and 5 meters for profiles 1, 2 and 3, respectively, and at 20 meters. The refractive profiles show that the refractive error at these points vanishes. However, the temperature profiles all exhibit some error at 20m. Presumably this error is due to the nonconstancy of atmospheric pressure.

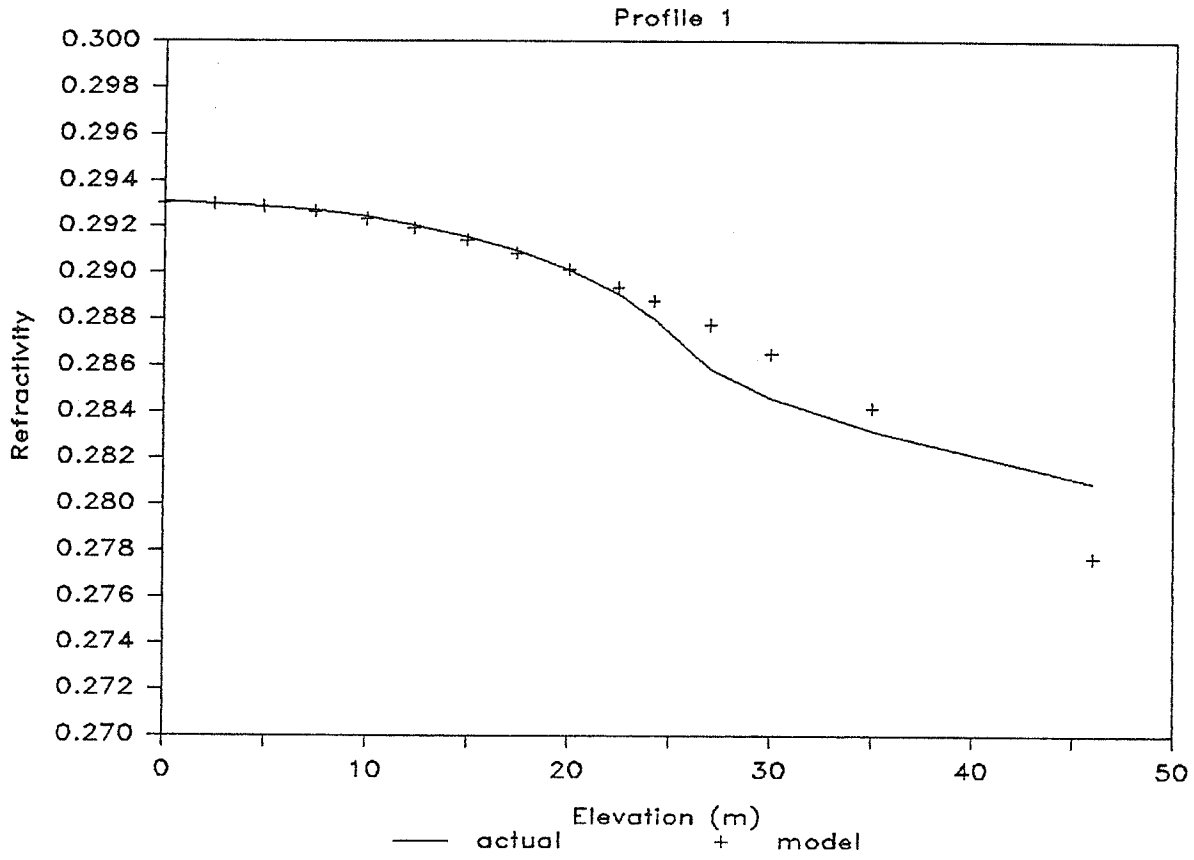

Fig. 4.4.1 Profile 1 refractivity. Cylindrical model.

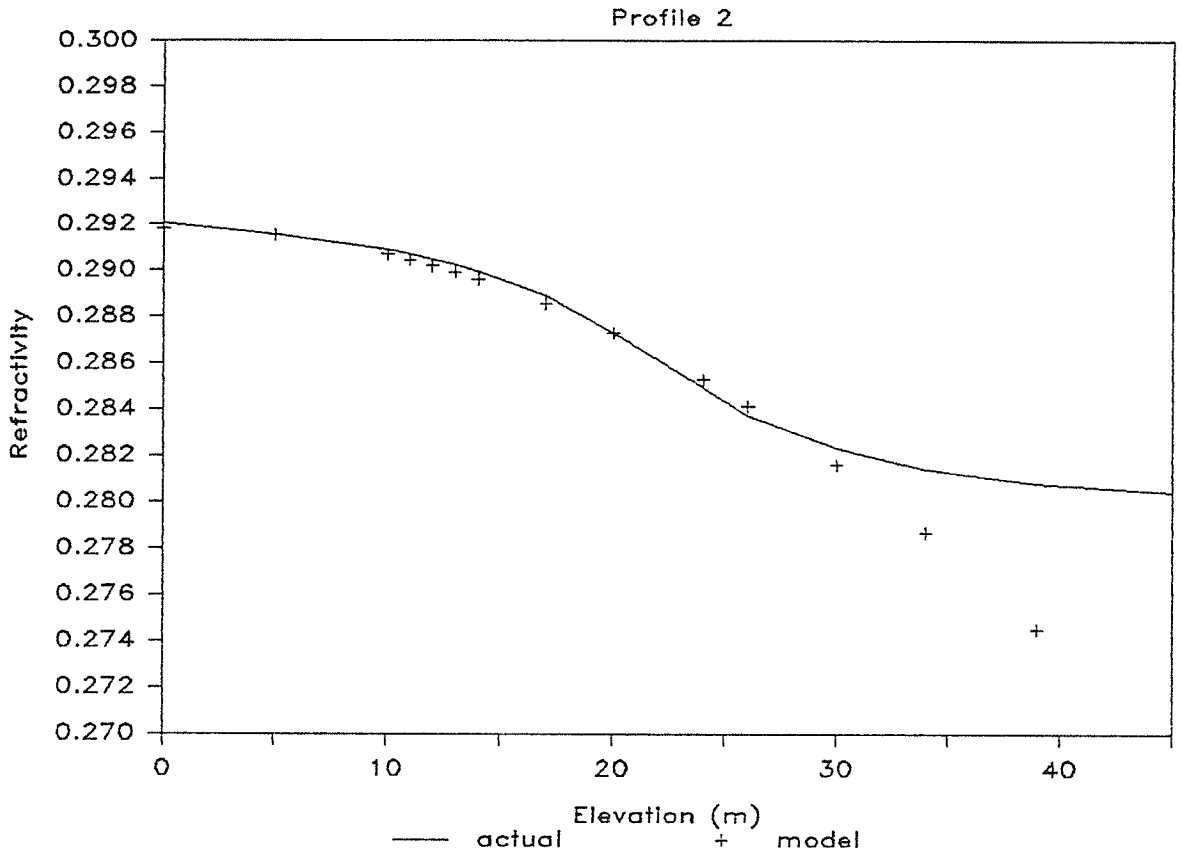

Fig. 4.4.2 Profile 2 refractivity. Cylindrical model.

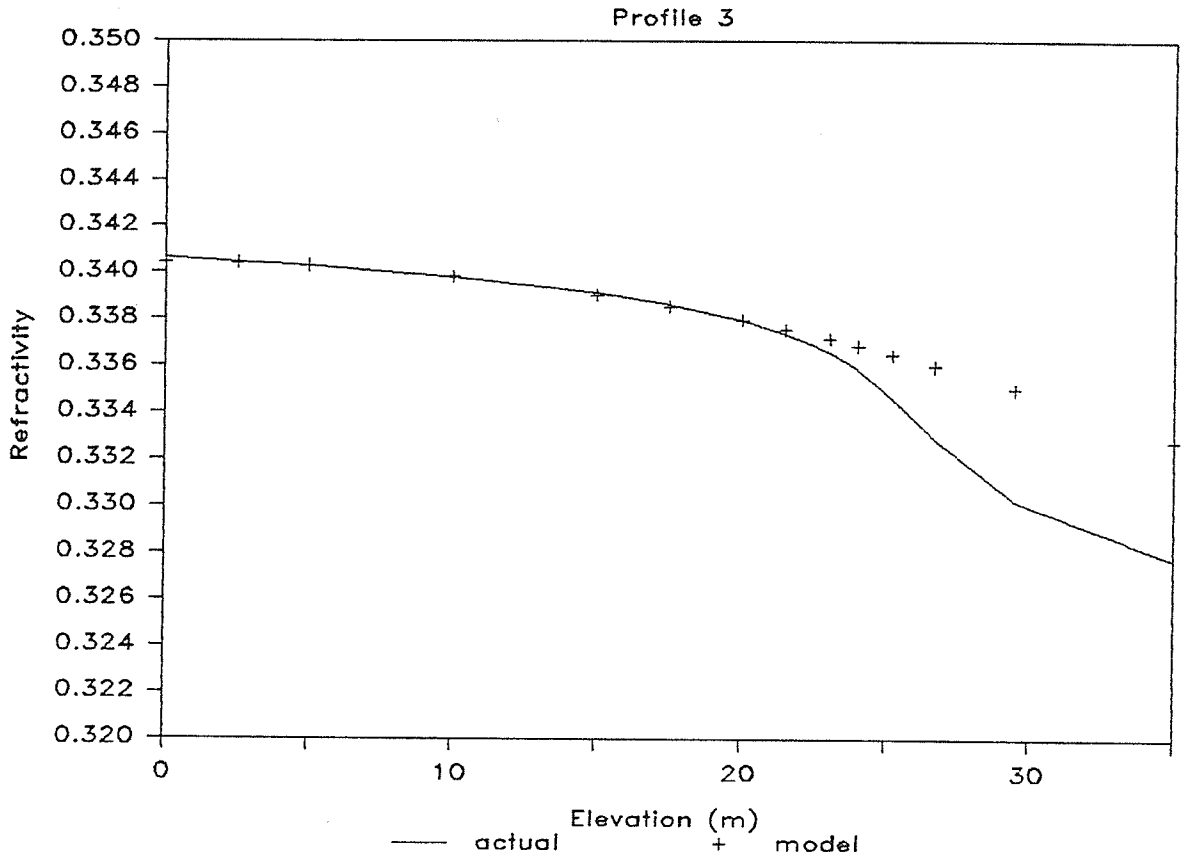

Fig. 4.4.3 Profile 3 refractivity. Cylindrical model.

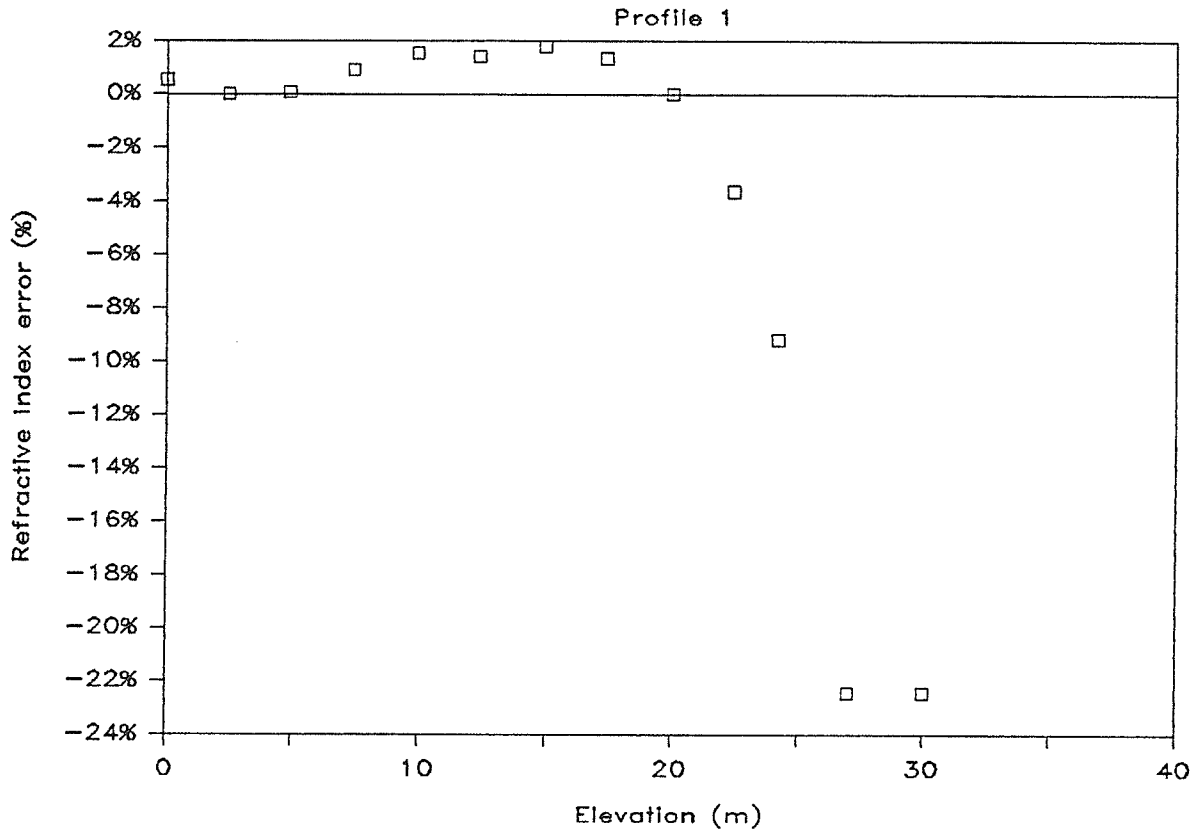

Fig. 4.4.4 Profile 1 refractivity errors. Cylindrical model.

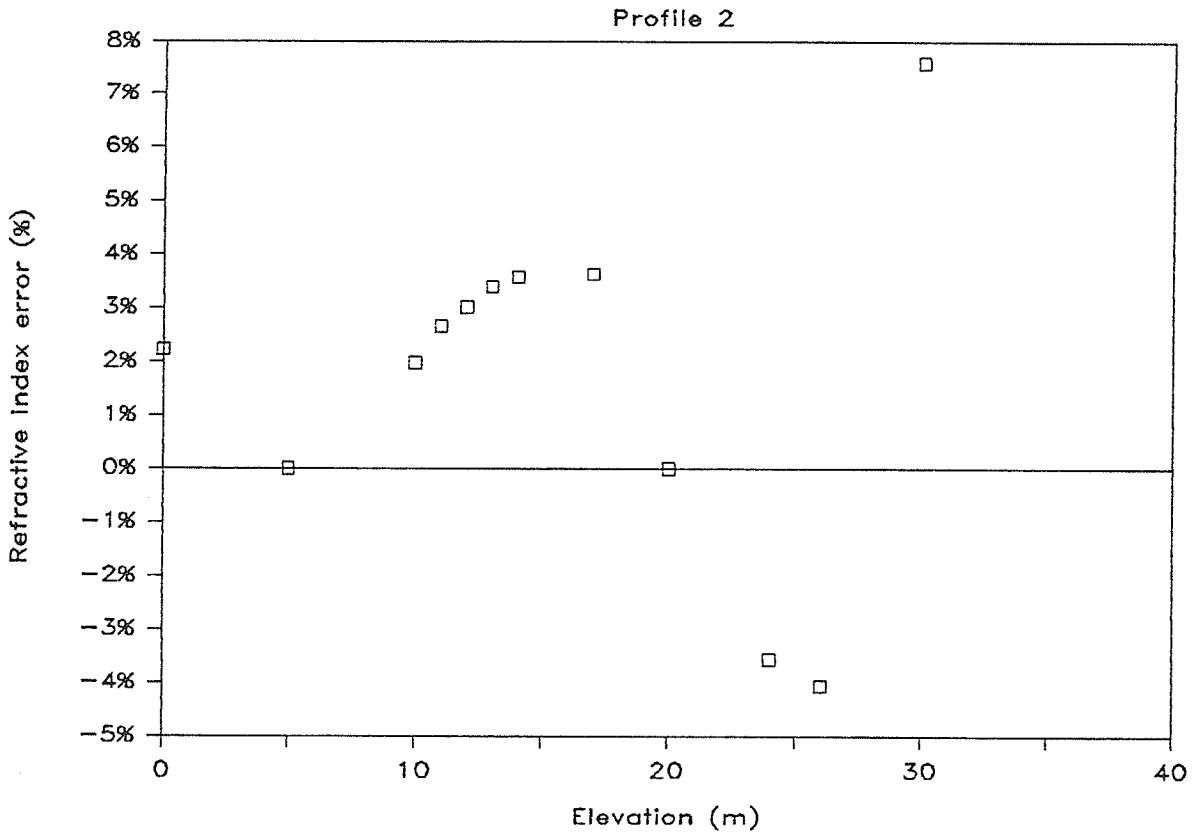

Fig. 4.4.5 Profile 2 refractivity errors. Cylindrical model.

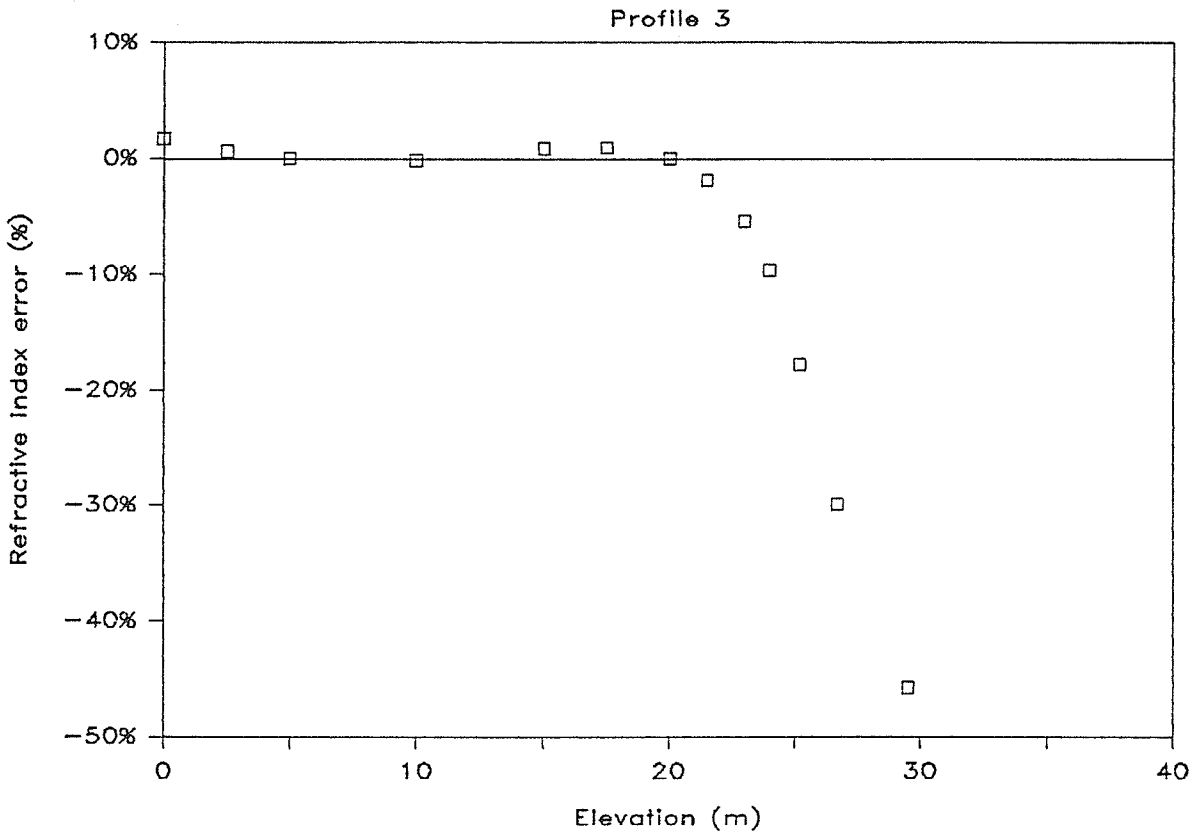

Fig. 4.4.6 Profile 3 refractivity errors. Cylindrical model.

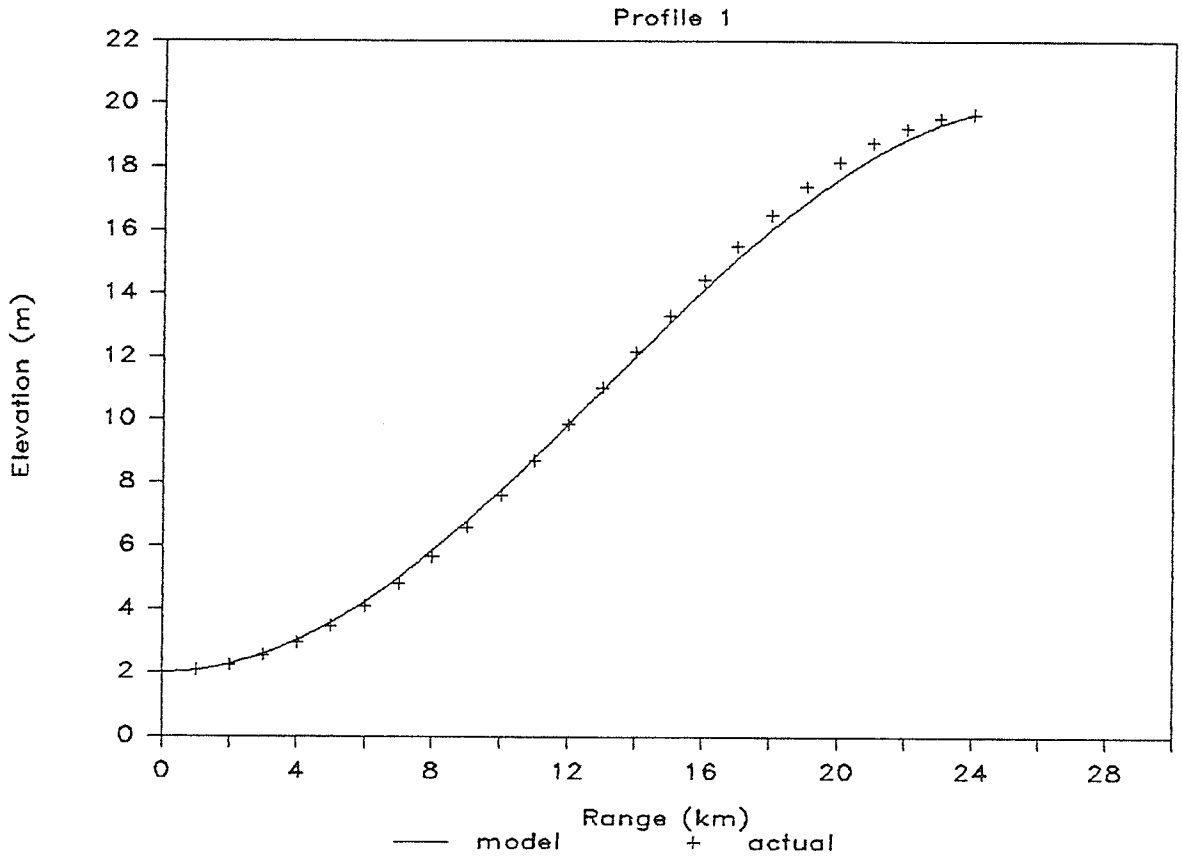

Fig. 4.4.7 Profile 1 ray traces. Cylindrical model.

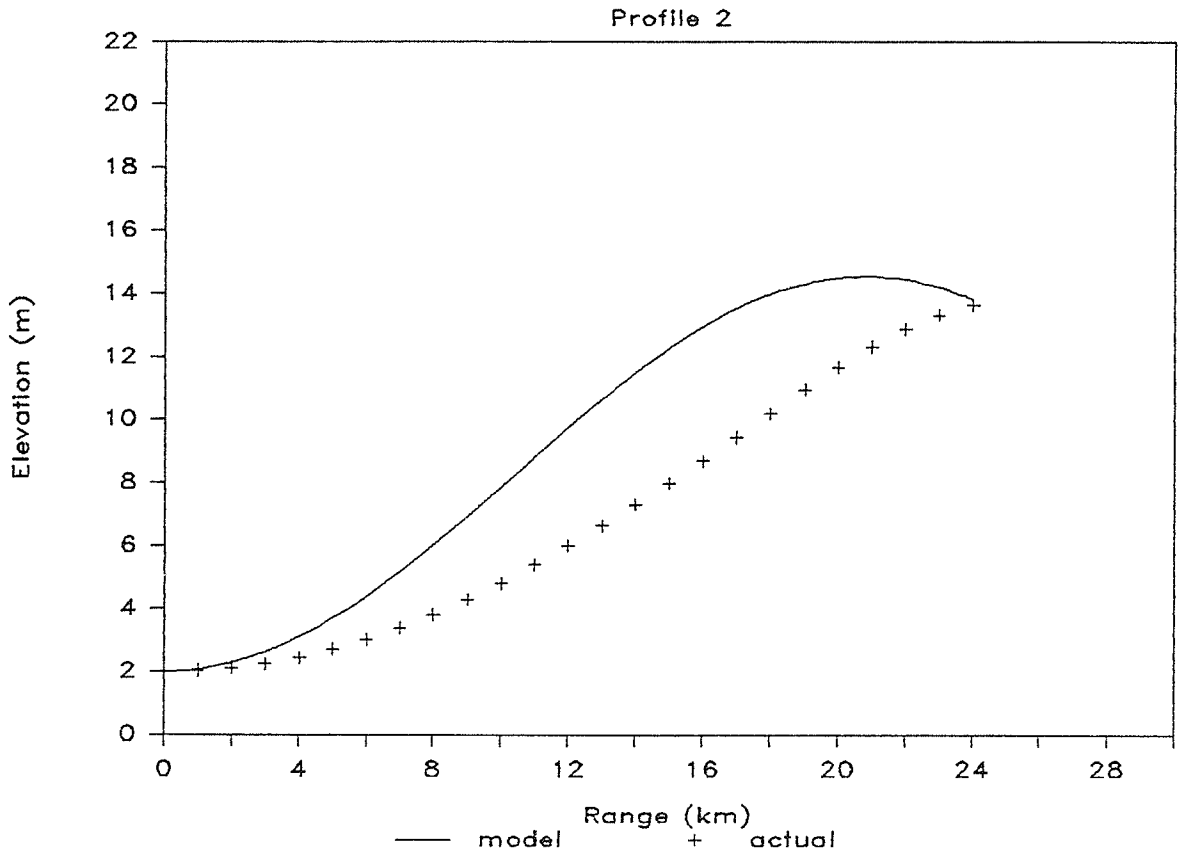

Fig. 4.4.8 Profile 2 ray traces. Cylindrical model.

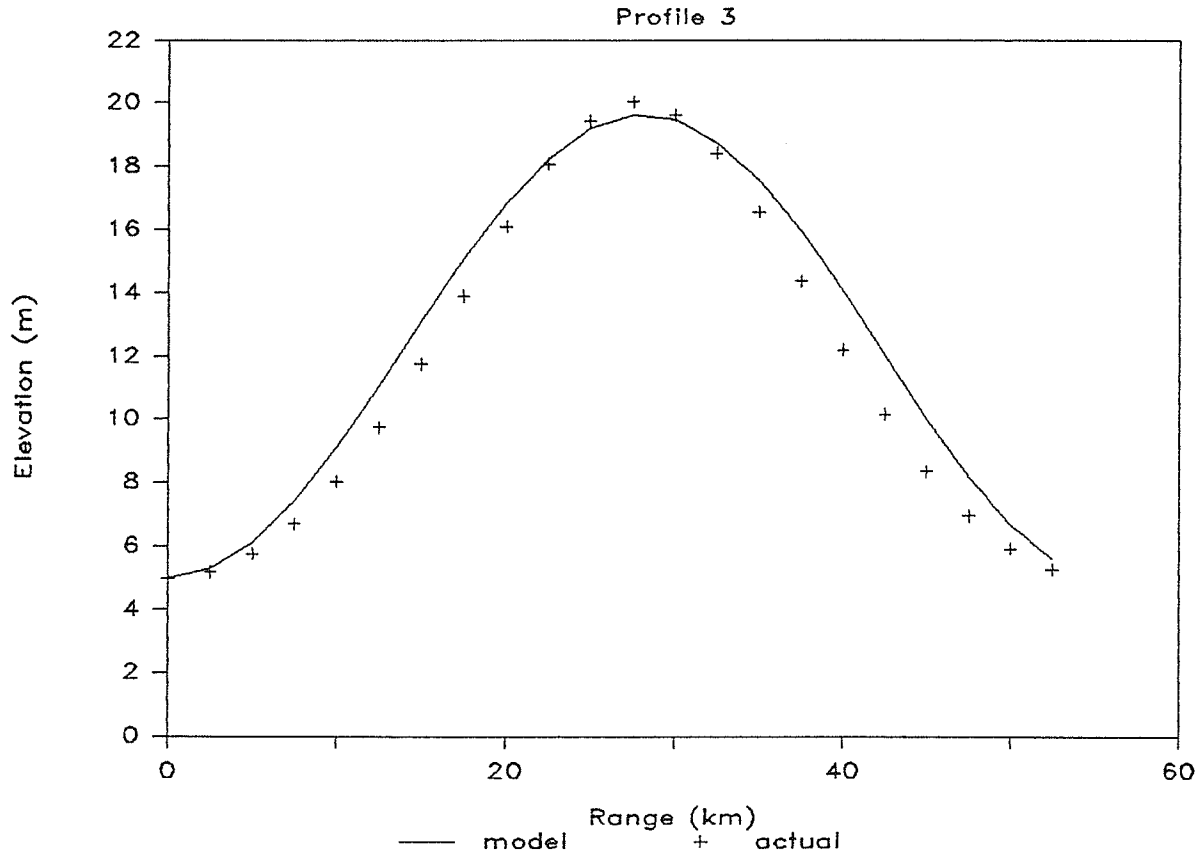

Fig. 4.4.9 Profile 3 ray traces. Cylindrical model.

It is clear that for small elevations, the model gives a more or less good fit. Above about 20 meters however, the curvature changes significantly and the fit becomes poor. This is not surprising. A quadratic approximation will employ, implicitly or otherwise, a second term of the Taylor expansion of the mapping that describes the surface. This approximation is useful for telling us what the surface is like close to a point but the accuracy of description will obviously decrease as we recede from the point, (unless, of course, the expansion of the mapping possesses nonvanishing terms only up to second order).

4.5 The Mechanics of Mirages

The previous section described a mechanical system analogous to the structure of the atmosphere that produces a superior mirage, that is, a temperature inversion. We considered there, a cylindrical trough opening upward. Clearly for a particle moving in this trough, the kinetic energy decreases as the particle rises up the wall of the trough, that is, as its altitude y increases. In § 4.1, we demonstrated the analogy between refractive index and kinetic energy. In this case the refractive index decreases with altitude, or equivalently, the temperature increases. If the cylinder were to open downward, then, kinetic energy would increase with increasing y and

hence temperature would decrease. Under these circumstances one could observe an inferior mirage.

The model is straightforward and allows an intuitive understanding of mirage phenomena, but finding a temperature profile with this model is a not a straightforward procedure. Right circular cylinders and small amplitudes make the problem solvable in an interactive manner, but there is at present no algorithmic way to relate optical data to the cylindrical model. Furthermore, any additional complications that would serve to extend the applicability of the model to higher elevations or more complicated atmospheric structures, would also increase the difficulty of the fitting procedure. Hence, although the model is intuitively attractive, it is computationally cumbersome (at best) and not easily extended.

We note here that this model produces effects similar to the geometrical model of the previous chapter, that is ray bundles that share a common spatial frequency. This follows immediately from the similar, trough-like, shapes of the profiles generated by each model.

This model falls into the same class of solutions as does Fraser's, that is, some sort of refractive profile is assumed and the optical data is fitted to it. While it is clearly effective in describing refractive profiles for small elevations, it fails to relate

optical data *uniquely* to profiles and hence any constructed profile must be verified independently. This is a serious defect. To be effective, a method for inverting optical data must allow us to estimate the fitting error.

Figures (4.5.1), (4.5.2) and (4.5.3) show model ray bundles for Profiles 1, 2 and 3 respectively. The model ray bundles demonstrate clearly that the cylindrical model can reproduce some interesting mirage phenomena: extreme magnification is seen in Profile 1 and focussing is evident in Profiles 2 and 3. Of these, the second will exist in any cylindrically modelled refractive profile, given sufficient target range, because of the periodic nature of the model ray path. The first focal point occurs at the first vertex of the ray with departure angle zero.

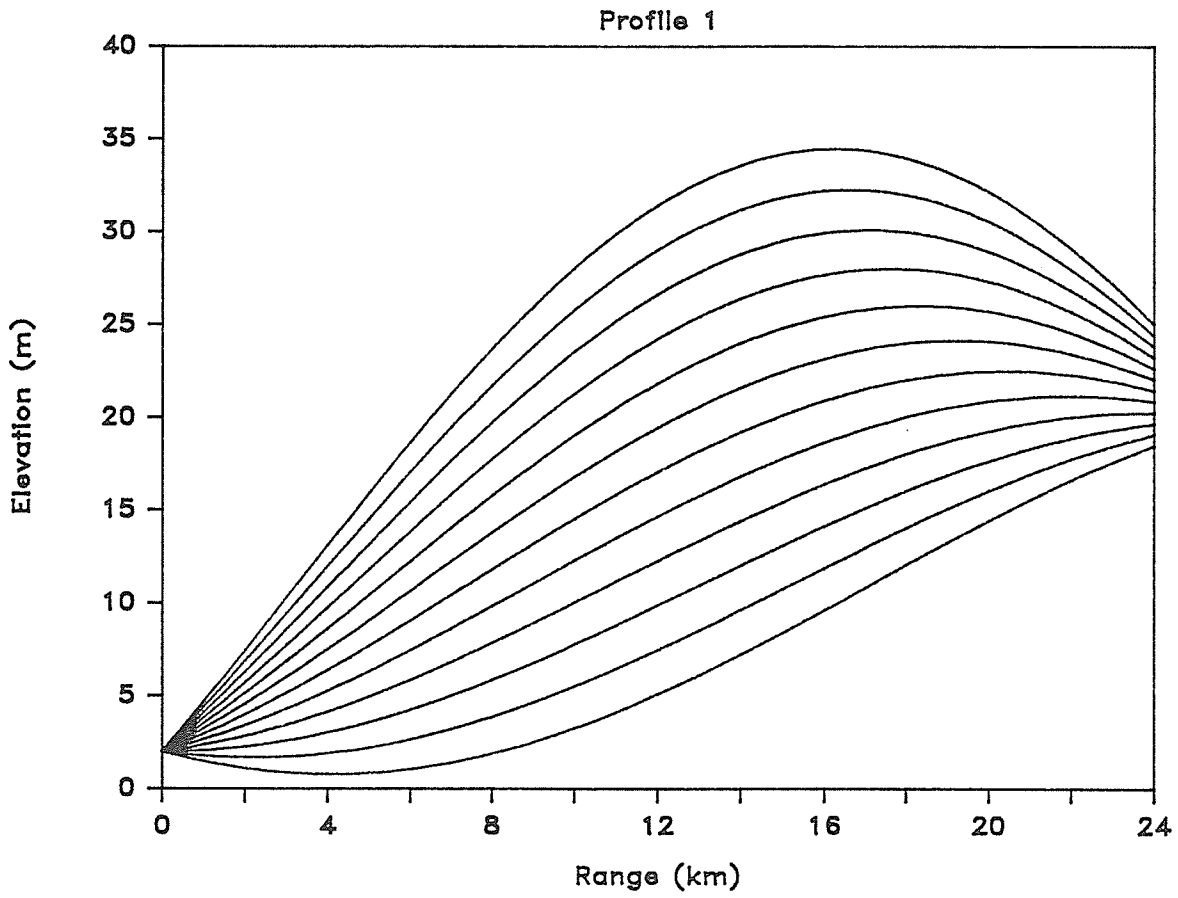

Fig. 4.5.1 Profile 1 ray traces with magnification.

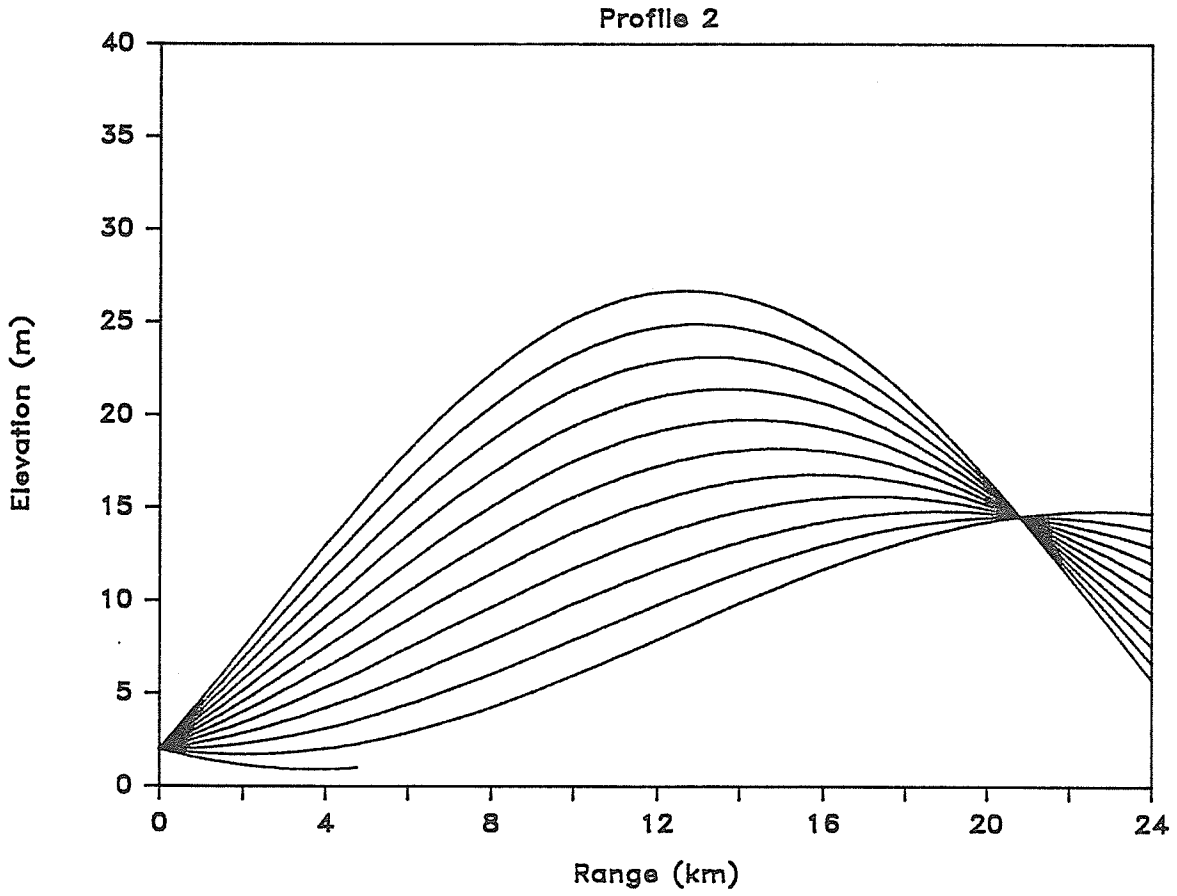

Fig. 4.5.2 Profile 2 ray traces with focussing.

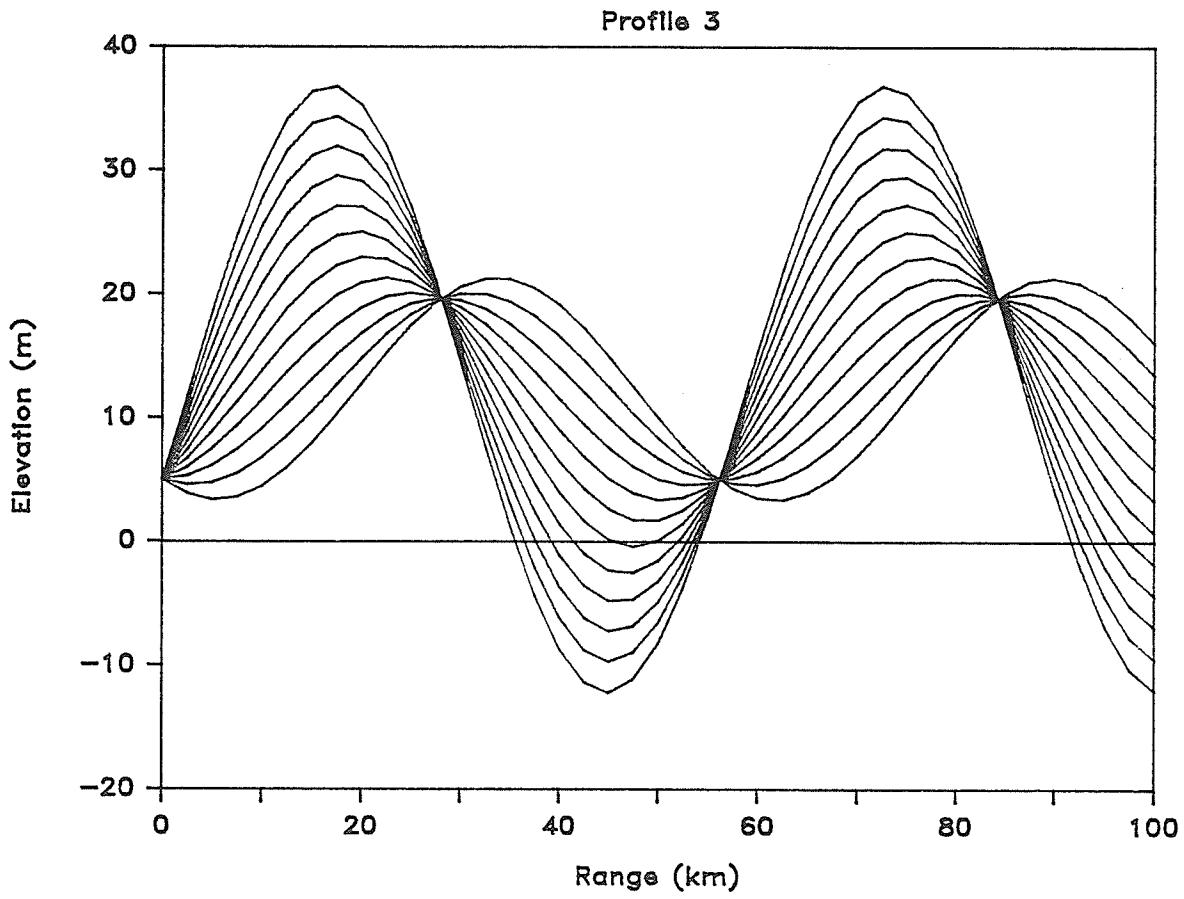

Fig. 4.5.3 Profile 3 ray traces with focussing.

CHAPTER 5: CONCLUSIONS

5.1 Fraser's Method

Fraser's transformation equations lead to a parametric form of the equation of the ray path, expressing ξ and ς as functions of parameter ϕ_t. He assumed a series expansion for the elevation variable ς in terms of the refractive variable τ. The expansion is truncated and the series coefficients determined from the optical data. The method was applied successfully to *inferior* mirage data. Its application to superior mirages failed to produce correct results.

Following Fraser, ς was expanded in a Maclaurin series in τ. A fit to superior mirage data was subsequently attempted for both a one term and a two term expansion.

The single term expansion resulted in a relation between image–object angular separation and temperature gradient, similar to a result due to Fleagle [5]. This relation was applied to Profile 1 and the rate of change of temperature calculated for several image–object angular elevation pairs. This led to a continuously changing temperature gradient and did not provide a close estimate of the actual gradient.

The two term expansion resulted in refractive profiles that either increased with elevation or decreased so slowly that temperature changed by less than 0.2° C over a vertical range of 40 meters. It was apparent that Fraser's method could not

be applied successfully to the superior mirages used here.

5.2 A Direct Solution

A formal solution of the ray equation was presented and its application to superior mirages investigated. The method allowed the calculation of refractive profile once a functional form for the ray path had been determined. In the case where the ray path can be described simply, the refractive profile can be given in closed form. For more complicated paths, the equations can be integrated numerically. Some profiles were presented and shown to be similar to results obtained by Lyusternik[6].

A parabolic path was chosen and fitted to the optical data. The resulting refractive profile was inaccurate. It was clear that while a parabola could be fitted to the data in a number of ways, the true ray was insufficiently parabolic over its entire course, to allow us to model it with a parabola.

It was noted that imposing radial symmetry upon the problem and solving the equations in polar coordinates led to unrealistic ray paths that could be inverted to produce profiles or realistic paths that were not easily inverted.

The problem of relating the profile derived from one ray in a mirage to the

profile derived from another ray in the same mirage, was examined. It was suggested that ray by ray analyses were not an appropriate method of attack and that a solution should be characterized by some parameter common to all paths.

5.3 An Analysis of the Ray Path

In Section 2.3 the consequences of restricting ray paths to the class of curves possessing one vertex and no points of inflection and having shallow vertical displacement was examined. It was demonstrated that this class of curves could bound the true ray path closely if the departure from the constraints was small.

5.4 Differential Geometry

A manifold with a specified metric was described and shown to have some interesting optical properties. The ray equation was derived from the geodesic equations of the manifold. Gaussian curvature K, was defined, and a differential equation relating refractive index and K was presented. This equation was solved for $K = 0$ and $K =$ constant.

The assumption that $K = 0$ led to an exponential refractive profile. Optical

data could not be fitted, so two points of known refractive index were used to determine the constants in the relation. The resulting profile was essentially linear over the vertical range of interest.

The assumption of constant K led to a more complicated exponential relation. This relation was fitted to three points of known refractive index for several profiles and the results presented. The fit in all cases produced profiles in excellent agreement with the true profile.

It was noted that in each case one of the fitting constants was close to unity. Assuming that it was unity allowed us to write the functional form of the refractive profile in a particularly simple manner

$$n = n_e \operatorname{sech}(ay)$$

Fitting this equation to two points of known refractive index resulted in a poorer fit but still, in comparison with the accuracy generally found in this field, quite good. This suggests that the thermodynamics of the bottom twenty meters of a mature inversion may be quite simple.

In order to account for the curvature of the earth, a radially symmetric manifold, with metric expressed in polar coordinates was defined. A differential equation defining Gaussian curvature in terms of this metric was solved. For K = 0 the re-

fractive profile was similar to that obtained in the Cartesian case. With K constant, no refractive profile could be determined at all. The implied scale size prevented a sensible solution from being obtained numerically. Imposing radial symmetry on the manifold served no purpose.

5.5 Cylindrical model

It was shown that a light ray will follow the same path as a mass particle if the refractive index of the medium through which the light passes has the same functional dependence on position as speed of the particle.

The kinematics of a particle of unit mass sliding without friction on the interior of a right circular cylinder was presented. It was shown that given the departure angle and initial and final displacements of the particle from an arbitrary reference level, the path could be described with two unknown parameters — the radius of the cylinder and the displacement of the reference level from the axis of the cylinder.

The vertical projection of the motion of the particle onto the $x - y$ plane will be the same as the path of a ray with the same departure angle and initial and final displacement from the same reference level. Two rays will then determine the unknown parameters. The relation between the radius of the cylinder and refractive

index is presented.

It was determined that optical data could not be fitted because of the periodic nature of the relation between target range and elevation. Rather, actual ray path data was used. The derived profiles produced interesting optical effects such as focussing and extreme magnification, but due to the fitting problems, the method is not well suited to inversion. It is however a good paedagogical tool.

CHAPTER 6: APPENDIX

6.1 Temperature Profiles

The profiles used in this thesis are presented in Tables 6.1, 6.2, and 6.3. Each table contains the ray elevations for each ray at 1000m intervals and the temperature at specified elevations. Graphs of rays paths are presented in Figs. (6.1.1), (6.1.2) and (6.1.3) and graphs of each profile in Figs. (6.1.4), (6.1.5) and (6.1.6).

6.2 Summation Convention

The Einstein summation convention usually referred to simply as the summation convention states that in any tensor equation, if an upper or contravariant index and lower or covariant index are represented by the same symbol, then summation over this symbol is implied. Hence the following identities

$$
\begin{aligned}
y^i x_i &= \sum_{i=1}^{2} y^i x_i = y^1 x_1 + y^2 x_2, \\
\Gamma_h{}^j{}_k &= g^{lj}\Gamma_{hlk} = g^{1j}\Gamma_{h1k} + g^{2j}\Gamma_{h2k}, \\
R_l{}^j{}_{hk} &= \frac{\partial \Gamma_l{}^j{}_h}{\partial x^k} - \frac{\partial \Gamma_l{}^j{}_k}{\partial x^h} + \Gamma_s{}^j{}_g \Gamma_l{}^s{}_h - \Gamma_s{}^j{}_h \Gamma_l{}^s{}_k \\
&= \frac{\partial \Gamma_l{}^j{}_h}{\partial x^k} - \frac{\partial \Gamma_l{}^j{}_k}{\partial x^h} + \Gamma_1{}^j{}_g \Gamma_l{}^1{}_h + \Gamma_2{}^j{}_k \Gamma_l{}^2{}_h - \Gamma_1{}^j{}_h \Gamma_l{}^1{}_k - \Gamma_2{}^j{}_h \Gamma_l{}^2{}_k.
\end{aligned}
\tag{6.2.1}
$$

(BG1)

Profile 1 ray elevations
Departure angle (minutes of arc)

Range (km)	-3	-2	-1	0	1	2	3	4	5	6	7
0	2.00	2.00	2.00	2.00	2.00	2.00	2.00	2.00	2.00	2.00	2.00
1	1.19	1.48	1.77	2.06	2.35	2.64	2.93	3.22	3.51	3.80	4.09
2	0.50	1.08	1.66	2.24	2.82	3.39	3.97	4.55	5.13	5.71	6.30
3	-0.08	0.80	1.67	2.54	3.39	4.25	5.12	5.98	6.84	7.71	8.58
4	0.00	0.63	1.80	2.95	4.07	5.22	6.36	7.51	8.65	9.79	10.92
5	0.00	0.59	2.05	3.47	4.86	6.28	7.70	9.11	10.51	11.89	13.26
6	0.00	0.67	2.42	4.09	5.75	7.44	9.10	10.75	12.37	13.97	15.57
7	0.00	0.87	2.90	4.82	6.74	8.67	10.56	12.40	14.21	16.02	17.80
8	0.00	1.19	3.49	5.66	7.81	9.95	12.01	14.02	16.01	17.97	19.90
9	0.00	1.63	4.19	6.58	8.95	11.25	13.45	15.61	17.72	19.79	21.79
10	0.00	2.19	5.00	7.61	10.14	12.55	14.86	17.11	19.30	21.40	23.36
11	0.00	2.87	5.90	8.70	11.34	13.82	16.21	18.50	20.70	22.73	24.50
12	0.00	3.66	6.90	9.84	12.54	15.07	17.47	19.74	21.83	23.66	25.05
13	0.00	4.55	7.99	11.01	13.71	16.24	18.60	20.79	22.68	24.14	24.99
14	0.00	5.55	9.14	12.17	14.85	17.33	19.57	21.55	23.12	24.14	24.30
15	0.00	6.64	10.33	13.31	15.93	18.28	20.37	22.04	23.12	23.67	23.07
16	0.00	7.83	11.54	14.42	16.93	19.09	20.90	22.25	22.66	22.75	21.42
17	0.00	9.07	12.73	15.51	17.82	19.73	21.16	22.19	21.79	21.42	19.48
18	0.00	10.37	13.89	16.49	18.56	20.20	21.15	21.85	20.64	19.82	17.35
19	0.00	11.67	15.03	17.39	19.14	20.42	20.85	21.23	19.23	18.00	15.09
20	0.00	12.96	16.10	18.16	19.56	20.35	20.28	20.34	17.65	16.05	12.77
21	0.00	14.23	17.08	18.77	19.83	20.01	19.46	19.20	15.94	14.00	10.43
22	0.00	15.45	17.95	19.23	19.94	19.45	18.47	17.90	14.13	11.92	8.10
23	0.00	16.60	18.66	19.52	19.89	18.73	17.33	16.45	12.29	9.82	5.83
24	0.00	17.65	19.22	19.66	19.68	17.85	16.06	14.90	10.43	7.75	3.65
25	0.00	18.56	19.62	19.64	19.32	16.83	14.69	13.29	8.58	5.74	1.58

Elev (m)	0.00	2.44	4.88	7.42	9.96	12.35	14.93
Temp (C)	- 0.96	-0.96	-0.93	-0.87	-0.71	-0.42	-0.06
Refractivity	0.29309	0.29300	0.29288	0.29272	0.29246	0.29206	0.29158

Elev (m)	17.37	20.00	22.44	24.20	27.00	30.00	35.00
Temp (C)	0.43	1.12	2.04	3.00	5.00	6.11	7.38
Refractivity	0.29097	0.29014	0.28908	0.28801	0.28584	0.28460	0.28314

Elev (m)	46.00	57.30	70.00
Temp (C)	9.25	10.60	11.75
Refractivity	0.28089	0.27917	0.27762

Table 6.1

(JN2)

Profile 2 ray elevations
Departure angle (minutes of arc)

Range (km)	-2	-1	0	1	2	3	4	5	6
0	2.00	2.00	2.00	2.00	2.00	2.00	2.00	2.00	2.00
1	1.45	1.74	2.03	2.32	2.61	2.90	3.19	3.48	3.77
2	0.95	1.53	2.11	2.69	3.28	3.86	4.44	5.02	5.60
3	0.51	1.38	2.25	3.13	4.00	4.87	5.74	6.60	7.46
4	0.12	1.29	2.45	3.62	4.78	5.93	7.07	8.21	9.35
5		1.25	2.71	4.16	5.61	7.01	8.42	9.83	11.25
6		1.27	3.02	4.76	6.46	8.12	9.80	11.47	13.10
7		1.35	3.38	5.41	7.34	9.25	11.18	13.04	14.83
8		1.48	3.81	6.09	8.24	10.41	12.52	14.50	16.37
9		1.67	4.29	6.80	9.17	11.55	13.76	15.78	17.69
10		1.91	4.82	7.52	10.12	12.62	14.85	16.86	18.64
11		2.22	5.41	8.28	11.07	13.60	15.74	17.68	19.22
12		2.57	6.02	9.05	11.98	14.44	16.45	18.11	19.41
13		2.99	6.66	9.86	12.80	15.09	16.95	18.17	19.22
14		3.46	7.32	10.67	13.52	15.54	17.19	17.84	18.64
15		3.99	8.00	11.46	14.11	15.80	17.05	17.13	17.68
16		4.57	8.71	12.18	14.52	15.86	16.60	16.11	16.36
17		5.21	9.45	12.82	14.74	15.73	15.94	14.88	14.82
18		5.88	10.21	13.35	14.77	15.41	15.10	13.47	13.09
19		6.58	10.96	13.76	14.60	14.89	14.05	11.93	11.24
20		7.30	11.67	14.03	14.23	14.18	12.85	10.30	9.34
21		8.04	12.31	14.13	13.68	13.29	11.53	8.67	7.45
22		8.81	12.86	14.03	12.99	12.27	10.15	7.06	5.59
23		9.61	13.31	13.77	12.19	11.17	8.77	5.47	3.76
24		10.42	13.63	13.37	11.30	10.02	7.41	3.92	1.99
25		11.22	13.82	12.83	10.36	8.87	6.08	2.42	0.27

Elev (m)	0.00	5.00	10.00	11.00	12.00	13.00	14.00
Temp (C)	0.00	0.30	0.75	0.88	1.06	1.26	1.50
Refractivity	0.29206	0.29156	0.29090	0.29072	0.29050	0.29025	0.28996

Elev (m)	17.00	20.00	24.00	26.00	30.00	34.00	39.00
Temp (C)	2.40	3.85	6.00	7.10	8.37	9.18	9.60
Refractivity	0.28890	0.28728	0.28493	0.28374	0.28232	0.28138	0.28079

Elev (m)	45.00
Temp (C)	9.80
Refractivity	0.28039

Table 6.2

(NZ802D)

Profile 3 ray elevations
Departure angle (minutes of arc)

Range (km)	-3	-2	-1	0	1	2	3	4	5	6	7
0.0	5.00	5.00	5.00	5.00	5.00	5.00	5.00	5.00	5.00	5.00	5.00
2.5	3.08	3.81	4.54	5.19	5.92	6.65	7.37	8.10	8.83	9.55	10.28
5.0	1.70	3.14	4.60	5.76	7.22	8.67	10.13	11.56	12.97	14.39	15.80
7.5	0.92	3.00	5.18	6.72	8.90	11.06	13.12	15.18	17.20	19.17	21.07
10.0	0.73	3.39	6.19	8.05	10.93	13.61	16.22	18.69	20.98	23.00	24.53
12.5	1.14	4.30	7.58	9.77	13.14	16.25	19.05	21.45	23.20	23.86	23.30
15.0	2.15	5.72	9.34	11.76	15.47	18.62	21.07	22.44	22.36	20.93	18.65
17.5	3.74	7.54	11.44	13.90	17.65	20.30	21.57	21.14	19.16	16.37	13.16
20.0	5.84	9.75	13.67	16.11	19.31	20.78	20.20	18.23	15.05	11.50	7.72
22.5	8.35	12.23	16.00	18.08	20.20	19.84	17.69	14.66	10.84	6.81	2.63
25.0	11.23	14.85	18.11	19.43	19.83	17.90	14.65	11.06	6.83	2.51	
27.5	14.27	17.42	19.59	20.04	18.51	15.38	11.59	7.64	3.21		
30.0	17.33	19.51	20.24	19.62	16.51	12.75	8.69	4.60	0.13		
32.5	19.93	20.70	19.59	18.42	14.20	10.24	6.12	2.03			
35.0	21.48	20.51	18.09	16.54	11.93	7.96	3.96	0.03			
37.5	21.23	19.02	15.98	14.36	9.80	6.06	2.31				
40.0	19.35	16.76	13.66	12.20	7.94	4.55	1.23				
42.5	16.59	14.14	11.42	10.17	6.47	3.53	0.75				
45.0	13.50	11.56	9.33	8.38	5.37	3.04	0.86				
47.5	10.48	9.12	7.56	6.96	4.68	3.07	1.58				
50.0	7.69	7.02	6.18	5.93	4.50	3.63	2.88				
52.5	5.27	5.30	5.17	5.28	4.85	4.72	4.74				
55.0	3.29	4.01	4.59	5.01	5.68	6.28	7.06				
57.5	1.84	3.23	4.54	5.12	6.89	8.23	9.77				
60.0	0.98	2.99	5.01	5.61	8.48	10.56	12.75				
62.5	0.72	3.27	5.93	6.49	10.45	13.09	15.85				
65.0	1.06	4.07	7.23	7.74	12.63	15.73	18.74				
67.5	1.99	5.40	8.91	9.38	14.94	18.19	20.89				
70.0	3.51	7.15	10.95	11.34	17.18	20.04	21.67				
72.5	5.56	9.28	13.16	13.44	19.00	20.80	20.44				
75.0	8.03	11.72	15.48	15.66	20.09	20.14	18.03				
77.5	10.87	14.31	17.67	17.70	20.03	18.34	15.03				
80.0	13.90	16.92	19.32	19.21	18.87	15.91	11.96				
82.5	16.98	19.15	20.20	19.98	17.00	13.27	9.02				
85.0	19.66	20.57	19.82	19.78	14.73	10.73	6.42				
87.5	21.37	20.66	18.49	18.73	12.43	8.38	4.20				
90.0	21.36	19.39	16.49	16.97	10.27	6.41	2.48				
92.5	19.64	17.26	14.18	14.83	8.33	4.81	1.33				
95.0	16.95	14.67	11.91	12.64	6.77	3.69	0.77				
97.5	13.87	12.06	9.78	10.58	5.59	3.09	0.82				
100	10.84	9.59	7.93	8.72	4.80	3.02	1.46				

Elev (m)	0.00	2.50	5.00	10.00	15.00	17.50	20.00
Temp (C)	-38.92	-38.90	-38.86	-38.70	-38.40	-38.14	-37.75
Refractivity	0.34062	0.34047	0.34029	0.33981	0.33912	0.33863	0.33794

Elev (m)	21.50	23.00	24.00	25.2	26.70	29.50	35.00
Temp (C)	-37.40	-36.90	-36.42	-35.6	-34.40	-32.60	-30.95
Refractivity	0.33737	0.33658	0.33585	0.33463	0.33287	0.33025	0.32774

Elev (m)	45.00	65.00	90.00
Temp (C)	-29.13	-26.55	-24.00
Refractivity	0.32484	0.32055	0.31617

Table 6.3

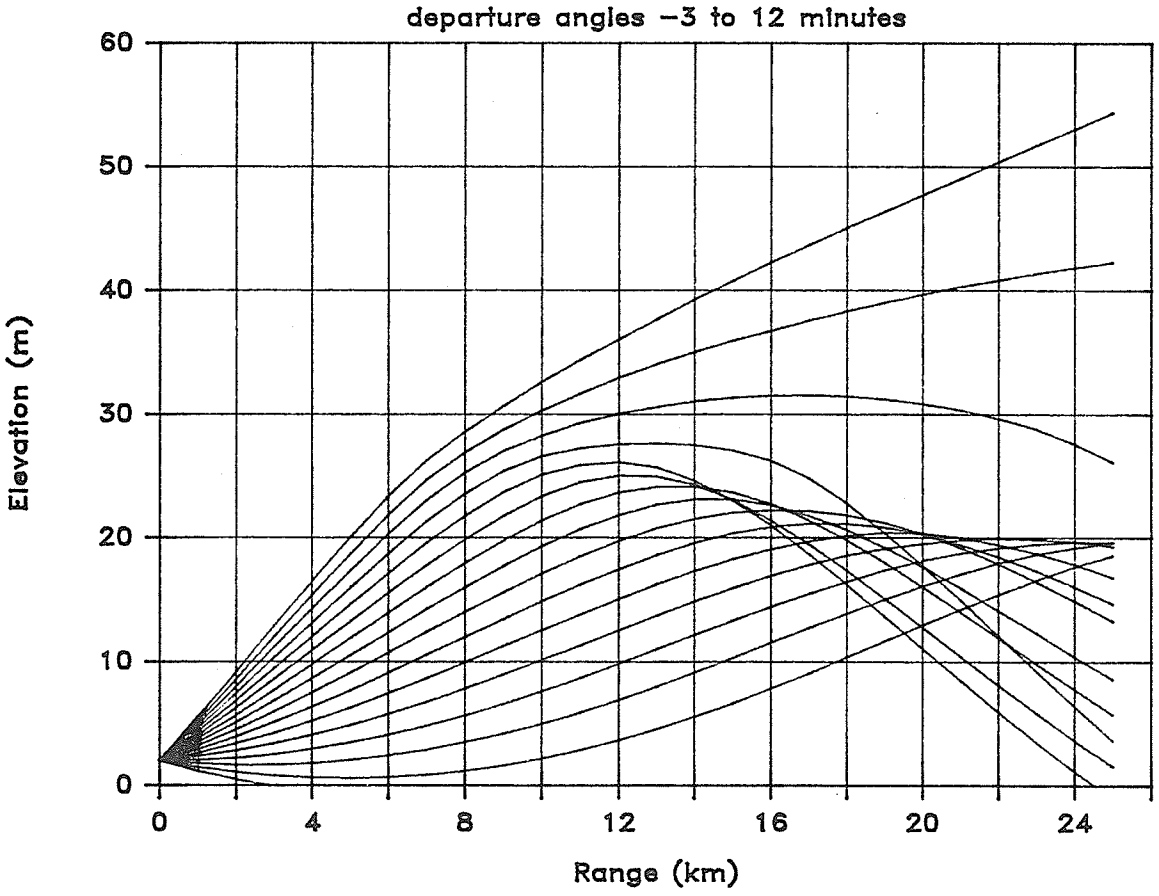

Fig. 6.1.1 Profile 1 — ray paths

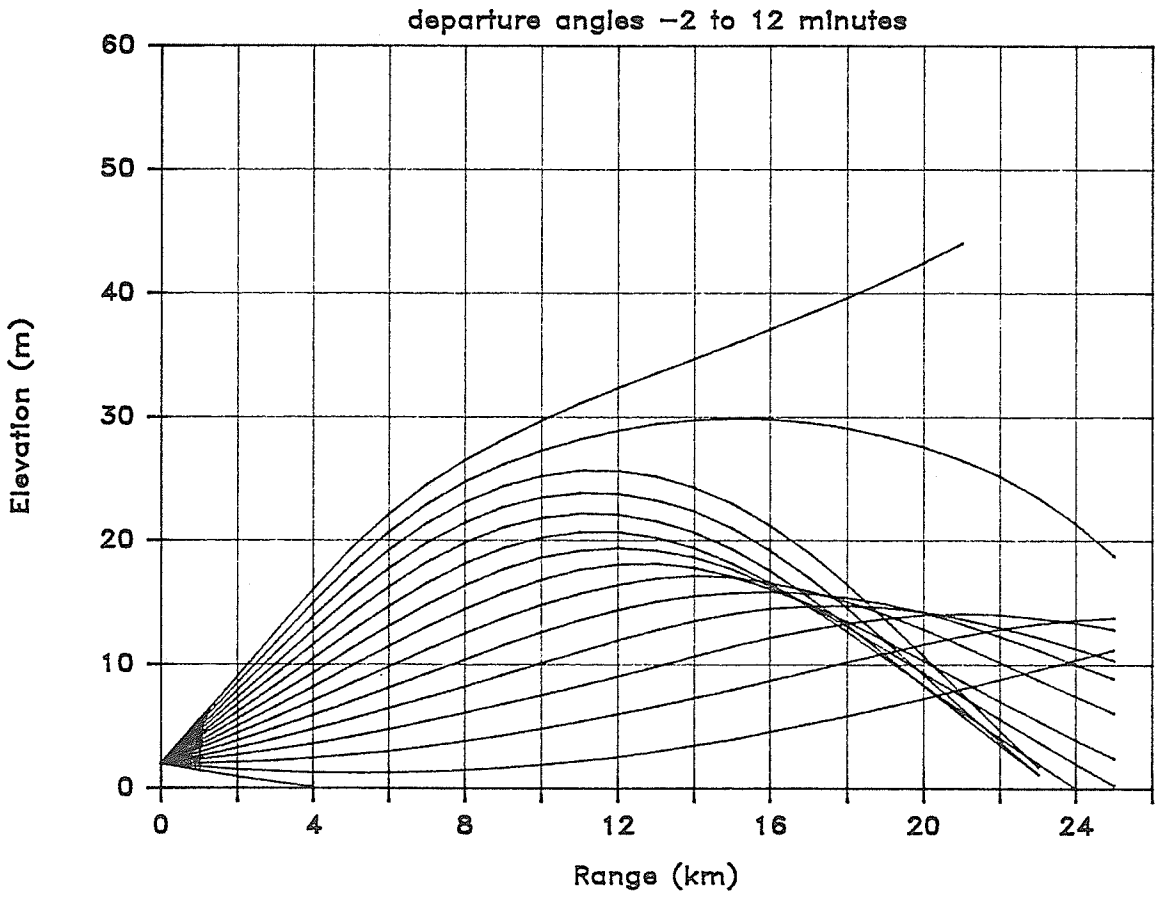

Fig. 6.1.2 Profile 2 — ray paths

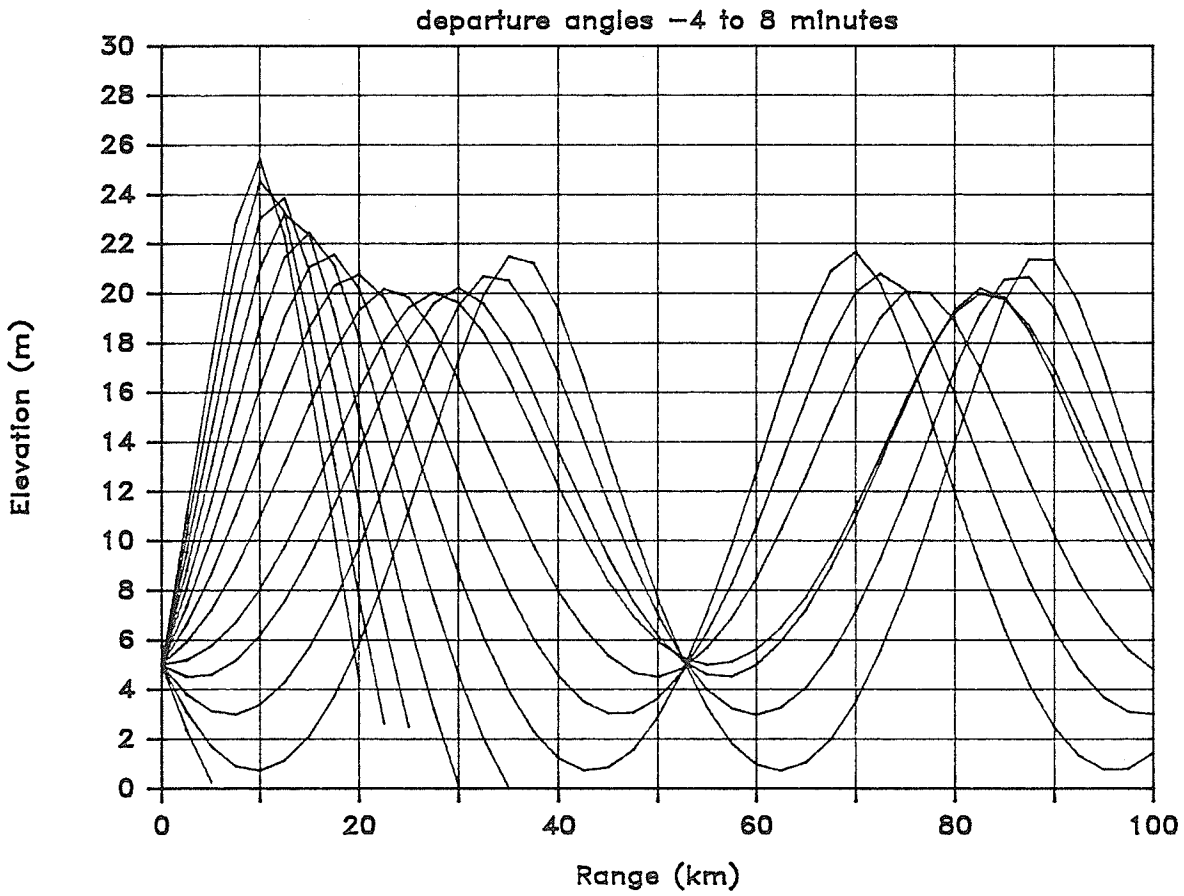

Fig. 6.1.3 Profile 3 — ray paths

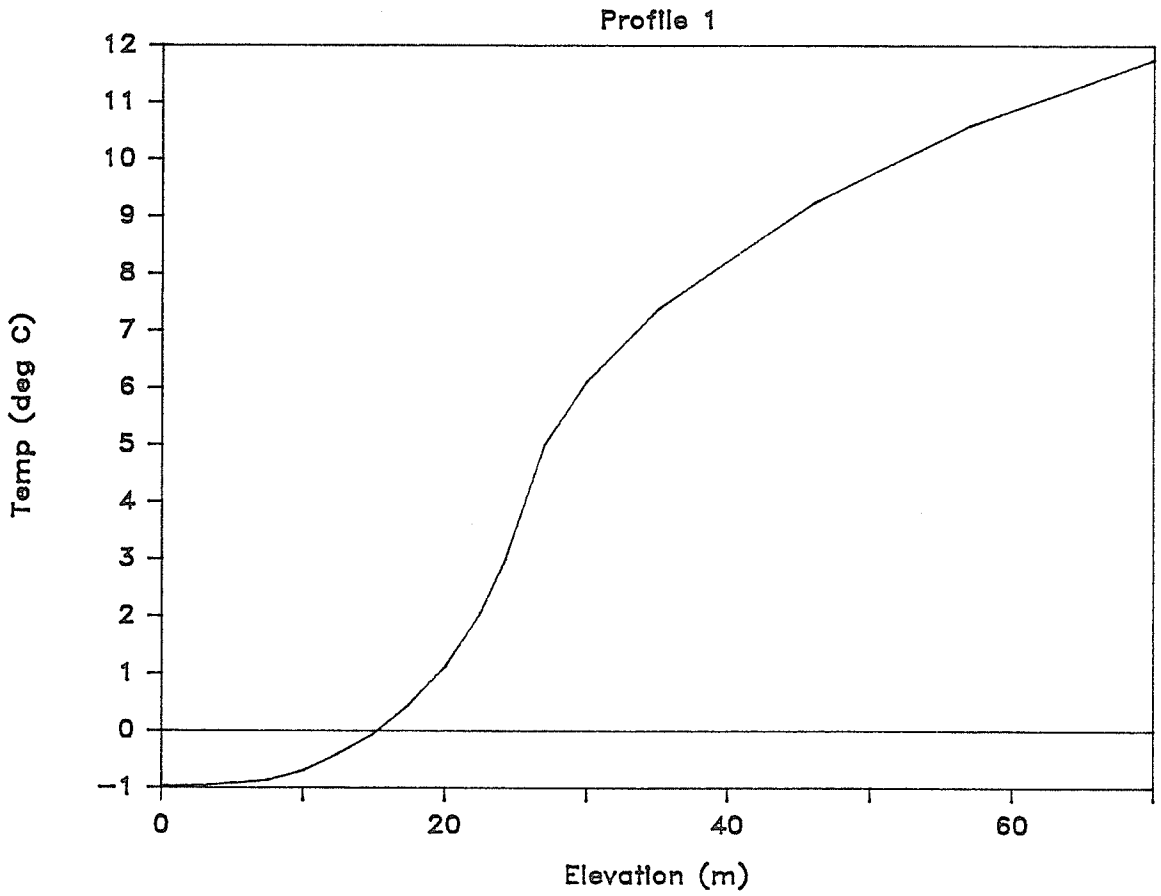

Fig. 6.1.4 Profile 1 temperature

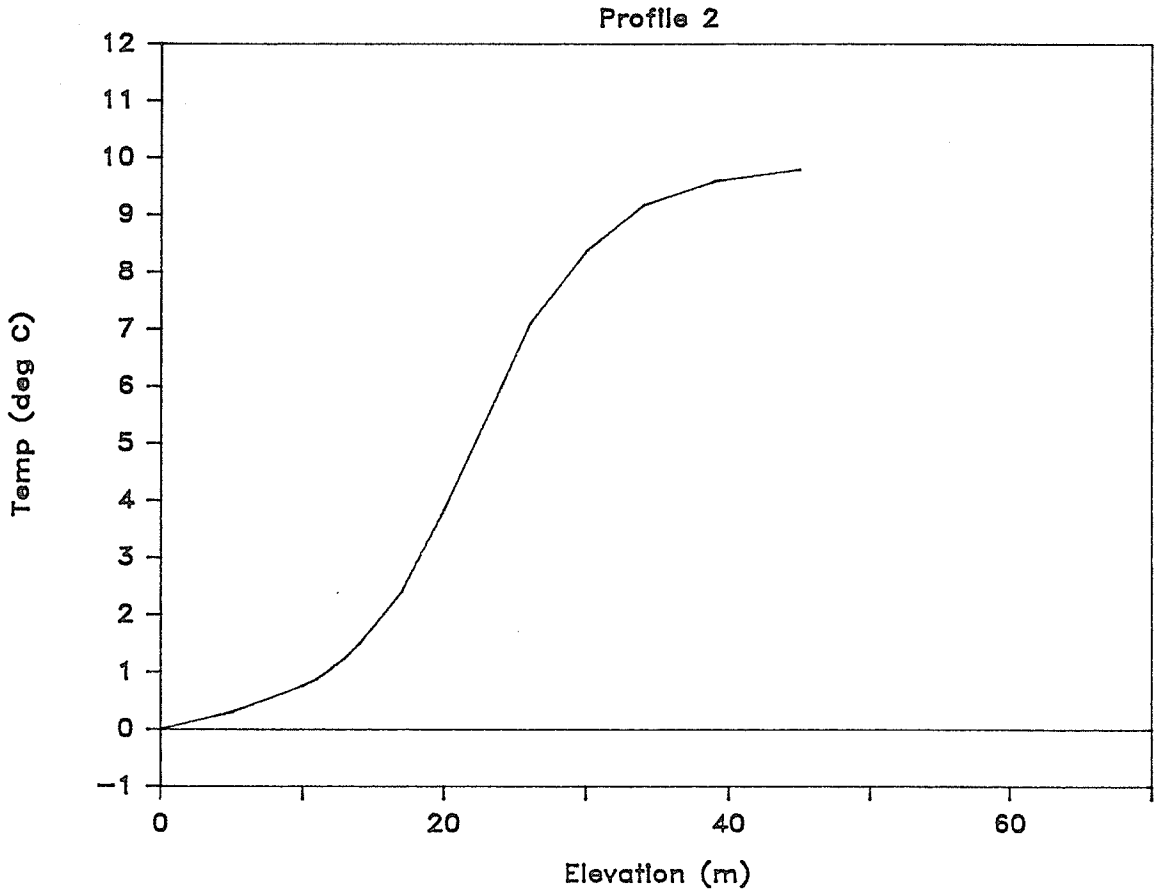

Fig. 6.1.5 Profile 2 temperature

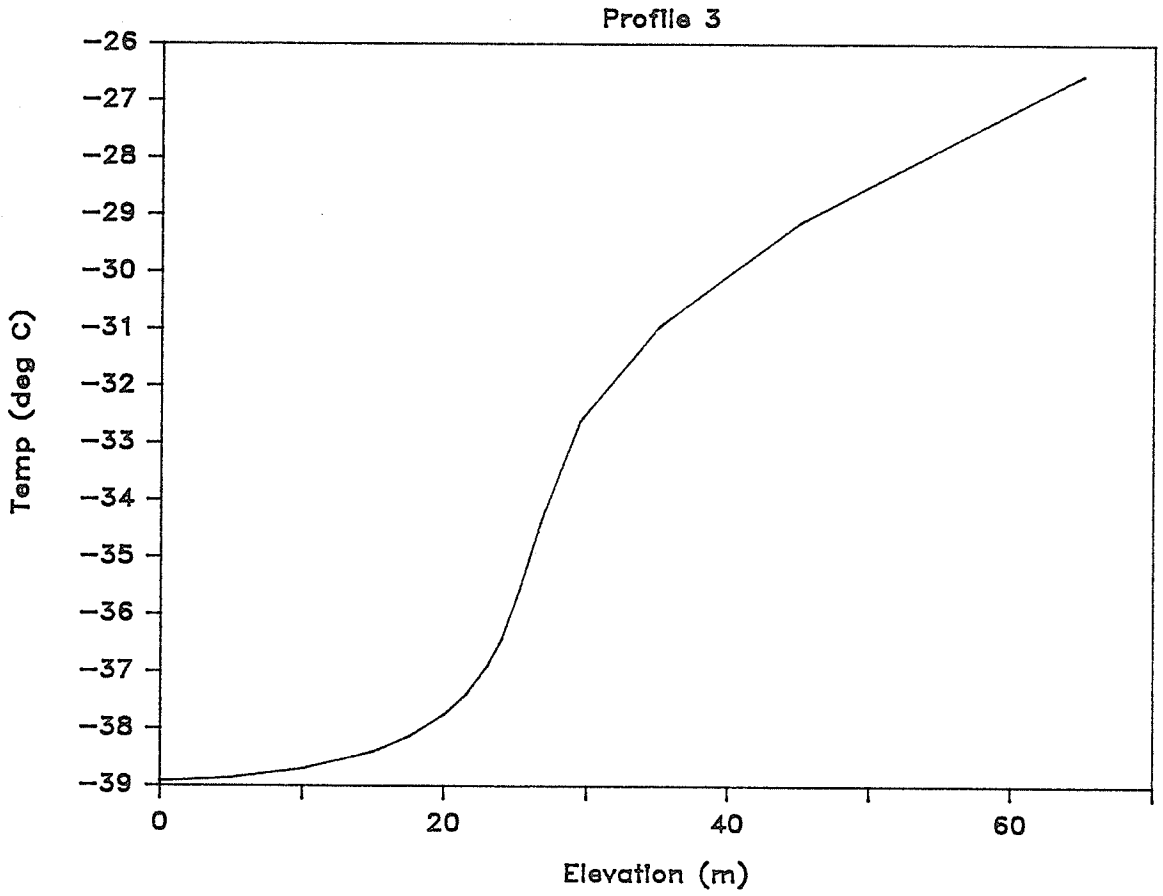

Fig. 6.1.6 Profile 3 temperature

6.3 Cartesian Geometry

Christoffel symbols of the first kind are defined by the relation

$$\Gamma_{hlk} = \frac{1}{2}\left(\frac{\partial g_{kl}}{\partial x^h} + \frac{\partial g_{lh}}{\partial x^k} - \frac{\partial g_{hk}}{\partial x^l}\right)$$

Then, given the metric of Eq. (3.2.2), we have

$$\begin{array}{llll} \Gamma_{111} = 0 & \Gamma_{212} = 0 & \Gamma_{121} = -n\,(dn/dy) & \Gamma_{211} = n\,(dn/dy) \\ \Gamma_{122} = 0 & \Gamma_{221} = 0 & \Gamma_{112} = n\,(dn/dy) & \Gamma_{222} = n\,(dn/dy) \end{array} \tag{6.3.1}$$

Christoffel symbols of the second kind are defined by the relation

$$\Gamma_h{}^j{}_k = g^{lj}\Gamma_{hlk} = g^{1j}\Gamma_{h1k} + g^{2j}\Gamma_{h2k}$$

The metric in Eq. (3.2.2) then gives us

$$\begin{array}{lll} \Gamma_1{}^1{}_1 = 0 & \Gamma_1{}^2{}_2 = 0 & \Gamma_1{}^2{}_1 = -(1/n)\,(dn/dy) \\ \Gamma_2{}^1{}_2 = 0 & \Gamma_2{}^2{}_1 = 0 & \Gamma_2{}^1{}_1 = (1/n)\,(dn/dy) \\ \Gamma_1{}^1{}_2 = (1/n)\,(dn/dy) & \Gamma_2{}^2{}_2 = (1/n)\,(dn/dy) & \end{array} \tag{6.3.2}$$

The mixed curvature tensor is defined by the relation

$$R_l{}^j{}_{hk} = \frac{\partial \Gamma_l{}^j{}_h}{\partial x^k} - \frac{\partial \Gamma_l{}^j{}_k}{\partial x^h} + \Gamma_1{}^j{}_g\Gamma_l{}^1{}_h + \Gamma_2{}^j{}_k\Gamma_l{}^2{}_h - \Gamma_1{}^j{}_h\Gamma_l{}^1{}_k - \Gamma_2{}^j{}_h\Gamma_l{}^2{}_k.$$

The non-vanishing components are

$$\begin{aligned} R_2{}^1{}_{12} &= -R_1{}^2{}_{12} = -R_2{}^1{}_{21} = R_1{}^2{}_{21} \\ &= -\frac{1}{n^2}\left(\frac{dn}{dy}\right)^2 + \frac{1}{n}\frac{d^2n}{dy^2} \end{aligned} \tag{6.3.3}$$

The covariant curvature tensor is defined by the relation

$$\begin{aligned} R_{lmhk} &= g_{jm} R_l{}^j{}_{hk} \\ &= g_{1m} R_l{}^1{}_{hk} + g_{2m} R_l{}^2{}_{hk} \end{aligned} \tag{6.3.4}$$

We need only the [1212] component of this tensor. It is

$$\begin{aligned} R_{1212} &= g_{12} R_1{}^1{}_{12} + g_{22} R_1{}^2{}_{12} \\ &= g_{22} R_1{}^2{}_{12} \\ &= \left(\frac{dn}{dy}\right)^2 - n\frac{d^2n}{dy^2}. \end{aligned} \tag{6.3.5}$$

Since $|g| = n^4$, we have

$$\begin{aligned} K &= R_{1212}/|g| \\ &= \frac{1}{n^4}\left(\frac{dn}{dr}\right)^2 - \frac{1}{n^3}\frac{d^2n}{dr^2}. \end{aligned} \tag{6.3.6}$$

6.4 Some Mirages

Some images and mirages are presented below. Figure 6.4.1 shows a normal view of the shore of the Beaufort Sea at Tuktoyaktuk, Northwest Territories. Figure 6.4.2 shows an real inverted, superior mirage of the same scene.

The image in Fig. 6.4.1 was digitized and a computer program used to manipulate it under the assumption that the air temperature was given by Profile 1. The resulting synthetic mirage is presented in Fig. 6.4.3. The major features of the real mirage, (that is the lifting and inversion of the mounds to the left and right) are

preserved in the synthetic mirage. The most significant feature missing from the synthetic image is the distorted but erect image of the shore. Examining the rays of Profile 1 in Fig. 6.1.1, it is clear that there are no rays contributing to an erect image for lower elevations.

Under the assumption that Gaussian curvature was constant, Profile 1 was fitted to Eq. 3.4.9. The resulting profile was used to construct the image in Fig. 6.4.4. This image is similar to Fig. 6.4.3, it possesses the same inversion and lifting and lacks the erect image of the shore because there are no rays from the target that reach the eye from lower elevations. The image differs in the degree of vertical magnification, causing it to be more like the real mirage than is Fig. 6.4.3. This is not to suggest that the real mirage arose as a consequence of constant curvature, but simply to demonstrate that such a simplifying assumption can lead to interesting refractive profiles.

Fig. 6.4.1 The shore of the Beaufort Sea at Tuktoyaktuk. Normal view.

Fig. 6.4.2 The shore of the Beaufort Sea at Tuktoyaktuk. Real mirage.

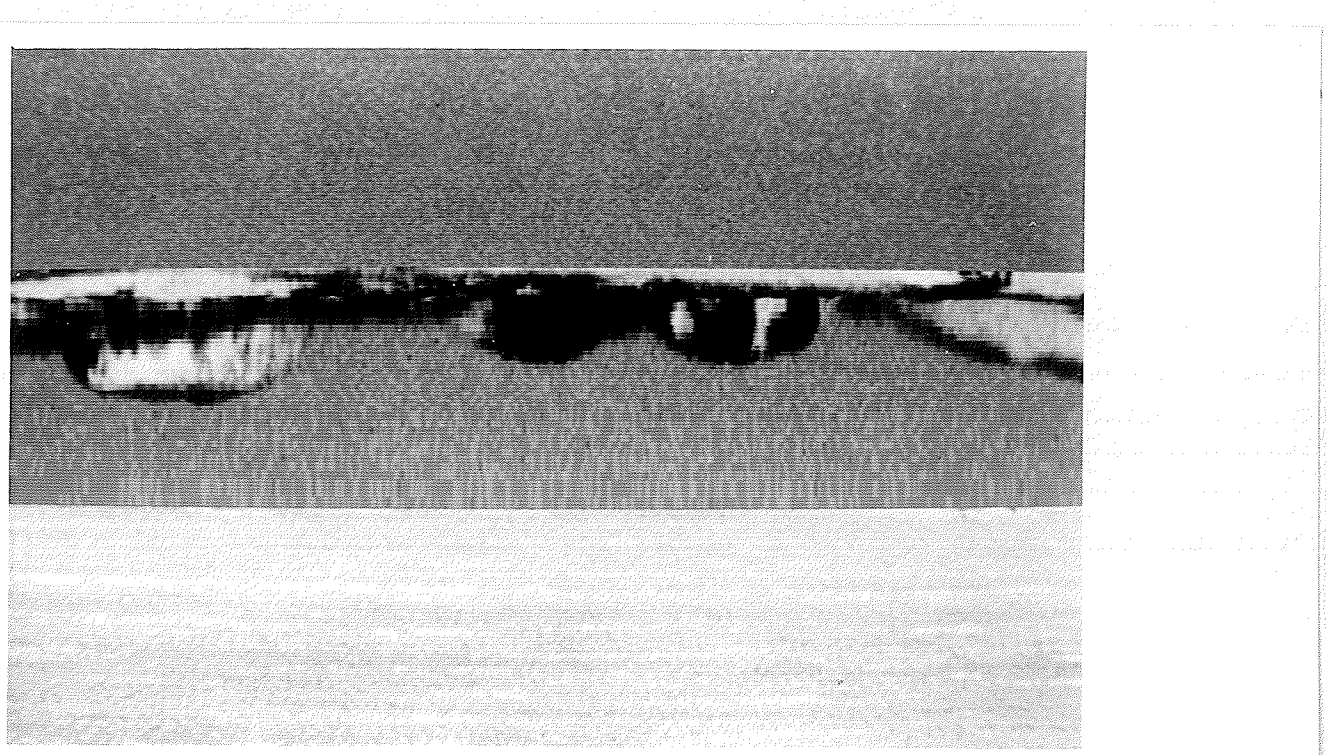

Fig. 6.4.3 Normal view modified by Profile 1, a synthetic mirage.

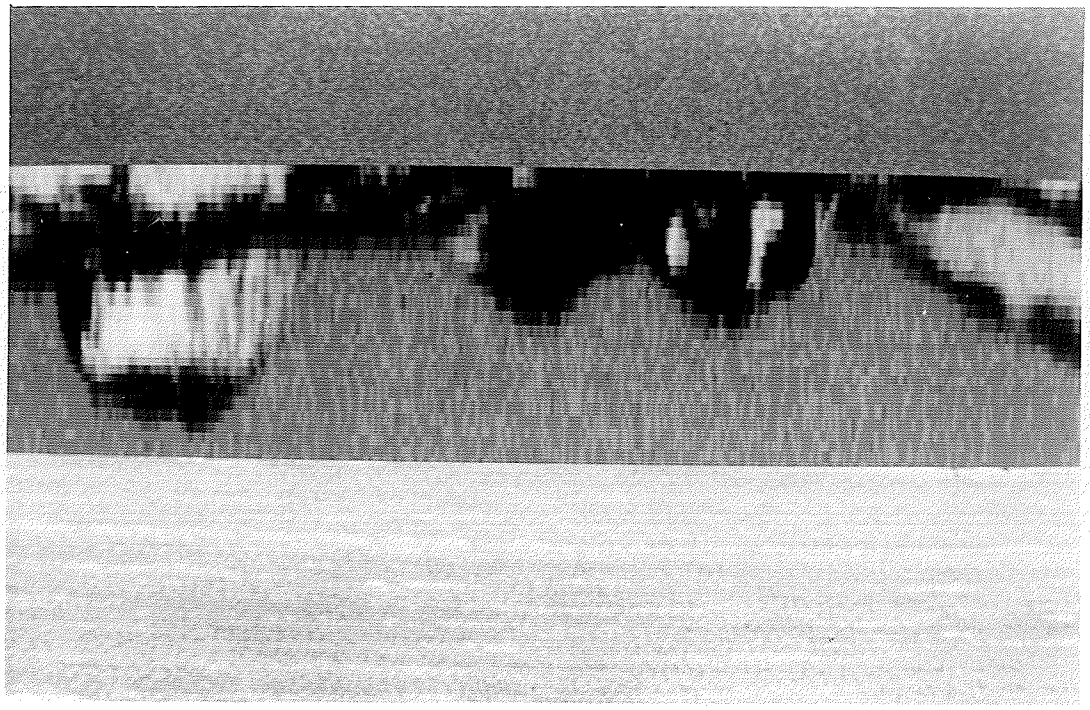

Fig. 6.4.4 Normal view modified by Eq. 3.4.9, a synthetic mirage.

6.5 Radially Symmetric Geometry

Christoffel symbols of the first kind are, given the metric of Eq. (3.5.2),

$$\begin{array}{lll} \Gamma_{211}=0 & \Gamma_{111}=n\,(dn/dr) & \Gamma_{122}=nr^2\,(dn/dr)+n^2r \\ \Gamma_{112}=0 & \Gamma_{221}=nr^2\,(dn/dr)+n^2r & \Gamma_{212}=-nr^2\,(dn/dr)-n^2r \\ \Gamma_{222}=0 & \Gamma_{121}=0 & \end{array} \tag{6.5.1}$$

Christoffel symbols of the second kind are

$$\begin{array}{lll} \Gamma_1{}^1{}_2=0 & \Gamma_1{}^2{}_1=0 & \Gamma_2{}^1{}_2=-(r/n)\,(rdn/dr+n) \\ \Gamma_2{}^1{}_1=0 & \Gamma_1{}^1{}_1=(1/n)\,(dn/dr) & \Gamma_1{}^2{}_2=(1/nr)\,(rdn/dr+n) \\ \Gamma_2{}^2{}_2=0 & \Gamma_2{}^2{}_1=(1/nr)\,(rdn/dr+n) & \end{array} \tag{6.5.2}$$

The non-vanishing components of the mixed curvature tensor are

$$\begin{aligned} R_2{}^1{}_{12} &= -R_1{}^2{}_{12}=-R_2{}^1{}_{21}=R_1{}^2{}_{21} \\ &= \frac{1}{n}\left[\frac{d^2n}{dr^2}-\frac{1}{n}\left(\frac{dn}{dr}\right)^2+\frac{1}{r}\frac{dn}{dr}\right] \end{aligned} \tag{6.5.3}$$

The [1212] component of the covariant curvature tensor is

$$\begin{aligned} R_{1212} &= g_{12}R_1{}^1{}_{12}+g_{22}R_1{}^2{}_{12} \\ &= g_{22}R_1{}^2{}_{12} \\ &= r^2\left(\frac{dn}{dr}\right)^2-r^2n\frac{d^2n}{dr^2}-rn\frac{dn}{dr}. \end{aligned} \tag{6.5.4}$$

Since $|g|=n^4r^2$, we have

$$\begin{aligned} K &= R_{1212}/|g| \\ &= -\frac{1}{n^3}\frac{d^2n}{dr^2}+\frac{1}{n^4}\left(\frac{dn}{dr}\right)^2-\frac{1}{n^3r}\frac{dn}{dr}. \end{aligned} \tag{6.5.5}$$

6.6 References

1. J.K. Sparkman, Jr. *A remote sensing technique using terrestrial refraction, for the study of low-level lapse rate*, Ph.D. Thesis, University of Wisconsin (1971).

2. A.B. Fraser, *Solutions of the refraction and extinction integrals for use in inversions and image formation*, Appl. Opt. **16**, 160-165 (1977).

3. W.H. Lehn, *Inversion of superior mirage data to compute temperature profiles*, J. Opt. Soc. Am. **73**, 1622-1625 (1977).

4. N.K. Johnson and O.F.T. Roberts, , Q.J.R. Meteorol. Soc. **51**, 131 (1925).

5. R.G. Fleagle, *The optical measurement of lapse rate*, Bull. Amer. Meteorol. Soc. **31**, 51 (1950).

6. L.A. Lyusternik, *Shortest Paths, Variational Problems*, (Pergamon, London, 1964).

7. W.H. Press et al. *Numerical Recipes, The Art of Scientific Computing*, (Cambridge, 1986).